Analytical Crashworthiness Methods Applied to Composite Structures

by

Keith W. Lehnhardt
B.S., United States Naval Academy, 1991

Submitted to the Department of Ocean Engineering and the Department of Mechanical Engineering in Partial Fulfillment of the Requirements for the Degrees of

Naval Engineer
and
Master of Science in Mechanical Engineering

at the
MASSACHUSETTS INSTITUTE OF TECHNOLOGY
June 1999

Signature of Author _____
Department of Ocean Engineering
13 May, 1999

Certified by _____
Tomasz Wierzbicki
Professor of Applied Mechanics
Thesis Supervisor

Certified by _____
James H. Williams, Jr.
SEPTE Professor of Engineering
Thesis Reader

Accepted by _____
Art Baggeroer
Ford Professor of Engineering
Chairman, Departmental Committee on Graduate Studies

Accepted by _____
Ain A. Sonin
Chairman, Departmental Committee on Graduate Studies
Department of Mechanical Engineering

Analytical Crashworthiness Methods Applied to Composite Structures

by

Keith W. Lehnhardt

Submitted to the Department of Ocean Engineering
on 13 May 1999, in partial fulfillment of the
requirements for the degrees of
Naval Engineer
and
Master of Science in Mechanical Engineering

Abstract

Several shell deformation models are developed for use in crashworthiness analysis of rotationally symmetric structures. These models use analytical techniques to predict the crushing force versus axial crush distance characteristics of both a rigid-plastic, hemispherical shell and an elastic, cylindrical shell loaded axially by a rigid flat plate. Additional methods are proposed to determine the effects of cutout sections and internal stiffening members on the crushing force capacity of the shells. These proposed methods are applied to determine the energy absorption capability of the composite/metal nose structure of a mini submarine subjected to a head-on impact with a flat rigid wall. The nose structure is composed of a stiffened composite shell that covers and is attached to the metal, forward, hemispherical portion of the pressure hull. The complex structure is simplified to a rotationally symmetric shell model and modified to account for the effects of stiffening elements and cutout sections. Laminated plate theory, a progressive composite failure method, and the models developed are then used to determine the structure's energy absorption capacity. The fairing structure is determined to be capable of absorbing the kinetic energy associated with an impact from an initial vehicle speed of 7.5 knots. Further, the entire nose structure (the fairing and forward pressure hull) is predicted to be able to absorb the kinetic energy from a 26.4 knot vehicle impact.

Thesis Supervisor: Tomasz Wierzbicki
Title: Professor of Applied Mechanics

Thesis Supervisor: James H. Williams, Jr.
Title: SEPTE Professor of Engineering

Contents

List of Tables

List of Figures

Chapter 1

Introduction

The Advanced Seal Delivery System (ASDS) (Figure (1-1)) is a highly sophisticated, mini-submarine 19.8 m long that displaces 60 metric tons submerged. It is designed to transport a team of Navy SEALs from a host submarine to a tactical point of insertion and back. While the transported SEALs are a formidable offense weapon, the ASDS itself has no offensive or defensive capabilities and must rely on stealth and its ability to "hide" in the water column to ensure the safe transport of its personnel. As such, the ASDS will be operating in close proximity to the ocean bottom in order to mask its underwater signature. This near bottom operating strategy presents some problems, however. The most pressing of these is the increased risk of impact with submerged objects or structures. For the safety of the embarked crew, it is paramount that a determination be made as to the crashworthiness of the ASDS and whether operational restrictions need to be imposed. In effect, a safety envelope needs to be developed which takes into account the depth, bottom type and impact angle to give a maximum safe operating speed. A natural starting point for this analysis is to look at how a front end impact will affect the forward structure of the vessel. This analysis, however, presents no small task. The complexity of this problem quickly becomes apparent when the structure types and problem variables are viewed:

- The structure of the nose section consists of various composite materials and steel including: glass woven cloth, carbon cloth, kevlar, vinylester, rubber, syntactic foam, and HY-80 steel.

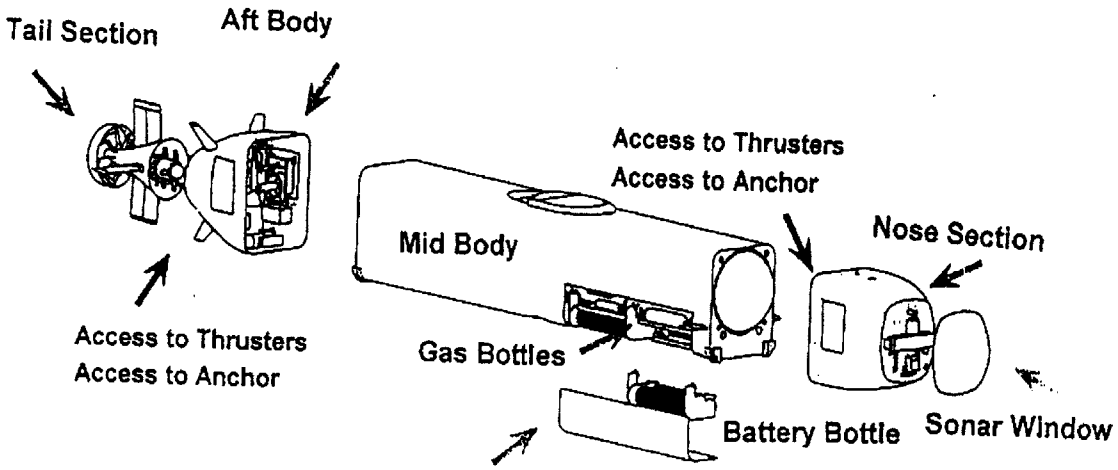

Figure 1-1: External Isometric View of the ASDS

- The variables of the problem include: depth, impact angle, speed, and bottom type.

Additionally, the interaction of the structural material and modes of failure during deformation and fracture are not well understood or predictable to a high degree of accuracy. In light of these complexities, using model testing to develop some empirical means of relating the structural behavior during a collision to key parameters such as impact angle, velocity, or crush distance would be the optimal analysis tool. However, due to the cost associated with such tests, this method is not feasible. Moving to the other end of the spectrum, a computer simulated "crash" test of the ASDS could, in theory, be used to ascertain the desired safety envelope at a substantially cheaper price and in an accelerated time frame. While modeling the full ASDS via computer simulation seems plausible on the surface, a little digging reveals that even the most sophisticated computer tools have not evolved far enough to accurately predict impact responses for such complex, composite/metal structures. With this in mind, it is apparent that neither model testing nor computer simulation alone can solve this problem. A middle road between these methods may be the required path. In effect, a combination of structural simplification and computer and analytical modeling will be used to complete the analysis. With all of this said, the overall objective of the project will be to determine a safe impact speed for the vehicle such that during an impact the pressure hull will not rupture and

the crew will be able to survive the collision.

As a first step in solving the problem, this thesis will analyze the energy absorbing potential of the composite nose fairing and forward pressure hull hemi-head structures during a head-on impact with a rigid wall structure. While this impact scenario is idealized and likely never to occur during actual operations, it will serve as a worst case impact and best case energy absorption scenario. This will be a worst case impact from the stand point that all kinetic energy will be absorbed by the structure in the form of deformation. No energy will be absorbed by the impacted structure or be maintained as vehicle kinetic energy. This is a best case energy absorption scenario in that the impact will allow the full utilization of the bow structure to absorb energy before the pressure hull is impacted. The reasoning behind looking at such a case first, is to ascertain the maximum energy absorption potential of the composite structure.

This analysis will progress in three phases:

- Deformation model development.
- Structural modeling of the ASDS nose structure.
- Energy absorption analysis.

The models developed include deformation relationships for a rigid-plastic, hemispherical and an elastic, cylindrical shell loaded axially by a rigid flat plate. A method is also included to approximate the reduced load carrying capacity caused by cutouts in the shell structure. Next, the composite shell of the nose fairing will be modeled using simplified, rotationally symmetric shells (i.e.- cylinders, frustum, and hemispheres). Internal stiffening members are incorporated into the model by "smearing" the effective area of each stiffener across portions of the inner surface of the shell to increase the effective thickness of the structure. Cutouts in the shell for components, such as thruster doors, video equipment, and lights are also modeled. Finally, the deformation relationships developed will be applied to the corresponding sections of the model to produce a force verse displacement relationship of the structure as it is crushed axially by a rigid flat plate. The energy absorption capability of the entire structure will then be determined and translated into the vehicle speed needed to produce such an impact.

Chapter 2

Development and Discussion of Analysis Tools

2.1 Crushing Response of a Hemispherical Shell Between Rigid Plates

2.1.1 Prior Research

Much attention has been devoted to the study of the energy absorbing characteristics of thin-walled, metal, dome structures [1]-[7]. The problem of large deformations of rigid-plastic, spherical shells being compressed between rigid plates was first studied by Updike [1]. A simplified yield condition and geometry was used to obtain a sequence of limit loads, thus producing a force-displacement relationship valid from a displacement of a few shell thicknesses to about 1/10th the shell radius. Wierzbicki [4] used similar geometric and deformation assumptions to derive a force-deflection relationship based on the optimization of bending and membrane energies valid theoretically until the plate deflection reaches half the radius of the shell. Comparison of [1] and [4] show that the force-displacement results predicted by each differ only slightly. Experimental testing of hemispherical shells was reported by Kitching [5] and Kinhead [5]. Kitching et al studied the quasi-static loading of hemispherical shells and observed experimentally three different stages of deformation for shells with radius to thickness ratios ranging from 36 to 460. Later, Kinkead performed experimental testing on shells with radius

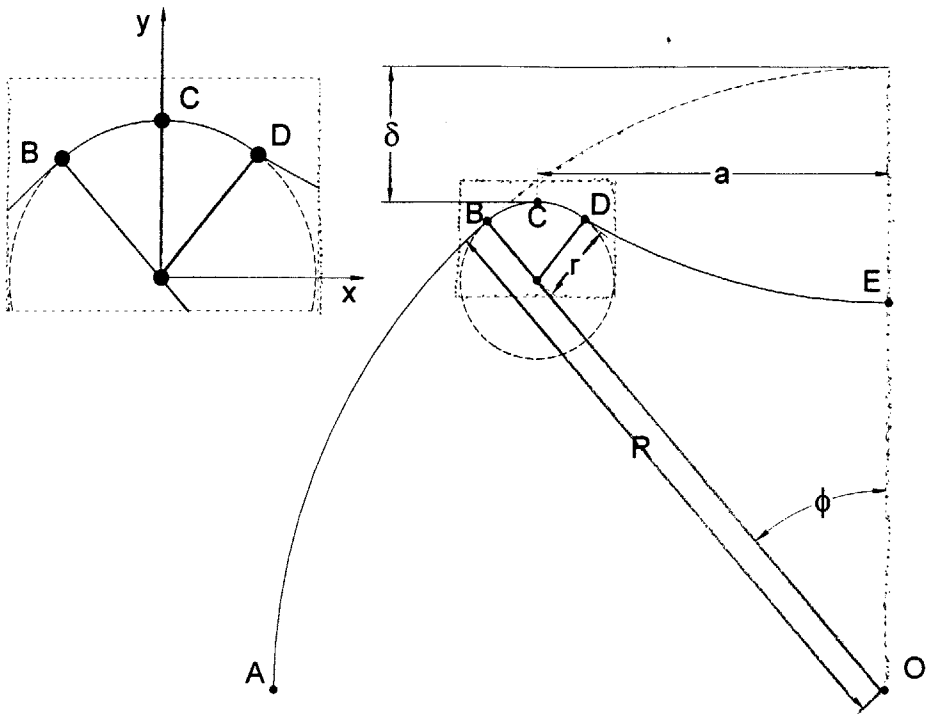

Figure 2-1: Geometry of Hemispherical Deformation Model.

to thickness values ranging from 8 to 32 and identified two vice three deformation stages. The loading characteristic observed by Kinhead were compared to values predicted by the methods of [1] and [4] and large differences were found. Gupta [7] developed another prediction method using a rigid plastic analysis which relies on two calibration constants that must be determined from curve fits of experimental data. The method proposed by Gupta showed good correlation with experimental results. This analysis develops a means of predicting the load-compression relationship of hemispherical shells using a rigid plastic analysis technique with an emphasis on creating a simple, analytical model whose accuracy is improved over that proposed in [1] and [4]. The model developed will utilize the same deformation model used by [1] and [4], but calculate the membrane energy using a simple strain averaging method. Additionally, the resulting relationship will be capable of analyzing material with differing compressive and tensile stresses.

2.1.2 Deformation Process

The spherical shell of radius R will be loaded from the top by a moving rigid plate with the base of the shell pinned to a fixed rigid plate. As the shell is loaded axially, a spherical dimple forms which is an inversion of the original shell curvature as shown in Figure (2-1). In this deformed state, surface AB remains rigid and undeformed. At point B, a circumferential plastic hinge increases the curvature of the shell, followed by rigid body translation between B and D and a reversal of curvature by the plastic hinge at D. The shell is subsequently unloaded and rigid body translation results on surface DE. As the shell deforms, the hinge circles at B and D move progressively outward. Deformation continues in this manner until the inverted portion of the shell at point E contacts the fixed rigid plate.

2.1.3 Deformation Model

Geometry

This analysis begins with a look at the various geometrical relationships that can be attained from the deformation model in Figure (2-1). First, the radius to the center of the toroidal surface (a) and the displacement of the moving rigid plate (δ) can be expressed in terms of the shell radius (R) and deformation angle (ϕ) as

$$a = R\sin\phi, \text{ and} \tag{2.1a}$$

$$\delta = R(1-\cos\phi) \tag{2.1b}$$

By differentiating Equations (2.1a) and (2.1b), the radial and axial velocities of the toroidal section and rigid plate become

$$\frac{da}{dt} = R(\cos\phi)\frac{d\phi}{dt}, \text{ and} \tag{2.2}$$

$$\frac{d\delta}{dt} = R(\sin\phi)\frac{d\phi}{dt} \tag{2.3}$$

By approximating $\cos\phi(t)$ using the first two terms of its Taylor expansion in Equation (2.1b) and rearranging, a simple equation relating the deformation angle to the rigid plate displacement can be deduced.

$$\phi = \sqrt{\frac{2\delta}{R}} \tag{2.4}$$

Turning now to the toroidal surface $\widehat{BCD}$, the average plastic hinge length (L) and toroidal surface area (A) can be calculated by the Equations (2.5a) and (2.5b).

$$L = 2\pi a, \text{ and} \tag{2.5a}$$

$$A = 4\pi r a \phi \tag{2.5b}$$

Additionally, the radial and rotational velocities of the plastic hinge at point B can be taken as

$$V = R\frac{d\phi}{dt} \tag{2.6}$$

$$\frac{d\theta}{dt} = \frac{V}{r} = \frac{R}{r}\frac{d\phi}{dt} \tag{2.7}$$

Finally, in order to simplify subsequent calculation, surface $\widehat{BCD}$ will be approximated as a parabolic surface of the form

$$y = \frac{1}{2}\frac{\varphi}{r\sin\varphi}x^2 + r(1-\cos\phi) \tag{2.8}$$

with the x and y axes oriented as shown in Figure (2.2.3).

Derivation of Membrane Stresses and Fully Plastic Bending Moment

Next, the membrane force (N) and fully plastic bending moment (M) relationships for a material having differing compressive (σ_c) and tensile (σ_t) flow stresses will be developed. As shown in Figure (2-2), when $\sigma_c \neq \sigma_t$ the neutral axis will shift away from the geometrical center of the cross section by an amount η. By using the fact that the neutral axis of a specimen subjected to a bending moment is located where the membrane force (N) is equal to zero, we are able to calculate a general expression for η in terms of shell thickness (t), σ_c, and σ_t as shown below

$$N = \int_0^{\frac{t}{2}+\eta} \sigma_t dz - \int_0^{\frac{t}{2}-\eta} \sigma_c dz = 0 \tag{2.9}$$

where both σ_t and σ_c are taken to be positive.. Upon integrating and solving for η, Equation

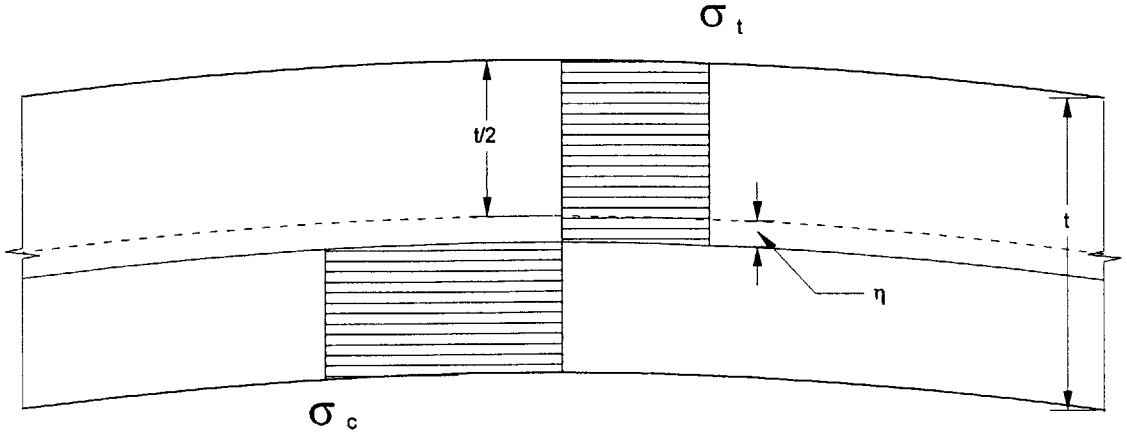

Figure 2-2: Membrane Stress and Fully Plastic Bending Moment Representation for Material having Differing Compressive and Tensile Flow Stresses.

(2.9) becomes

$$\eta = \frac{1}{2} t \frac{\sigma_c - \sigma_t}{\sigma_c + \sigma_t} \tag{2.10}$$

With η calculated, general expressions for N and M can be derived as follows:

$$\begin{aligned} N &= \int_0^t \sigma_c dz \\ M &= \int_0^{\frac{t}{2}+\eta} \sigma_t z dz + \int_0^{\frac{t}{2}-\eta} \sigma_c z dz \end{aligned}$$

Note that the regions of membrane deformation are compressive in nature while the bending forces are both tensile and compressive. After integrating, substituting Equation (2.10) for η, and setting $\alpha = 2\frac{\sigma_t}{\sigma_c+\sigma_t}$, the total membrane force and fully plastic bending moments become

$$N = \sigma_c t \tag{2.11}$$

$$M = \frac{1}{2}\sigma_c t^2 \frac{\sigma_t}{\sigma_c + \sigma_t} = \frac{\sigma_c t^2}{4}\alpha \tag{2.12}$$

In order verify the validity of Equations (2.11) and (2.12), σ_c can be set equal to σ_t which results in a symmetric stress profile throughout the specimen. In such a case Equations (2.11) and (2.12) reduce to the standard expressions for the fully plastic membrane force and bending moment.

Energy Balance

The principle of virtual velocities will be used to relate the rate at which energy is being introduced to the system to the rate at which it is being absorbed. Equation (2.13) states that the rate at which energy is applied to the shell must exactly match the rate at which it is being absorbed by the bending and membrane effects in the shell.

$$\overset{(1)}{P\frac{d\delta}{dt}}=\overset{(2)}{\frac{dE_b}{dt}}+\overset{(3)}{\frac{dE_m}{dt}} \tag{2.13}$$

The remainder of this section will further develop each of the terms in Equation (2.13). Starting first with the left hand side of Equation (2.13), term (1) can be rewritten in a different form by using Equation (2.3) as follows

$$P\frac{d\delta}{dt} = PR\sin\phi\frac{d\phi}{dt} \tag{2.14}$$

The second term of Equation (2.13) represents the rate at which energy is absorbed by the shell due to bending processes. Using the deformation model shown in Figure (2-1), it is plainly seen that bending energy will be absorbed at two discrete locations – plastic hinges B and D. This component can be quantified by the following expression

$$\frac{dE_b}{dt} = \sum_{i=B,D} M_i\frac{d\theta}{dt}L_i \tag{2.15a}$$

Equation (2.15a) can be further simplified by making the following assertions

- the magnitudes of the bending moment and rate of angular rotation at hinges B and D are equal.
- the total hinge length $\sum_{i=B,D} L_i$ can be rewritten as $2L$ (where L is the average hinge length.

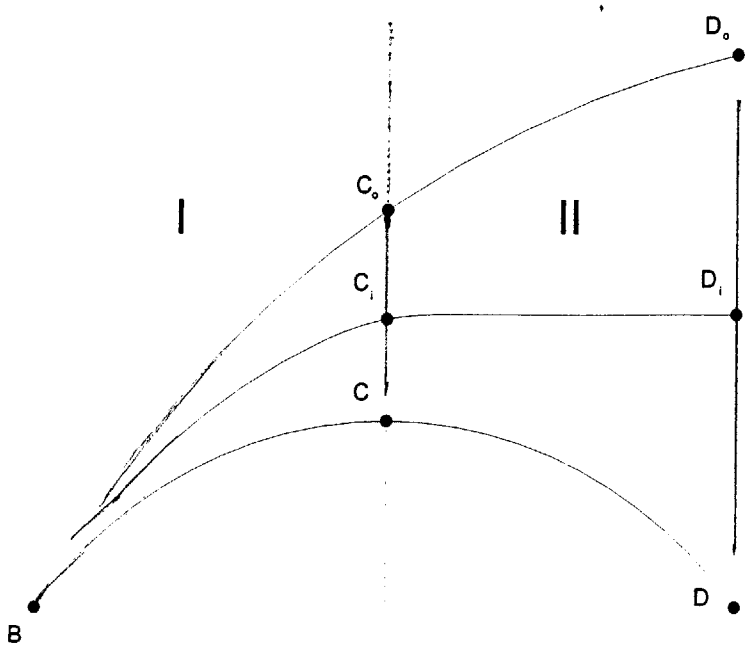

Figure 2-3: Deformation of Surface BCD.

Using these simplifications and Equations (2.1a), (2.5a), and (2.7), Equation (2.15a) can be expressed in the following form:

$$\frac{dE_b}{dt} = 4\pi R^2 \sin\phi \frac{M}{r}\frac{d\phi}{dt} \tag{2.16}$$

The final term in Equation (2.13) accounts for the membrane energy dissipated on surface $\widehat{BCD}$ and can be written as:

$$\frac{dE_m}{dt} = NA\frac{d\varepsilon}{dt} \tag{2.17}$$

where $\frac{d\varepsilon}{dt}$ is the instantaneous rate of strain experienced by surface $\widehat{BCD}$. As a simplification, the average strain rate, $\frac{d\varepsilon_{av}}{dt}$, will be used in place of the instantaneous strain rate. Figure (2-3) shows a detailed view of the deforming surface $\widehat{BCD}$. The average strain of this surface will be calculated by dividing the surface into two subsurfaces, calculating the average strain on each, and then averaging the strains from each region to get the final average strain. This

statement can be expressed mathematically as

$$\varepsilon_{av} = \frac{\varepsilon_{I_{av}} + \varepsilon_{II_{av}}}{2} \tag{2.18}$$

where $\varepsilon_{I_{av}}$ and $\varepsilon_{II_{av}}$ are the average strains experienced as surfaces $\widehat{BC_o}$ (region 1) and $\widehat{C_oD_o}$ (region 2) deform to $\widehat{BC}$and $\widehat{CD}$ respectively. Looking first at region I, the strain can be written in terms of initial and final curvatures of the $\widehat{BC}$.

$$\varepsilon_I = \varepsilon_{I_f} - \varepsilon_{I_o} = \frac{1}{2}\left(\frac{dy}{dx}\right)^2 - \frac{1}{2}\phi^2 \tag{2.19a}$$

In general, the average strain in region I can be formulated as:

$$\varepsilon_{I_{av}} = \frac{1}{r\sin\phi}\int_0^{r\sin\phi} \varepsilon_I dx \tag{2.20}$$

Upon substitution of Equation (2.19a), integration and simplification, Equation (2.20) reduces to

$$\varepsilon_{I_{av}} = \frac{1}{3}\phi^2 \tag{2.21}$$

The strain in region II requires an additional step to calculate. While the strain in region I is purely compressive for the entire deformation, the strain in region II is initially compressive for the first part of deformation and then tensile for the remainder of the deformation. So, the average strain will be calculated for the compressive phase as surface $\widehat{C_oD_o}$ is deformed to an intermediate flat surface $\widehat{C_iD_i}$ and also for the tensile phase as the shell further deforms to surface $\widehat{CD}$. With this, the average strain in region II can be calculated in the same manner as in region I. The details of the calculation follow.

$$\begin{aligned}
\varepsilon_{II_{av}} &= \varepsilon_{II_{av_{compressive}}} + \varepsilon_{II_{av_{tensile}}} \\
\varepsilon_{II_{av}} &= \frac{1}{r\sin\phi}\int_0^{r\sin\phi}\left[\left(\varepsilon_{II_{f_{compressive}}} - \varepsilon_{II_{o_{compressive}}}\right) + \left(\varepsilon_{II_{ftensile}} - \varepsilon_{II_{o_{tensile}}}\right)\right]dx \\
\varepsilon_{II_{av}} &= \frac{1}{r\sin\phi}\int_0^{r\sin\phi}\left[\left(\frac{1}{2}\phi^2 - 0\right) + \left(0 - \frac{1}{2}\left(\frac{dy}{dx}\right)^2\right)\right]dx \\
\varepsilon_{II_{av}} &= \frac{2}{3}\phi^2
\end{aligned} \tag{2.22}$$

With the average strain calculated in both regions, we can now determine the average strain of the entire surface $\widehat{BCD}$ by substituting Equations (2.21) and (2.22) into Equation (2.18). Subsequently, the average strain rate can be calculated by simple differentiation of the average strain as follows.

$$\varepsilon_{av} = \frac{1}{2}\phi^2 \tag{2.23}$$

$$\frac{d\varepsilon_{av}}{dt} = \phi\frac{d\phi}{dt} \tag{2.24}$$

Now a final expression for the rate at which energy is absorbed by membrane forces can be realized by substituting Equations (2.5b), (2.1a) and (2.24) into Equation (2.17).

$$\frac{dE_m}{dt} = 4\pi r N R \sin\phi\phi^2\frac{d\phi}{dt} \tag{2.25}$$

New expressions have now been formulated for each term in Equation (2.13). By substituting the new expressions (Equations (2.14), (2.16), and (2.25)) into Equation (2.13) and solving for the instantaneous crushing force (P), the following result is obtained

$$P = 4\pi\left(\frac{RM + Nr^2\phi^2}{r}\right) \tag{2.26}$$

Further, the mean crushing force ($\overline{P}$) can be calculated and minimized with respect to the toroidal radius (r) to obtain an optimal toroidal radius.

$$\overline{P} = \frac{P}{2\pi M} = 2\left(\frac{R}{r} + r\frac{N}{M}\phi^2\right) \tag{2.27}$$

$$\frac{d\overline{P}}{dr} = 2\left(\frac{N}{M}\phi^2 - \frac{R}{r^2}\right) = 0$$

$$\left(\frac{1}{r_{opt}}\right) = \phi\sqrt{\frac{N}{RM}} \tag{2.28}$$

By substituting the optimal toroidal radius back into Equation (2.27) and using the fact that at the optimal radius the membrane and bending contributions are equal, the mean crushing force can be expressed more simply as

$$\overline{P}_{opt} = 4\phi R\sqrt{\frac{N}{RM}} \tag{2.29}$$

Equation (2.29) can be rewritten in terms of plate displacement and shell thickness by using Equations (2.4), (2.11), and (2.12).

$$\overline{P}_{opt} = 8\sqrt{\frac{2\delta}{t\alpha}} \tag{2.30}$$

Finally, the optimal instantaneous crushing force becomes

$$P_{opt} = 4\pi\sqrt{2}\sigma_c\alpha^{\frac{1}{2}}t^{\frac{3}{2}}\delta^{\frac{1}{2}} \tag{2.31}$$

2.2 Derivation of Cylindrical Tube Equation

2.2.1 Prior Research

The deformation and energy absorption characteristics of thin-walled, composite, cylindrical shells have been studies for many years by many researchers. [8]-[15]. Farley [10]-[13] and Hull [14] have performed extensive testing on composite shell samples composed of various materials using different lay-up conditions. Both quasi-static and dynamic loading situations were investigated. These studies did much to further the knowledge base in the areas of determining crushing modes and their controlling mechanisms. They also showed that there was no explicit set of rules that could be generalized for all composites types. Material lay-up pattern, crushing speed, fiber volume fraction, and radius to laminate thickness ratio all play key roles in determining the deformation characteristics of the shell. From these studies, complicated numerical models have been established for use in predicting the failure of very simple composite structures. The degree of success realized by these models has varied in even simple situations. The vast majority of the work described has been directed toward understanding the deformation of composites on the micro- and macroscopic scales. Hanefi and Wierzbicki [15] took a more global approach to a similar deformation problem. They developed a simple model that was used to predict the energy absorption characteristics of a combined metallic/composite tube structure in axial compression. The model coupled a rigid plastic analysis of the metal tube with a compressive perfectly plastic and tensile elastic analysis of the composite material. The

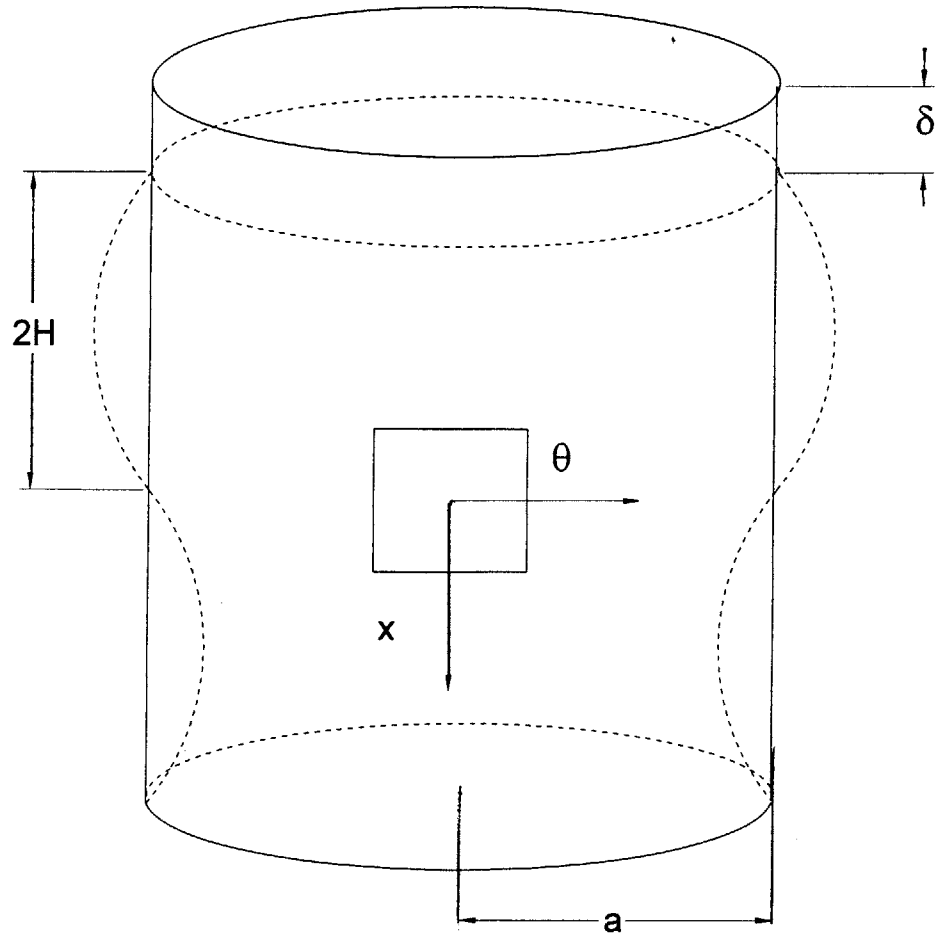

Figure 2-4: Deformation Model for Cylindrical Thin-walled Structure.

predicted results matched well with experimental data. In this analysis, a global failure approach will also be taken. A deformation model will be developed using elastic principles to determine the force deflection and energy deflection characteristics of a thin-walled, cylindrical shell loaded axially. Bending and in-plane stiffnesses will be step-wise varied to account for stiffness variations as plys fail within the structure. Finally, a simple result will be established for a material exhibiting constant and identical flexural and inplane stiffness properties.

2.2.2 Deformation Process

Figure 2-4 shows a representation of two buckling lobes of the cylinder during deformation where δ denotes the axial crush distance, a is the radius of the cylinder, and $2H$ is the half

length of the buckling lobe generated. As the cylinder is crushed axially by a distance δ, the cylinder will form an axisymmetric, elastic buckling pattern with a wave length equal to $2H$. Deformation takes place both in the form of bending and circumferential strain. The material will behave elastically until its elastic limits are reached with subsequent deformation occurring with the material in a progressively degraded state. The material degradation takes place through a step-wise reduction of the material's flexural and circumferential elastic moduli and material thickness. The process continues progressively through all buckling lobes formed.

2.2.3 Deformation Model

The principle of virtual work (Equation (2.32)) will be used as the starting relationship from which to derive an expression relating the crushing force (P) to the axial crush distance (δ). Equation (2.32) states that the energy applied to the cylinder through an external force (1) must be exactly equal to the energy absorbed by the structure in the form of circumferential (2) and bending (3) strains.

$$\overset{(1)}{P}d\delta = \int_V (\overset{(2)}{\sigma_\theta} d\varepsilon_\theta + \overset{(3)}{\sigma_x} d\varepsilon_x) dV \tag{2.32}$$

$$\sigma_\theta = E\varepsilon_\theta \text{ and } \sigma_x = E\varepsilon_x \tag{2.33}$$

$$Pd\delta = \int_V (E\varepsilon_\theta d\varepsilon_\theta + E\varepsilon_x d\varepsilon_x) dV \tag{2.34}$$

Because the deformation will be elastic, Equation (2.32) can be simplified using the elastic relationships between stress and strain (Equation (2.33)) to obtain Equation (2.34). Figure (2-5) shows a detailed view of the deformation of a single buckling lobe with parameters pertinent to the analysis labeled. Using this figure, expressions can be derived in terms of the variables shown for the incremental volume (dV), strains (ε_x and ε_θ), and incremental strains ($d\varepsilon_x$ and $d\varepsilon_\theta$). First, inextensibility will be assumed for the shell as it buckles, making dV constant over the deformation process and having the following value:

$$dV = 4\pi atH \tag{2.35}$$

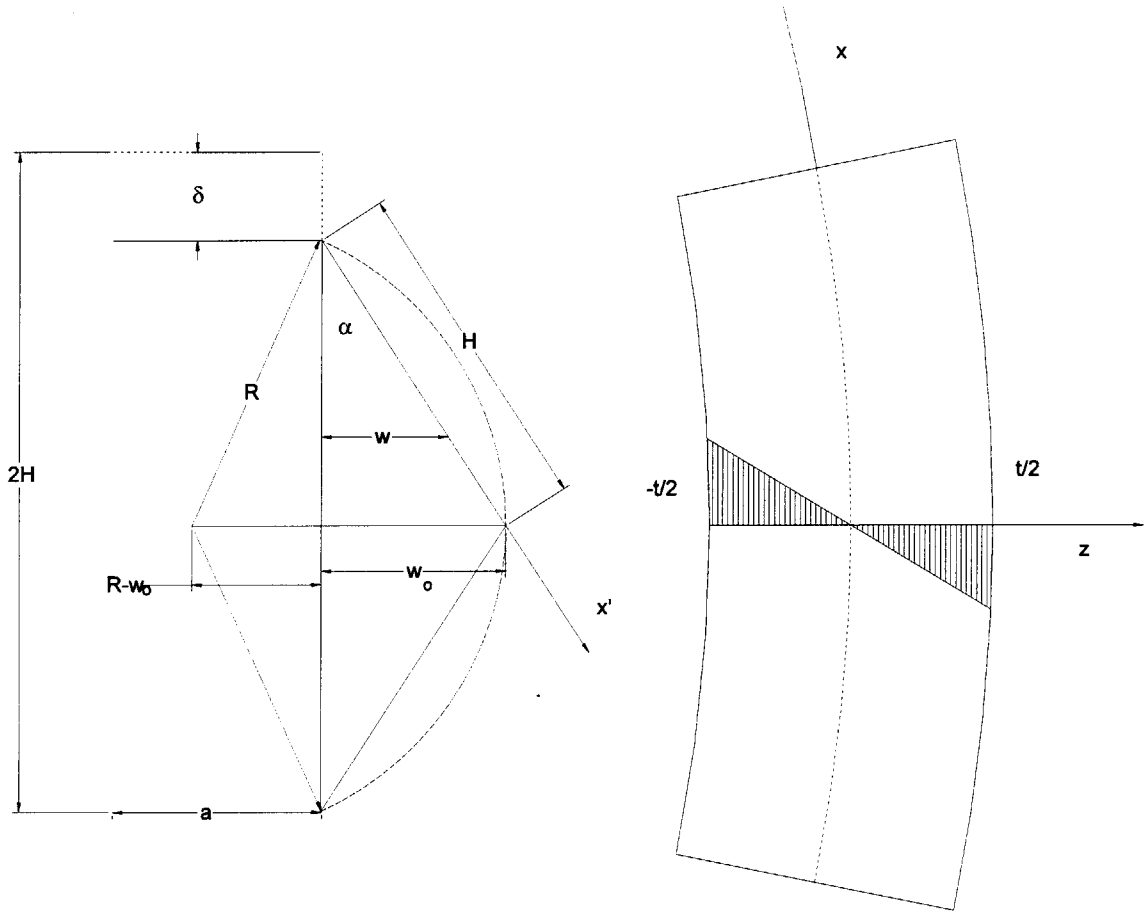

Figure 2-5: Detailed View of the Deformed Cylinder Section.

Next, the circumferential strain can be expressed as the ratio of the outward deflection of the shell (w) to the original shell radius. The actual deflection is measured from the original surface of the shell to the deformed surface and varies from 0 at the being of the lobe to a maximum value of w_o at the midpoint, and then back to 0 at the end of the lobe. In order to simplify future calculations, a linear deflection profile ($w(x') = \frac{x'}{H} w_o$) is used to approximate the actual deflection profile as shown in Figure (2-5). Using this linear relationship, ε_θ and $d\varepsilon_\theta$ can be expressed as

$$\varepsilon_\theta = \frac{w}{a} = \frac{x'}{aH} w_o \tag{2.36}$$

$$d\varepsilon_\theta = \frac{x'}{aH} dw_o \tag{2.37}$$

The bending strain component can be determined by using the curvature of the shell section (κ) and the position within the thickness of the material (z) as is shown in Equation (2.38). This variation of the bending strain throughout the shell thickness will be assumed linear with maximums occurring at $\frac{t}{2}$ and $-\frac{t}{2}$ and no strain occurring at the mid-plane. Further, plane sections will remain plane as shell curvature increases.

$$\varepsilon_x = z\kappa = \frac{z}{R} \tag{2.38}$$

However, the radius of curvature (R) is related to the half lobe length and the maximum circumferential deflection by Equation (2.39)

$$\begin{aligned} R^2 - (R - w_o)^2 &= H^2 - w_o^2 \\ R &= \frac{H^2}{2w_o} \end{aligned} \tag{2.39}$$

Substitution of Equation (2.39) into Equation (2.38) yields the final expressions for ε_x and $d\varepsilon_x$ (Equations (2.40) and (2.41)).

$$\varepsilon_x = \frac{2z}{H^2} w_o \tag{2.40}$$

$$d\varepsilon_x = \frac{2z}{H^2} dw_o \tag{2.41}$$

Now, Equations (2.35)-(2.37) and (2.40) can be substituted back into Equation (2.34) to obtain the following:

$$Pd\delta = \left(\frac{(4\pi at)}{a^2H^2} \int_0^H E_m(x')^2 dx' + \frac{8E_f}{H^4}(4\pi aH) \int_0^{\frac{t}{2}} z^2 dz \right) w_o dw_o \tag{2.42}$$

If the flexural and membrane Young's moduli can be assumed equal and constant throughout the deformation process, Equation (2.42) can be further simplified to Equation (2.43).

$$Pd\delta = \frac{4}{3}\pi E \left[\frac{tH}{a} + \frac{at^3}{H^3} \right] w_o dw_o \tag{2.43}$$

Previous work [18] has proven that the elastic, buckling lobe length of a cylinder can be related to the shell radius and thickness by

$$\begin{aligned} 2H &= 1.72\sqrt{at} \\ H &\approx \sqrt{at} \end{aligned} \tag{2.44}$$

Using Equation (2.44), Equation (??) can be reduced to

$$\begin{aligned} Pd\delta &\approx \frac{4}{3}\pi E \left[\frac{t\sqrt{at}}{a} + \frac{at^3}{at\sqrt{at}} \right] w_o dw_o \\ Pd\delta &\approx \frac{4}{3}\pi E \left[t\sqrt{\frac{t}{a}} + t\sqrt{\frac{t}{a}} \right] w_o dw_o \\ Pd\delta &\approx \frac{8}{3}\pi E t\sqrt{\frac{t}{a}} w_o dw_o \end{aligned} \tag{2.45}$$

A final simplification can be made to Equation (2.45) by relating δ to w_o. Using Figure (2-5) the following geometric relationships can be generated.

$$\sin(\alpha) = \frac{w_o}{H} \tag{2.46}$$

$$\cos(\alpha) = 1 - \frac{\delta}{2H} \tag{2.47}$$

By squaring and adding Equations (2.46) and (2.47), the relationships are combined in the following form

$$1 = \left[\frac{w_o}{H}\right]^2 + \left[1 - \frac{\delta}{2H}\right]^2 \tag{2.48}$$

After differentiating, rearranging and substituting Equation (2.44), the desired relationship is achieved

$$w_o dw_o \approx \left[\sqrt{at} - \frac{\delta}{2}\right] \frac{d\delta}{2}$$

This expression can now be substituted back into Equation (2.45) to obtain the final expression relating the crushing force applied to the axial deflection of the cylinder.

$$P(\delta) \approx \frac{4}{3}\pi E \left[t^2 - t\sqrt{\frac{t}{a}}\frac{\delta}{2}\right] \tag{2.49}$$

As previously states, Equation (2.49) applies to materials with equal and constant flexural and circumferential Young's moduli. If these conditions are not met, the more general expression (Equation (2.42)) must be used.

2.2.4 Correction for Open Sections

Open sections or cutouts in a shell will effectively reduce the load required to deform the shell in the local region of the cutout. These cutouts could even change the local deformation mode of the structure or change the order in which the overall structure deforms. For simplicity, this analysis will include only the reduction in loading capacity for several reasons. The relationships previously developed, Equations (2.26) and (2.49), are valid only for the failure modes assumed; so, a change in failure modes (i.e.- from axisymmetric shell yielding to lobar buckling for example) will not be captured here in. While this seems like a fairly unreasonable assumption, the reader is reminded that the objective of this analysis is to determine the *maximum* energy absorption capability of the structure. The development of Equations (2.31) and (2.49) assume failure modes which produce this maximum. So, a shift to a different mode would produce a lower energy absorption. With the assumption that the failure mode remains unchanged at the cutouts, it does not make sense to consider the order in which parts of the structure collapse because the same amount of energy will be absorbed regardless of the collapse sequence. So, the

only effect that will be considered is the reduction of strength caused by the loss of material. This effect will be approximated by multiplying the applied load of an intact shell by a reduction factor in the local vicinity of the cutout. This reduction factor will be proportional to the remaining shell area divided by the material present in an intact shell of the same dimensions (Equation (2.50))

$$\begin{aligned} F(\delta)_{corrected} &= F(\delta)_{uncorrected}\varepsilon(\delta) \text{ where} \\ \varepsilon(\delta) &= \left[\frac{(\mathrm{A}_{\text{complete shell}}(\delta) - \mathrm{A}_{\text{removed material}}(\delta))}{\mathrm{A}_{\text{complete shell}}(\delta)}\right]\xi \end{aligned} \tag{2.50}$$

While this area ratio is part of the reduction effect, it does not capture all aspects. Other factors, such as cutout geometry, affect the load carrying capacity of the structure around the cutout. While these other effects are recognizable, a theoretical derivation of their effect is impractical. This effect must be determined experimentally. The experimental correction factor would be used to match experimental test data with theoretical predictions and is expressed as ξ in Equation (2.50). Since no experimental calibration was done during the course of this thesis, ξ will be set equal to 1 until future evaluation determines its correct value.

Hemispherical Dome

For the hemispherical dome, the cutout sections will be assumed to be circular with diameter D as shown in Figure (2-6). From Figure (2-6) it is apparent that the correction factor can be stated in terms of the average plastic hinge radius (a(δ)) and angle $\phi(\delta)$ as follows:

$$\begin{aligned} \varepsilon(\delta) &= \left(\frac{(\text{Average Hinge Diameter-Length of Open Section})}{\text{Average Hinge Diameter}}\right)\xi_{hemisphere} \\ \varepsilon(\delta) &= \left(\frac{2\pi a(\delta) - \phi(\delta)a(\delta)}{2\pi a(\delta)}\right)\xi_{hemisphere} = \left(1 - \frac{\phi(\delta)}{2\pi}\right)\xi_{hemisphere} \end{aligned} \tag{2.51}$$

The task now becomes to express $\phi(\delta)$ in terms of known quantities. Figures (2-7) and (2-8) show more detailed views of the side and top of the shell respectively with pertinent dimensions labeled in each figure.

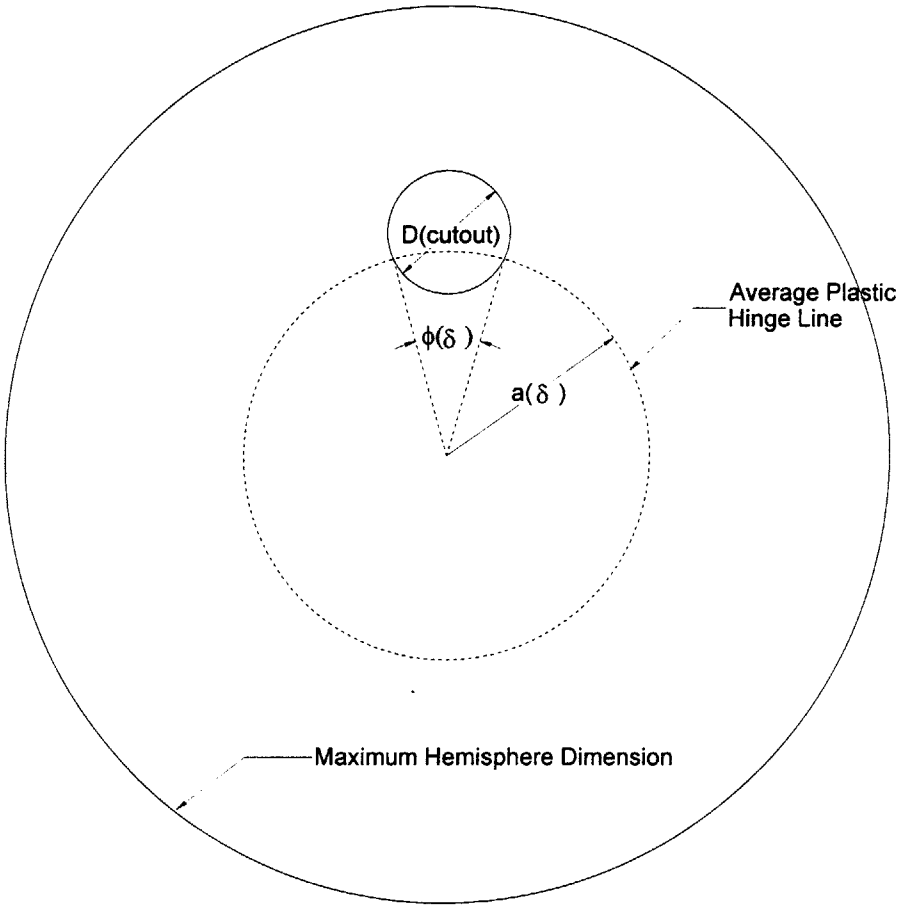

Figure 2-6: Top View of Hemispherical Dome with a Single Circular Cutout Section.

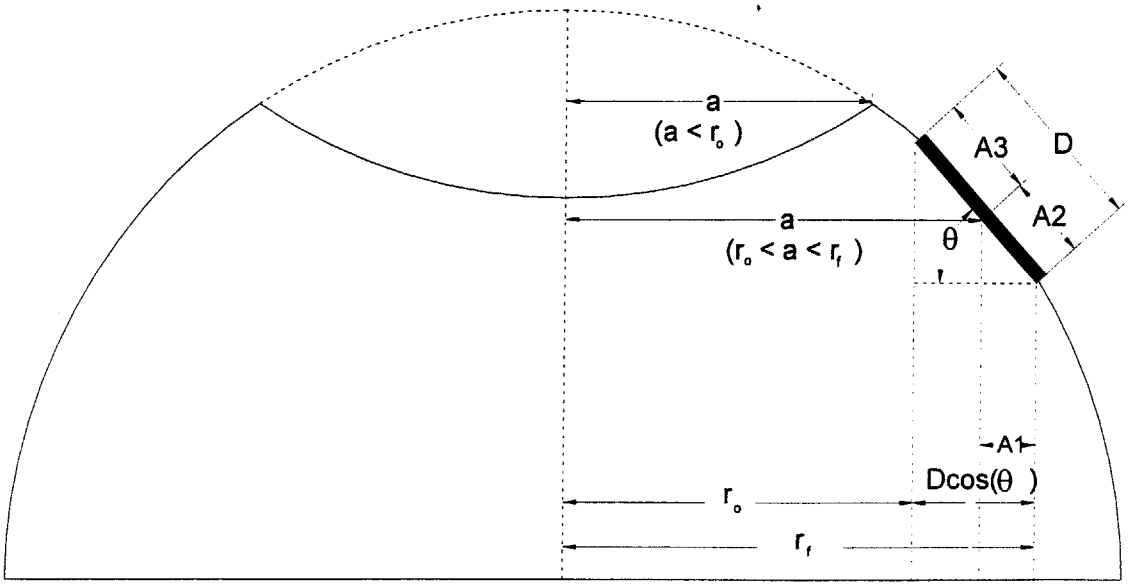

Figure 2-7: Geometrical Relationship of Parameters Used in the Derivation of the Correction Factor for Open Sections in a Dome Structure (side view).

From these figures, the following geometric relationships can be established:

$$\begin{aligned} A1 &= r_o + D\cos\theta - a(\delta) \\ A2 &= \frac{A1}{\cos\theta} \\ A3 &= D - A2 \\ A4 &= \frac{D}{2} - A3 = A2 - \frac{D}{2} \\ A5 &= \sqrt{\left(\frac{D}{2}\right)^2 - A4^2} \end{aligned} \tag{2.52}$$

$\phi(\delta)$ can now be expressed in terms of the initial radius at which the cutout is encountered (r_o), cutout diameter (D), cutout inclination angle (θ), and average plastic hinge radius as shown in Equation (2.53).

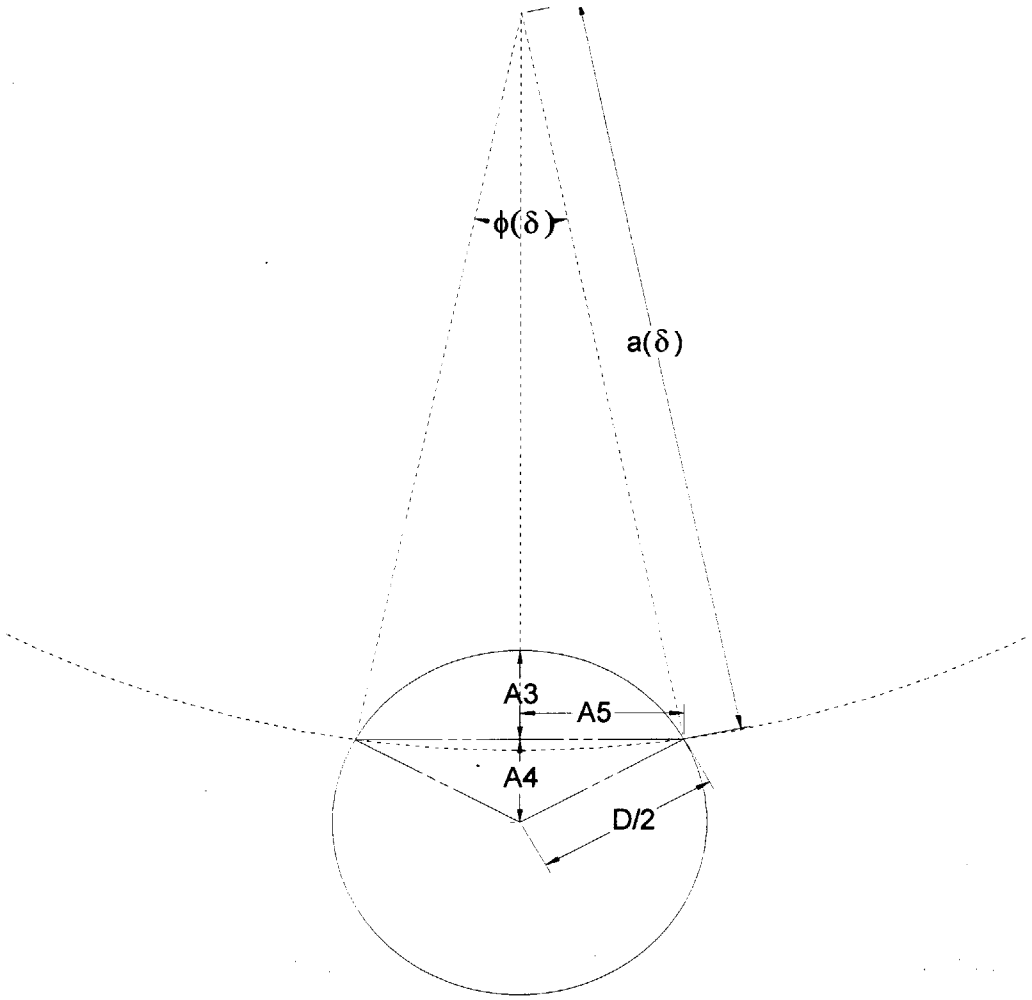

Figure 2-8: Geometrical Relationship of Parameters Used in the Derivation of the Correction Factor for Open Sections in a Dome Structure (top view).

$$\begin{aligned}\phi(\delta) &= 2\arcsin\left(\frac{A5}{a(\delta)}\right)\\ \phi(\delta) &= 2\arcsin\left(\frac{\sqrt{\left(\frac{r_o+D\cos\theta-a(\delta)}{\cos\theta}\right)\left(D-\left(\frac{r_o+D\cos\theta-a(\delta)}{\cos\theta}\right)\right)}}{a(\delta)}\right)\end{aligned} \tag{2.53}$$

Next, a(δ) can be related directly to the radius of the hemisphere (R) and the crush distance of the shell (δ) by the following:

$$a(\delta) = \sqrt{R^2-(R-\delta)^2} = \sqrt{\delta(2R-\delta)} \tag{2.54}$$

Finally, substitution of Equation (2.54) into (2.53) and the result into (2.51) yields the desired result for the correction factor (Equation (2.55))

$$\varepsilon(\delta) = \left[1-\frac{1}{\pi}\arcsin\left(\frac{\sqrt{\left(\frac{r_o+D\cos\theta-\sqrt{\delta(2R-\delta)}}{\cos\theta}\right)\left(D-\left(\frac{r_o+D\cos\theta-\sqrt{\delta(2R-\delta)}}{\cos\theta}\right)\right)}}{\sqrt{\delta(2R-\delta)}}\right)\right]\xi_{hemisphere} \tag{2.55}$$

Cylindrical Shell

The same principles described in Section (2.2.4) will also be used to estimate the effect of cutout sections in the cylindrical section with the exception that the cutout shape will be much simpler. The cutouts in the cylindrical section will be rectangular in shape, and thus, the material removed will not vary with axial crush distance. So, using Equation (2.50) and again assuming that $\xi = 1$, the correction factor of the cylinder can be expressed as

$$\begin{aligned}\varepsilon &= \frac{2\pi a - n\varphi a}{2\pi a} = 1-\frac{n\varphi}{2\pi} \text{ where}\\ n &= \text{Number of cutouts}\\ \varphi &= \text{Angular extent of cutout}\end{aligned} \tag{2.56}$$

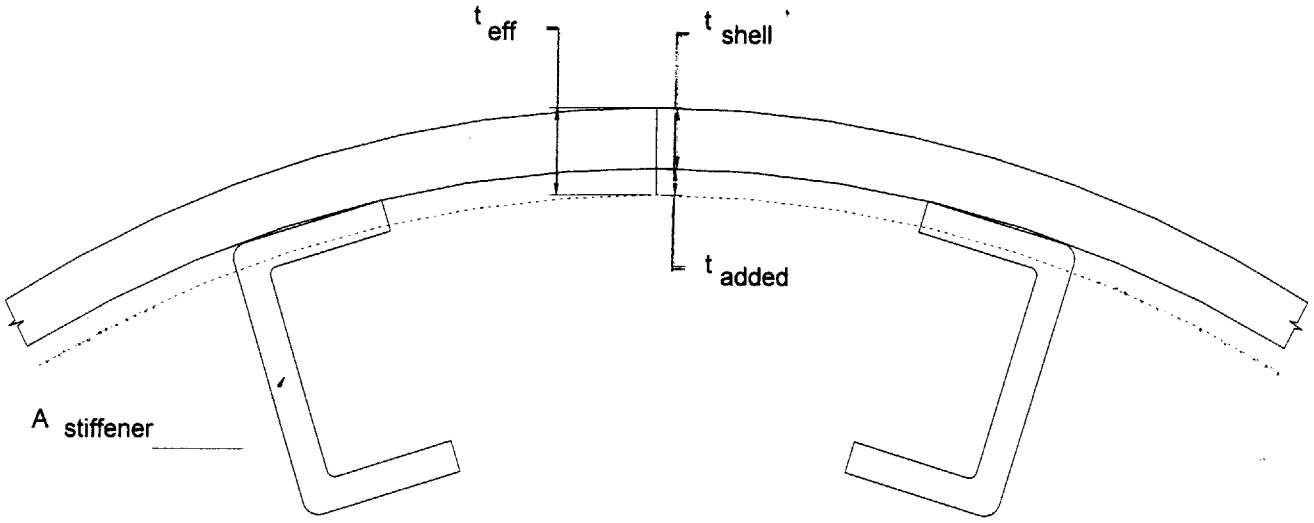

Figure 2-9: Stiffener Smearing Process.

2.2.5 Effect of Shell Stiffeners

The energy dissipation effects of shell stiffeners can be taken into account using Equations (2.31) and (2.49) by assuming that these structural members are "smeared" across the surface of the shell so as to produce a new effective shell thickness. This process is illustrated in Figure (2-9). If the material properties of the stiffeners are identical to those of the shell material, their cross sectional area is distributed across the surface of the shell such that the new effective thickness (t_{eff}) can be determined by the following expression

$$t_{eff} = t_{shell} + \frac{\sum_{i=1}^{n} A_i}{2\pi a} \tag{2.57}$$

where A_i is the cross sectional area of the i^{th} stiffener, n is the total number of stiffeners, a is the shell radius, and t_{shell} is the shell thickness. If the shell and stiffener materials have different properties, the force distribution over the effective cross section must be made consistent with the force distribution prior to the "smearing" process by using the following relationship

$$P_{eff} = P_{shell} + P_{stiffeners} \tag{2.58}$$

By substituting the appropriate relationships and assuming that P_{eff} will be calculated using the shell properties, Equation (2.58) can be written as

$$2\pi a t_{eff} E_{shell} \varepsilon = 2\pi a t_{shell} E_{shell} \varepsilon + \sum_{i=1}^{n} A_i E_i \varepsilon$$

which can be solved to determine the effective shell thickness

$$t_{eff} = t_{shell} + \frac{1}{2\pi a E_1} \sum_{i=1}^{n} A_i E_i \tag{2.59}$$

When $E_1 = E_2 = ... = E_n$ in Equation (2.59), Equation (2.57) is recovered.

Chapter 3

Modeling and Analysis of ASDS Composite Shell Structure

With the analysis tools developed, focus now shifts to the modeling and analysis phase of the project. First, a model will be developed for the actual ASDS nose fairing structure and forward hemi-head of the pressure hull using simple, rotationally symmetric, geometric shapes for the shell. Stiffeners and cutout sections will be incorporated using the techniques discussed in Section (2). Next, the analysis tools developed in Section (2) will be applied to determine the crushing force to axial crush distance relationship and energy absorption capability of the structure. Finally, a maximum impact speed will be calculated by equating the energy absorbed in the collision to the kinetic energy possessed by the vehicle just prior to the impact.

3.1 ASDS Modeling

3.1.1 Actual Structure

The forward portion of the ASDS consists of a hemispherical pressure hull and a composite fairing structure. The hemispherical pressure hull section is constructed of HY-80 steel and is welded to the cylindrical portion of the hull to form a water tight boundary. The ASDS nose fairing (see Figure (3-1)) is a composite structure attached to the forward end of the pressure hull by eight titanium clevises. The structure has an overall length of 2.94 m and a

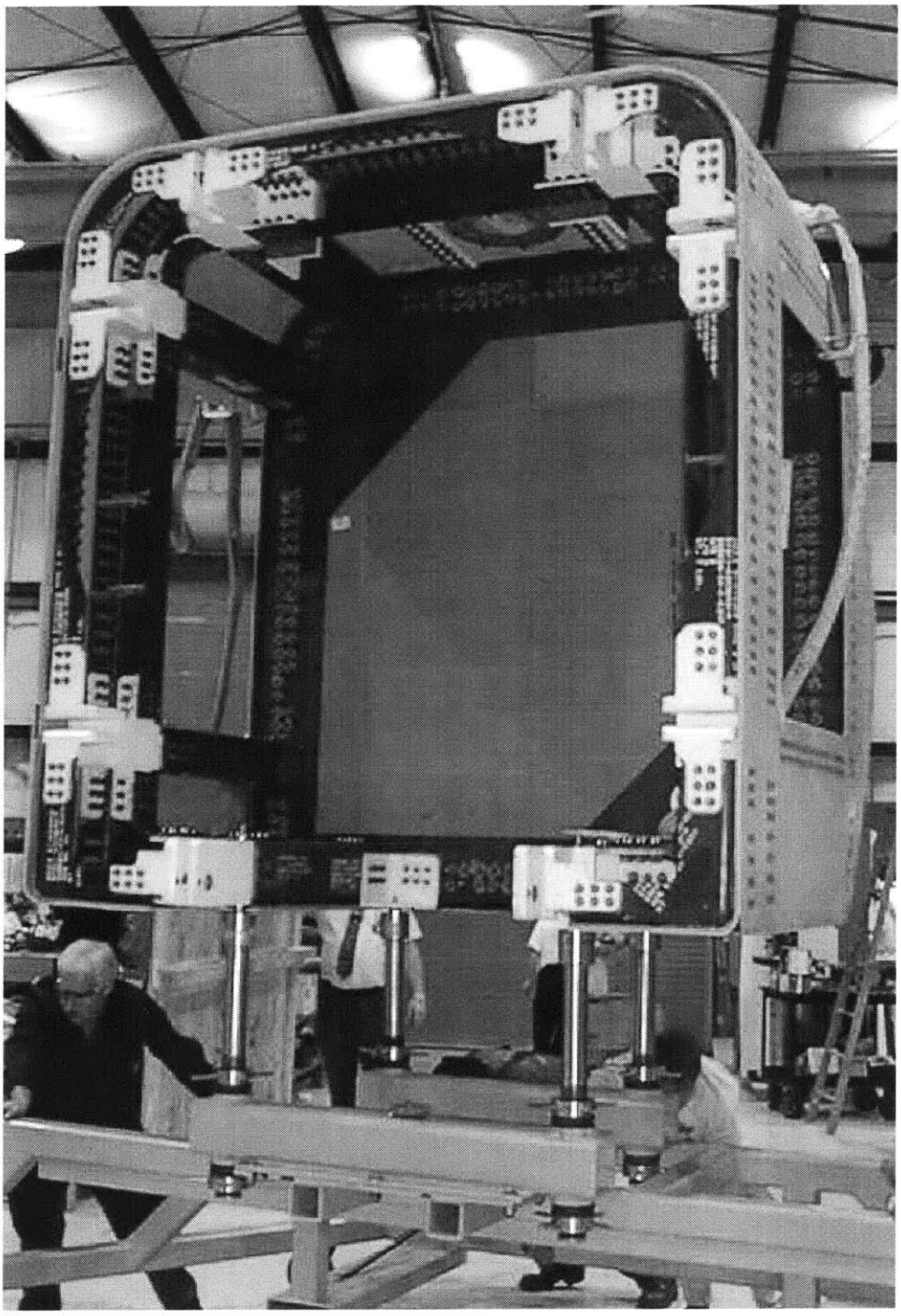

Figure 3-1: The Actual ASDS Nose Fairing Structure Showing Internal Components (Viewed from Aft Looking Forward).

Property	A	B	C	D	E
E_1 (x 10^6 psi)	3	11.6	4.7	.0013	16.4
E_2 (x 10^6 psi)	2.7	10.6	4.7	.0013	16.4
E_3 (x 10^6 psi)	.55	.37	.45	-	-
$\nu_{1,2}$	.15	.124	.15	.499	.31
Fiber Content	.5	.5	.5	-	-
Tensile Strength					
Axial (X) (ksi)	39.1	75	56	-	125
Transverse(Y) (ksi)	39.1	75	56	-	125
Compressive Strength					
Axial (X') (ksi)	33.8	68	14	-	125
Transverse (Y') (ksi)	33.8	68	14	-	125
Shear Strength (S) (ksi)	9.41	7.5	4.5	-	77
A-E-Glass (1583)/Epoxy (7780) woven cloth B-Carbon woven cloth (6K 5HS satin weave IM7) C-Kevlar (K285)/ epoxy (7714) woven cloth D-Rubber core material E-Titanium clevise material (Ti 6Al-4V)					

Table 3.1: Properties of Materials Used in ASDS Nose Fairng.

pseudo-rectangular cross section with maximum dimensions of 2.21 m high and 2.06 m wide. The structure itself consists of an outer shell constructed from E-Glass (1583) /Epoxy (7780) preimpregnated (prepreg) woven cloth in a single mold process. Internally, the shell is stiffened by a network of longitudinal and transverse woven carbon cloth (6K 5HS Satin Weave IM7) beams which are bolted to the shell and interconnected by titanium clevis fittings. Attached to the front end of the shell is a sonar dome comprised of a BFGoodrich Rho-Cor material system. This system consists of Kevlar (K285)/Epoxy (7714) prepreg woven cloth with a rubber core material. The properties for the various material systems described are contained in Table (3.1). Cutouts have been made in shell and the sonar dome to accommodate such equipment as thrusters, the forward anchor, lights and video cameras.

3.1.2 Simplified Model

The actual structural design of the ASDS had to be simplified to rotationally symmetric shapes before the analysis tools developed in Section (2) could be applied. A representation of the model developed is shown in Figure (3-2). For the forward pressure hull, no modeling idealizations needed to be made since the structure was already rotationally symmetric and

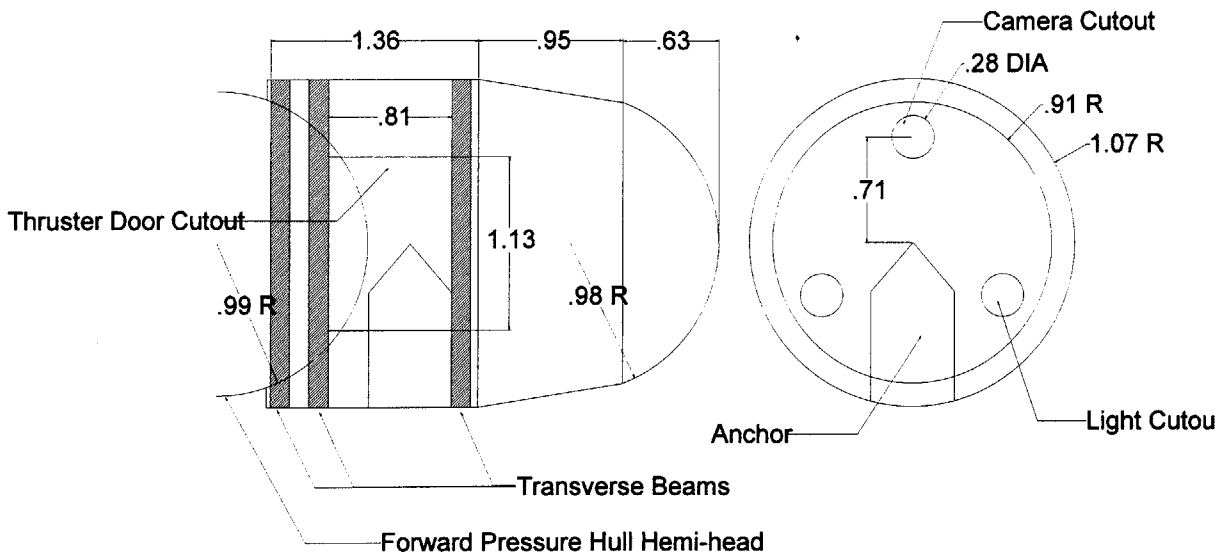

Figure 3-2: Model of ASDS Forward Section (Dimensions in meters).

hemispherical in shape. The pressure hull has a .99 m radius and an undisclosed thickness. The actual thickness of the structure is held as confidential by the U.S. Navy so as not to reveal the operational diving depth of the vessel. For this analysis, a notional thickness of 19 mm will be used. The sonar dome was modeled as a spherical dome section using the axial depth of the actual sonar dome and a base radius equal to the average of the height and width of the actual sonar dome. The thickness and lay-up construction was taken to be that of the actual structure. Three cutout sections simulating the locations of the camera and lights were located on the model 120° apart at the same radial distance. The actual and model sonar dome dimensions are summarized in Table (3.2). The shell structure was modeled using a combination of a frustum for the forward portion of the shell that transitions into the sonar dome and a stiffened cylinder for the after section. The radius of the cylindrical section was taken to be the average of the maximum height and width of the actual structure. The frustum was used as a transition section between the sonar dome and the cylindrical section and uses the corresponding radius at each end to fix its dimensions. For the frustum section, the shell thickness was taken to be that of the actual material. The thickness of the cylindrical section was taken to be an effective thickness calculated using Equation (2.59) to account for the added structural stiffness of the longitudinal carbon beams. The transverse beams were not utilized

Actual	Parameter	Model
.64	**Axial Depth (m)**	.635
1.91	**Height (m)**	-
1.75	**Width (m)**	-
1.83	**Average (m)**	-
-	**Radius (m)**	.91
9.6	**Thickness (mm)**	9.6
	Camera Cutout	
.28	Diameter (m)	.28
0°	Orientation	0°
.71	Radial Distance (m)	.71
	Light Cutout 1	
.28	Diameter (m)	.28
-147°	Orientation	-120°
.72	Radial Distance	.71
	Light Cutout 2	
.28	Diameter (m)	.28
148°	Orientation	120°
.69	Radial Distance	.71

Table 3.2: Comparison of Actual and Modeled Sonar Dome Dimensions.

in the effective thickness calculation because their energy absorption in an orthogonal impact is would be minimal. Instead, these beams were used to define nodal points for buckling waves. Table (3.3) summarizes the actual and modeled dimensions of the shell section. Two cutout sections 1.13 m high by .81 m wide were included in the cylindrical section to account for the openings created by the forward thruster doors. (It is assumed that during a collision imminent situation, the thruster doors would be open and the thrusters in use.) Additionally, the titanium clevises (used to attach the internal beams together and to the pressure hull) and the anchor were treated as rigid objects.

3.2 Analysis

3.2.1 Impact sequence

As stated previously in Section (1), this analysis will investigate an head-on impact with a flat, rigid wall. Structural deformation will initiate at the bow as the sonar dome is impacted first. The deformation will progress .635 m through the sonar dome, .95 m through the frustum

Actual	Parameter	Model
Cylindrical Section		
1.36	Length (m)	1.36
2.21	Height (m)	
2.06	Width (m)	
2.14	Average	
-	Radius (m)	1.07
12.8	Thickness (mm)	35
Frustral Section		
.95	Length (m)	.95
-	Fwd Radius (m) (Sonar Dome Radius)	.91
-	Aft Radius (m) (Cylinder Section Radius)	1.07
10.1	Thickness (mm)	10.1

Table 3.3: Comparison of Actual and Modeled Nose Shell Section Parameters.

section of the nose shell, and .18 m into the cylindrical section before the anchor makes contact with the wall. At this point, some of the crushing load is transferred to the pressure hull via the anchor and simultaneous deformation of the cylindrical section and the pressure hull results for another .66 m. The deformation process ends when the after most transverse beams and titanium cleaves make contact with the wall.

3.2.2 Sonar Dome

Equation (2.31) will be used to determine the crushing force required to deform the structure throughout the progressive crushing of the sonar dome. Implicit in the use of this equation is that the structure can be modeled using rigid-plastic techniques. While it is understood that in general composite structures behave in a more brittle than ductile way, kevlar composites have been shown to buckle under axial loading in modes similar to those seen in metal structures [19]. This behavior coupled with the fact that the structure has a rubber core was used to justify the use of this analysis technique on this component.

The sonar dome is composed of 22 plys of kevlar cloth laid-up symmetrically sandwiching a 3.81 mm rubber core ($[90, 0]_5, 0,$ rubber core$, 0, [90, 0]_5$) for a total laminate thickness of 9.4 mm. The compressive and tensile flow stresses were calculated using a combination of laminated plate theory and a progressive failure analysis [21]. The detailed calculations are shown in

Appendix (A) and, for brevity sake, only an summary of the process and the result will be included here. First, the material properties of the ply (listed in Table (3.1)) were used to determine the undamaged 0° ply stiffness characteristics. These properties were then modified using techniques of [21] to determine the reduced stiffness of the 0° ply with matrix and fiber damage. The stiffnesses were calculated using the following relationship:

$$Q = \begin{bmatrix} \frac{E_1}{1-\nu_1\nu_2} & \frac{\nu_2 E_1}{1-\nu_1\nu_2} & 0 \\ \frac{\nu_1 E_2}{1-\nu_1\nu_2} & \frac{E_2}{1-\nu_1\nu_2} & 0 \\ 0 & 0 & E_3 \end{bmatrix} \tag{3.1}$$

The stiffnesses were then rotated to a 90° ply orientation. The stiffness of the rubber core material was also determined from Equation (3.1) by setting $E_1 = E_2$, $\nu_1 = \nu_2$, and $E_3 = \frac{2E_1}{1+\nu_1}$. The overall laminate stiffness was then calculated using the following:

$$A^* = \frac{1}{h_{\text{laminate}}}\left(N_{0°}h_{0°}Q_{0°} + N_{90°}h_{90°}Q_{90°} + N_{rubber}h_{rubber}Q_{rubber}\right) \text{ where}$$

N_x = Total number of "x" plys

h = Thickness of individual ply

Q = Stiffness of individual ply

Next, stress space strength parameters were calculated from the material test data provided in Table (3.1) using Equations (3.2) and (3.3) and the generalized von Mises value of $-\frac{1}{2}$ for $F^*_{1,2}$.

$$F_{i,j} = \begin{bmatrix} \frac{1}{XX'} & \frac{F^*_{1,2}}{\sqrt{XX'YY'}} & 0 \\ \frac{F^*_{1,2}}{\sqrt{XX'YY'}} & \frac{1}{YY'} & 0 \\ 0 & 0 & \frac{1}{S^2} \end{bmatrix} \tag{3.2}$$

$$F_i = \begin{bmatrix} \frac{1}{X} - \frac{1}{X'} \\ \frac{1}{Y} - \frac{1}{Y'} \end{bmatrix} \tag{3.3}$$

The strain space strength parameters and failure envelopes could then be determined through

the relationships in Equations (3.4)-(3.6).

$$G_{k,l} = F_{i,j}Q_{i,k}Q_{j,l} \tag{3.4}$$

$$G_j = F_iQ_{i,j} \tag{3.5}$$

$$G_{i,j}\varepsilon_i\varepsilon_j + G_j\varepsilon_i = 1 \tag{3.6}$$

A progressive failure model [22] was then used to approximate the stress strain relationship of the material under pure compressive and tensile loadings (oriented in the 0° ply direction). The progressive failure model allows for a rough prediction of post first ply failure behavior of the laminate. The model works by calculating the strain of first ply failure for the assumed load condition and then determines the stress using the undamaged laminate stiffness ($\{\sigma\} = A^*\{\varepsilon\}$). After first ply failure, the limiting ply is failed to a degraded state, a new laminate stiffness is calculated, and the next ply failure strain and stress is determined. A ply can be damaged at most twice – once by degraded matrix and the final by fiber failure. In certain cases, based on the properties of the plys used, the degraded ply failure strains can be less than that of the undamaged ply. For this condition, the ply failure occurs after its undamaged failure envelope is surpassed. The tensile and compressive stress versus. strain estimates are shown in Figure (3-3).

The compressive (σ_{co}) and tensile (σ_{to}) flow stresses were then determined to be 8.41 MPa and 53.35 MPa respectively using Equation (3.7).

$$\sigma_o = \frac{1}{\varepsilon_f}\int_0^{\varepsilon_f} \sigma d\varepsilon \tag{3.7}$$

Now, the crushing force ($P_{\text{sonar dome}}$) and cumulative energy absorption ($E_{\text{sonar dome}}$) of the sonar dome can be determined from Equation (2.31) and (3.8) with the cutout correction factor (Equation (2.55)) applied to the crushing force over the appropriate regions of the shell.

$$E = \int_0^{\delta} P(\delta)d\delta \tag{3.8}$$

The resulting crushing force and cumulative energy absorption profiles for an axial crush distance (δ) are shown in Figure (3-4). Here it is seen that the total energy absorbed for a crush

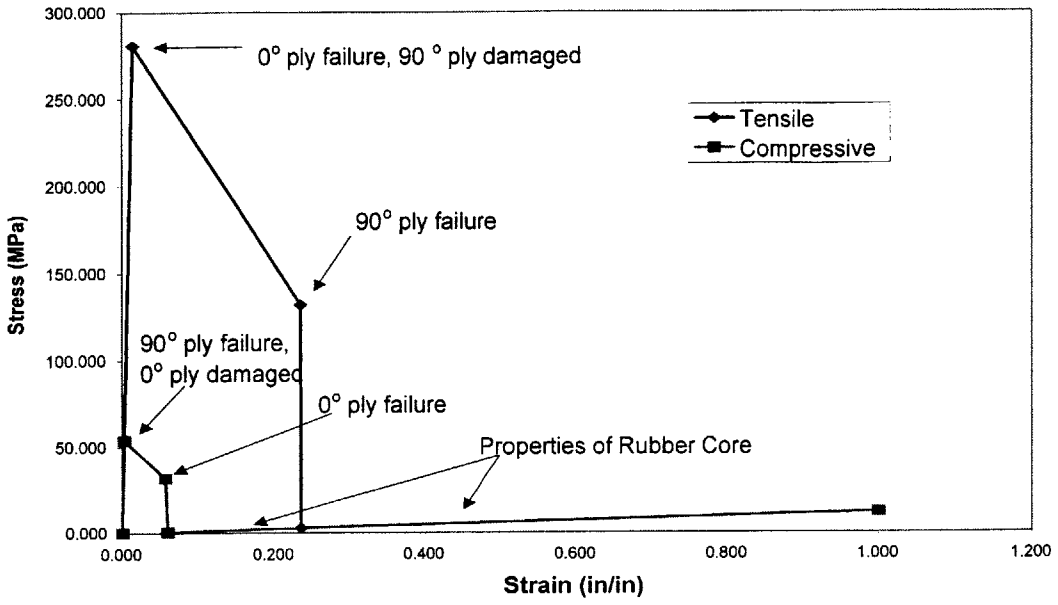

Figure 3-3: Compressive and Tensile Stress vs Strain Estimates Calculated using the Progressive Failure Method.

distance of .635 m is .058 MJ. This figure also clearly shows the effect of the cutouts on the crushing force curve.

3.2.3 Frustum Section of Nose Shell

The frustum section is composed of a 22 ply, E-Glass (1583)/Epoxy (7780), woven cloth composite system laid up symmetrically $([90, 45, 0, -45]_2, 90, 45, 0, 0, 45, 90, [90, 45, 0, -45]_2)$ for a laminate thickness of 10.1 mm. The analysis of the frustum section was done by approximating the frustum as a cylinder with a radius equal to the average of the forward and after radii of the frustum and using the analysis discussed in Section (2.2.3). The details of these calculations are contained in Appendix (B). In order to use this technique, the appropriate circumferential (E_θ) and flexural (E_f) Young's moduli needed to be determined. The method described in Section (3.2.2) was initially used to determine the strain space failure envelopes for each of the ply orientations used in the laminate. Subsequently, the failure envelopes were used to develop an E_2 versus. tensile, transverse strain relationship using the progressive failure technique described previously. E_2 was chosen as the circumferential strain Young's moduli because as the buckling

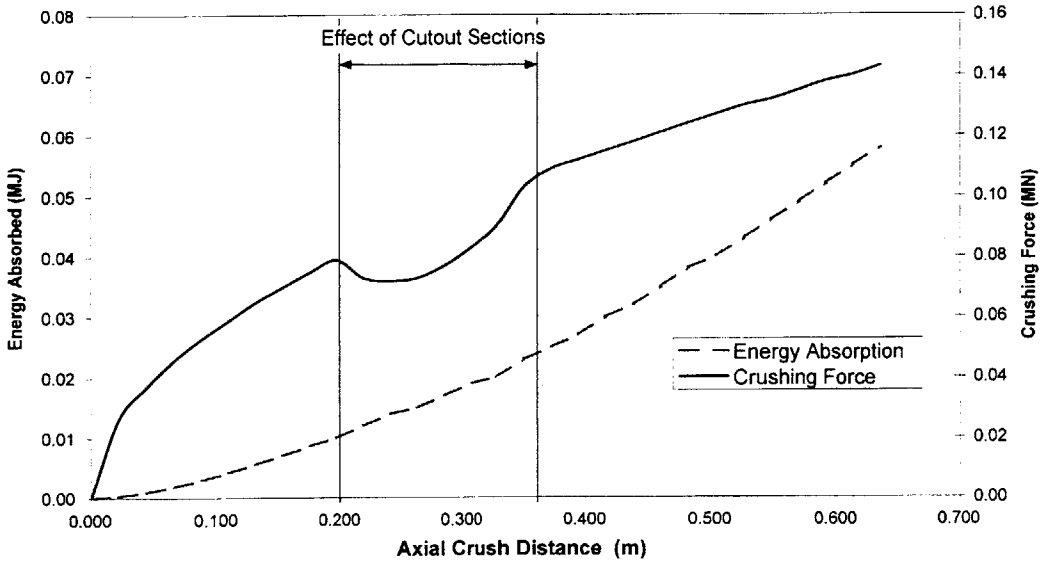

Figure 3-4: Crushing Force and Cumulative Energy Absorption as a Function of Axial Displacement for the Sonar Dome.

lobes are formed and bulge outward and inward, the laminate will be strained in the 2-direction with respect to the laminate orientation. In reality, both compressive (bulging inward) and tensile (bulging outward) strains will be experienced and thus, different E_2 versus. strain relationships will result. However, because the compressive and tensile strengths of the plys are approximately equal (Table (3.1)), the difference is small and only the tensile E_2 versus. strain relationships will be used to simplify the analysis. Figure (3-5) shows the E_2 versus. strain relationship that was determined as well as the order of ply failure.

The actual circumferential strain was then calculated as a function of $x^{'}$ and δ using Equations (2.36), (2.48), and (2.44). This relationship is shown in Equation (3.9).

$$\varepsilon_\theta = \frac{x^{'}}{aH} w_o = \frac{x^{'}\delta}{a\sqrt{at}} \sqrt{\frac{\sqrt{at}}{\delta} - \frac{1}{4}} \tag{3.9}$$

Since the circumferential strain varies both with $x^{'}$ and δ and E_2 varies with δ, E_θ will vary with both $x^{'}$ and δ. E_θ was then calculated for discrete values of $x^{'}$ and δ in preparation for a numerical integration scheme to be used in Equation (2.42).

To determine E_f, a relationship between flexural strain (ε_f) and the axial crushing distance

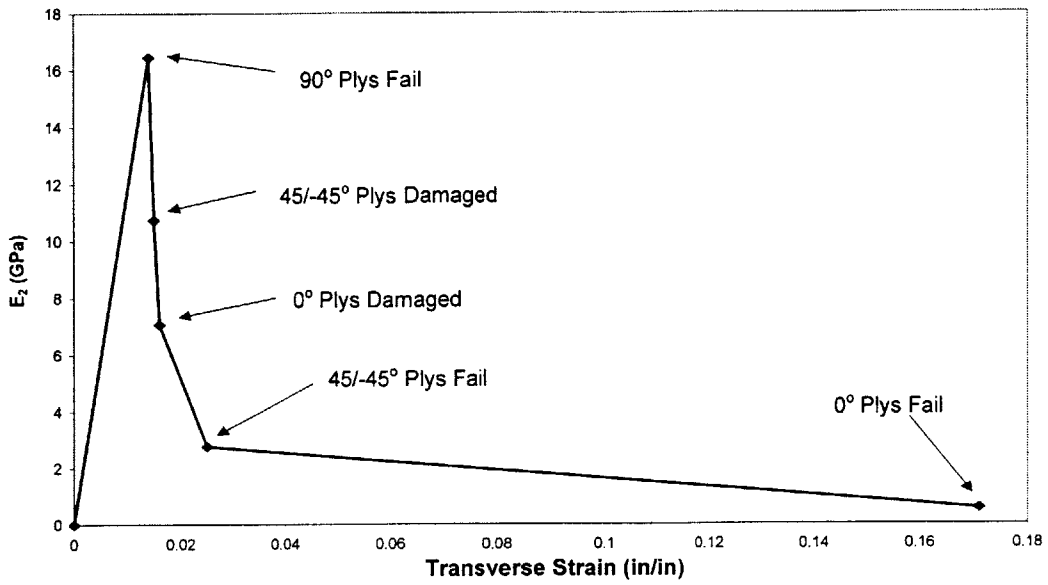

Figure 3-5: Transverse Young's Modulus Variations with Pure Tensile, Transverse Strain for Frustum Section.

(δ) was first developed using Equations (2.38), (2.39), and (2.48). (see Equation (3.10))

$$\varepsilon_f = \frac{2z}{at}\sqrt{\delta\sqrt{at} - \frac{\delta^2}{4}} \tag{3.10}$$

Equation (3.10) was then used to determine a ε_f versus. δ curve for each ply over the entire crushing distance for one buckling lobe ($2\sqrt{at}$). For each, the strain was determined at the midplane of the individual plys. Using these plots and the strain failure envelopes, the displacement at which each ply failed in tension could be determined. Figure (3-6) shows how this process was done for the 0° oriented plys in the laminate.

Flexural stiffness (D*), E_f, and laminate thickness (t) were then recalculated after each ply failure using Equations (3.11)-(3.13).

$$[D^*] = \frac{12}{t^3}\int_{-\frac{t}{2}}^{\frac{t}{2}} [Q]z^2 dz \tag{3.11}$$

$$E_f = \left\{\left([D^*]^{-1}\right)_{1,1}\right\}^{-1} \tag{3.12}$$

$$t = nh \text{ where} \tag{3.13}$$

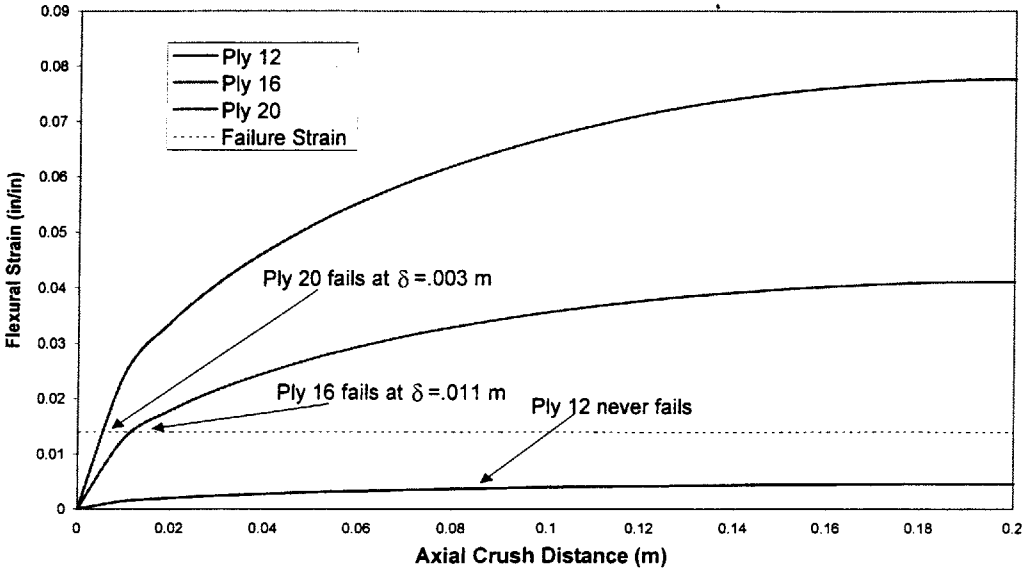

Figure 3-6: Flexural Strain to Axial Crush Distance Relationships for the 0 Degree Oriented Plys in the Frustum Laminate.

$$n = \text{number of intact plys}$$

$$h = \text{ply thickness}$$

Figure (3-7) shows the variations in E_f and t as δ increases. Notice also that as more plys fail, E_f becomes more erratic and diverges further and further from the in-plane modulus. This is expected since the laminate starts out homogenized and gradually de-homogenizes as each successive ply fails.

The crushing load and cumulative energy absorption can now be determined as a function of axial crushing distance (Figure (3-8)) using Equations (2.42) and (3.8). Since neither E_θ nor E_f was constant or equal during the deformation process, the simplified form of Equation (2.42) could not be used here. Figure (3-8) shows that five buckling lobes form as the frustum is crushed and that a total energy absorption of .105 MJ is realized.

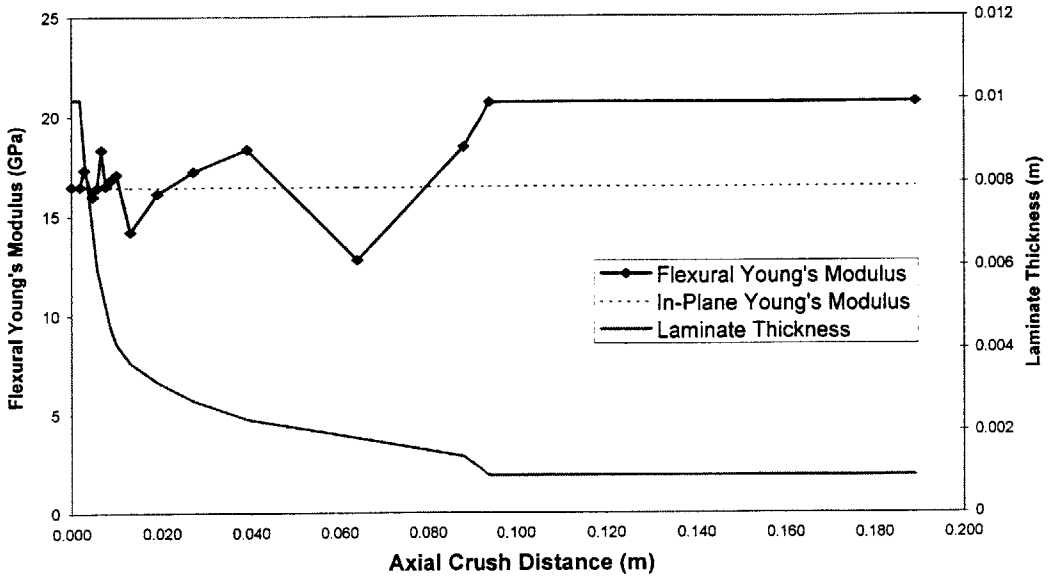

Figure 3-7: Flexural Young's Modulus and Laminate Thickness Variation with Axial Crush Distance of the Frustum Section.

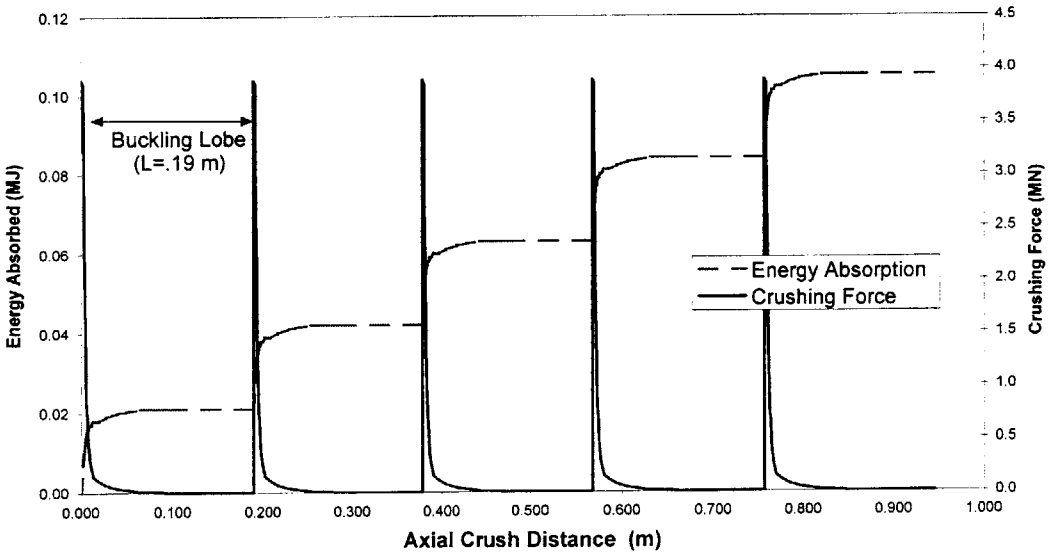

Figure 3-8: Crushing Load and Cumulative Energy Absorption Characteristics of the Frustum Section.

3.2.4 Cylindrical Section of Nose Shell

This outer shell of the stiffened, cylindrical section is composed a 28 ply, E-Glass (1583)/Epoxy (7780), woven cloth composite system laid up symmetrically ($[90, 45, 0, -45]_2, 90, 45, 0, 0, 45, 90, [90, 45, 0, -45]_2$) for a laminate thickness of 12.8 mm. Additional support is provided by an internal, frame structure constructed using carbon, woven cloth (6K 5HS satin weave IM7), composite, C-channel beams. The beams are 32 plys thick for a laminate thickness of 11 mm and laid-up symmetrically in the following configuration: $[90,45,0,-45]_4[90,45,0,-45]_4$. The shell analysis was accomplished by the same process as described in Section (3.2.3) and is shown in detail in Appendix (C). However, the effect of the stiffeners still needed to be taken into account. This was done by "smearing" the stiffeners into the shell and then calculating an effective thickness (t_{eff}) using Equation (2.57). The detailed stiffener and t_{eff} calculations are included in Appendices (C) and (D) with the t_{eff} determined to be 35 mm. An effective buckling lobe length was then determined based on t_{eff}. The crushing force and cumulative energy absorption could then be determined using Equations (2.42) and (3.8). Figure (3-9) shows the force and energy profiles at various displacements and also, that the cylinder was only allowed to crush .84 m in two buckling lobes while Table (3.3) indicates that the section is 1.36 m long and should buckle in three lobes. This reduction in length was due to the effects of the transverse beam structures. The forward beam and titanium fittings served to force a nodal point at the beginning of the thruster door section as seen in Figure (3-2). The after beams and rigid titanium clevises at the aft portion of the thruster door create another node point and serve to terminate the deformation process. So, only the .84 m shell and stiffener portion between the forward and after beams will deform during the impact. .49 MJ of energy are absorbed during this deformation.

3.2.5 Analysis of Forward Hemi-head of Pressure Hull

The forward pressure hull hemi-head is a metallic structure constructed from HY-80. As previously stated, the thickness used in the analysis will be assumed to be 19 mm due to the confidentiality of the actual thickness. The deformation starts as the forward anchor contacts the collision boundary and is pushed back into the pressure hull. The deformation is assumed to be of the form described in Section (2.1) and, as such, Equation (2.31) will be used to de-

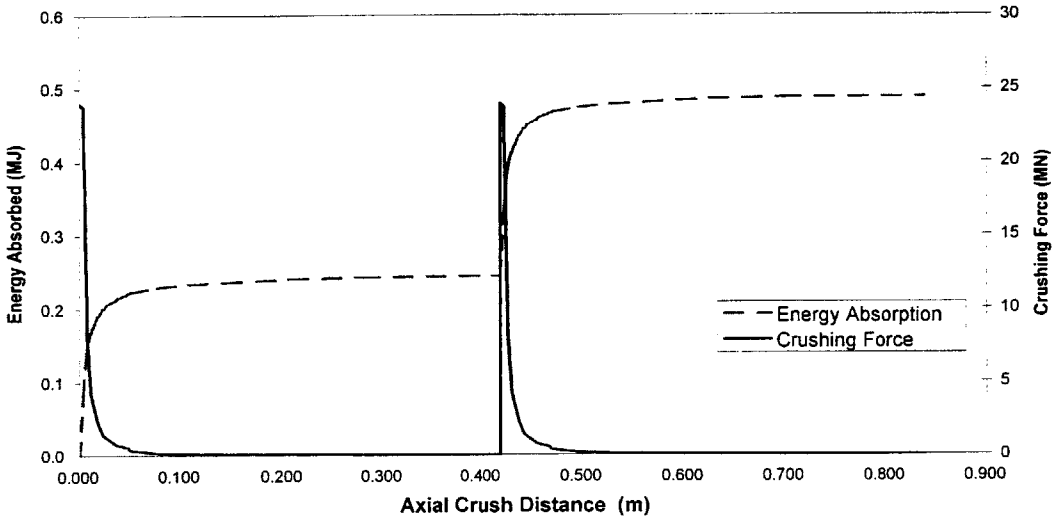

Figure 3-9: Crushing Force and Cumulative Energy Absorption of the Cylinder Section of the Nose Shell.

termine the crushing force. The flow stress was calculated from a partial stress versus. strain curve using Equation (3.7). The detailed calculations and the stress versus. strain profile used are included in Appendix (E), and the crushing force and cumulative energy absorption versus. displacement results are shown in Figure (3-10). Throughout this analysis, it is assumed that the forward hemi-head remains water tight. Further analysis must be performed to determine the point at which the pressure hull fails. By allowing the pressure hull to deform to the full axial extent allowed for the nose shell, 7.566 MJ of energy will be absorbed.

3.2.6 Kinetic Energy Calculations

After determining the energy absorption capability of each modeled nose fairing component, a determination of the kinetic energy possessed by the ASDS was needed for various speeds. The kinetic energy was determined using Equation (3.14)

$$KE_{ASDS} = \frac{1}{2}(m_{vehicle} + m_{added})v^2 \tag{3.14}$$

where $m_{vehicle}$ is the submerged mass, m_{added} is the added mass, and v is the speed of the vehicle.

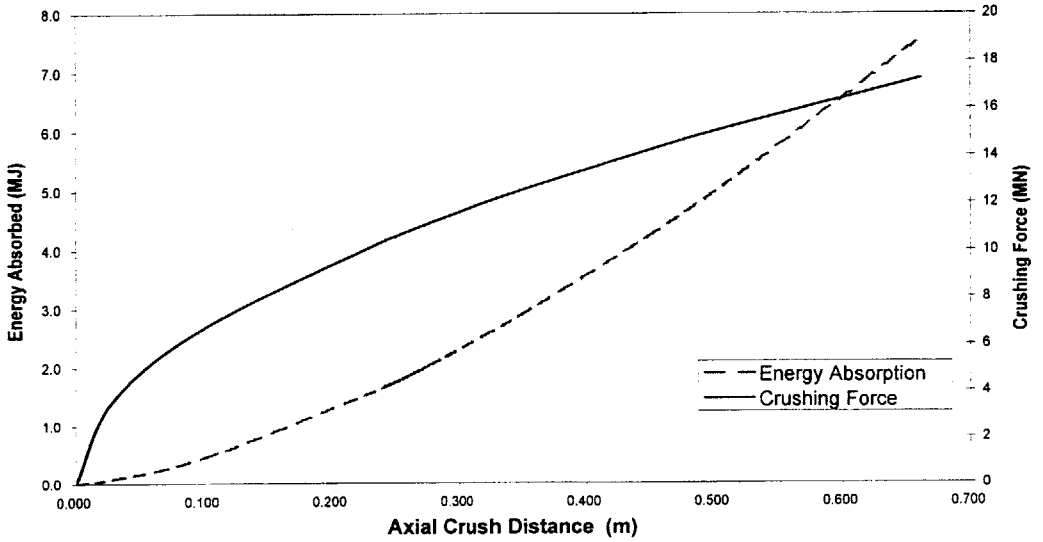

Figure 3-10: Crushing Force and Cumulative Energy Absorption for the Forward Pressure Hull Hemi-head.

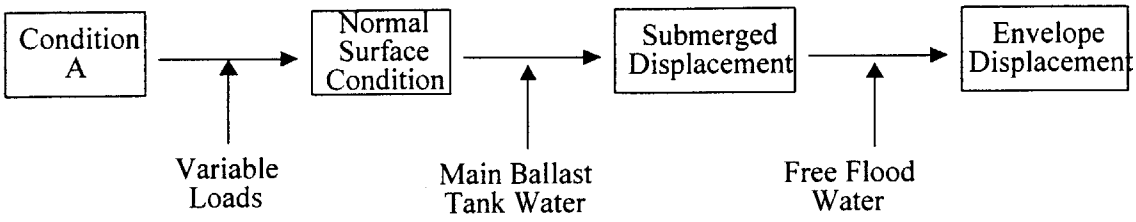

Figure 3-11: Description of Standard Submarine Weight Terms

Parameter	Weight (metric tons)
NSC	56.2
Main Ballast Tanks	4.8
Free Flood	27
Δ_{env}	88

Table 3.4: ASDS Weights

The submerged mass of the vehicle was calculated using the ASDS weight report [16]. Weight reports for submarines are standardized and broken down into categories of weights based on the operating condition of the submarine. Figure (3-11) shows a brief summary of the standard terminology used in submarine weight analysis and how each relates to the other. Condition A is the dry vehicle weight. When the variable load (variable ballast tank water, personnel, etc.) is added, the new weight created is the normal surfaced condition (NSC). The main ballast tanks are filled with water to submerge the vehicle; so, the weight of this water added to the NSC becomes the submerged displacement (Δ_{sub}). Finally, during submergence, non-water tight free flood areas (i.e.-between the fairings and the pressure hull) fill with water. This water, while in pressure equilibrium with the surrounding water, moves with the submarine as it transits, and when its weight is added to Δ_{sub} the resultant is the envelope displacement (Δ_{env}). For this case, it is this Δ_{env} that is required for the analysis. Table (3.4) shows the various weights used to determine the envelope displacement.

Next, the added mass was determined. Since this vehicle is relatively slender, it is expected that the added mass in surge will not be large. However, two approximations were made using a sphere and an ellipsoid. The size of the sphere was set such that the frontal area was equal to that of the ASDS (Figure (3-12)). Once the sphere dimensions are known, the added mass can be calculated using Equation (3.15)

$$\begin{aligned} m_{\text{added sphere}} &= \frac{1}{2}\rho_{water}V_{sphere} = \frac{2}{3}\pi\rho_{water}R^3_{sphere} = 4.5 \text{ metric tons} \\ (\text{where } \rho_{water} &= 1.025\frac{\text{metric tons}}{\text{m}^3}) \end{aligned} \tag{3.15}$$

The added mass of the vehicle was also approximated using an ellipsoid with the frontal area

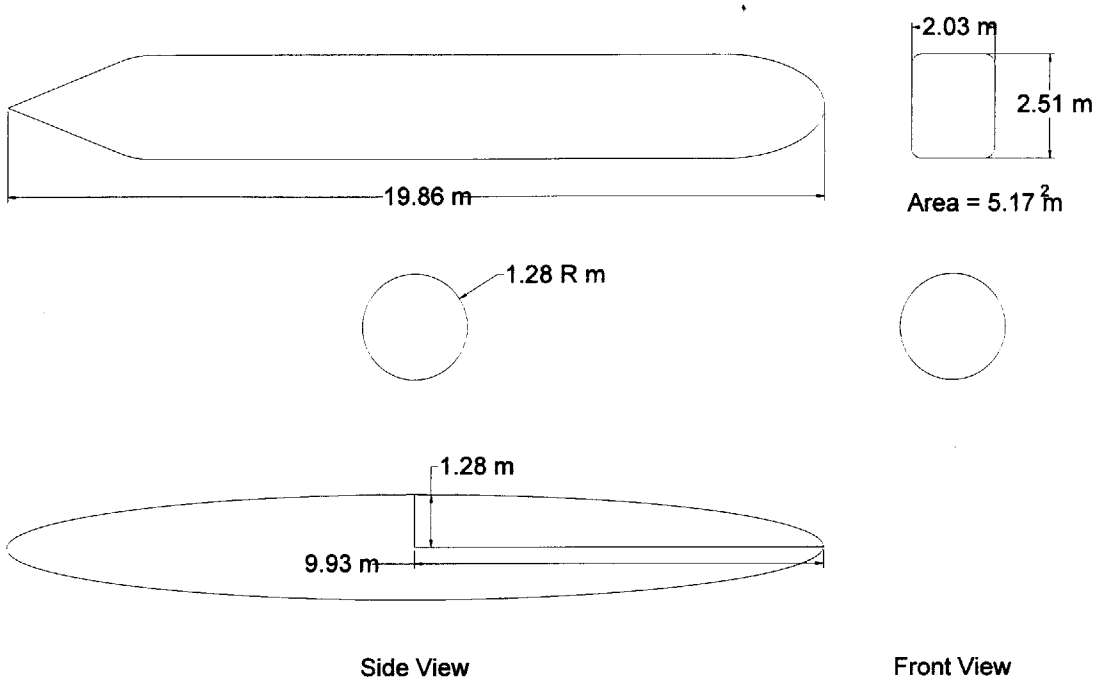

Figure 3-12: Dimensions Used During Added Mass Calculations

equal to that of the ASDS (as in the case of the sphere) and a major axis length equal to that of the overall vehicle (Figure (3-12)). The added mass of the ellipsoid can then be determined using Equation (3.16) and the graphs from [17] for the added mass coefficient (C_a)

$$m_{\text{added ellipsoid}} = C_a \frac{4}{3}\pi\rho_{water}ab^2 = 2.1 \text{ metric tons (where } C_a = .13) \tag{3.16}$$

Since the actual vehicle shape is not as bluff as a sphere, yet not as fine as an ellipse, the added mass of the vehicle lies somewhere between the two calculated values. So, the average value was used as the vehicle added mass. Now, the kinetic energy possessed by the ASDS at various speeds can be determined using Equation (3.14) as shown in Figure (3-13).

3.3 Results

With the energy absorption of each section determined, the overall energy absorption of the nose structure can be determined by summing the energy absorbed by each section throughout the

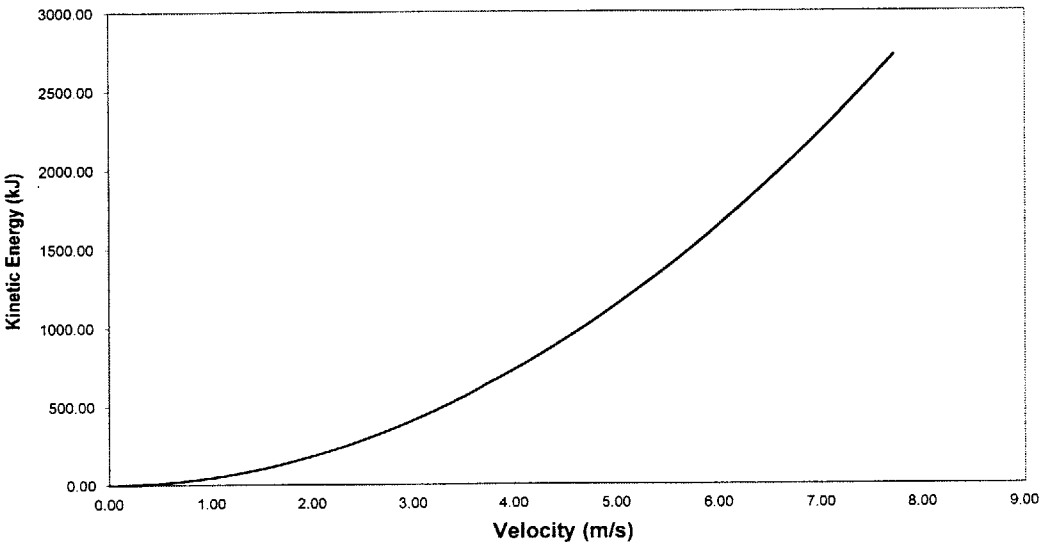

Figure 3-13: Vehicle Kinetic Energy for Various Speeds.

impact sequence. Figures (3-14) and (3-15) show the integrated crushing force and cumulative energy absorption profiles for the entire deformation process. Two curves are shown in Figure (3-15) depicting the energy absorption of the nose structure with and without the effects of the pressure hull included. Additionally, the kinetic energy curve shown in Figure (3-15) is overlaid on this plot. Using the curves in Figure (3-15) initial speed versus. crush distance assessments can be made. Without the pressure hull included, the nose structure can absorb .67 MJ of energy which would allow the complete absorption of all kinetic energy possessed by the vehicle with an initial speed of 7.5 knots. If the effects of the pressure hull are included, a total of 8.235 MJ of energy can be absorbed. This equate to an initial vehicle velocity of 26.4 knots. As previously stated, the point at which the pressure hull will fail during its deformation was not determined; so, a the safe impact speed for the vehicle cannot yet be determined. However, when this point is determined, Figure (3-15) will provide this safe speed estimate.

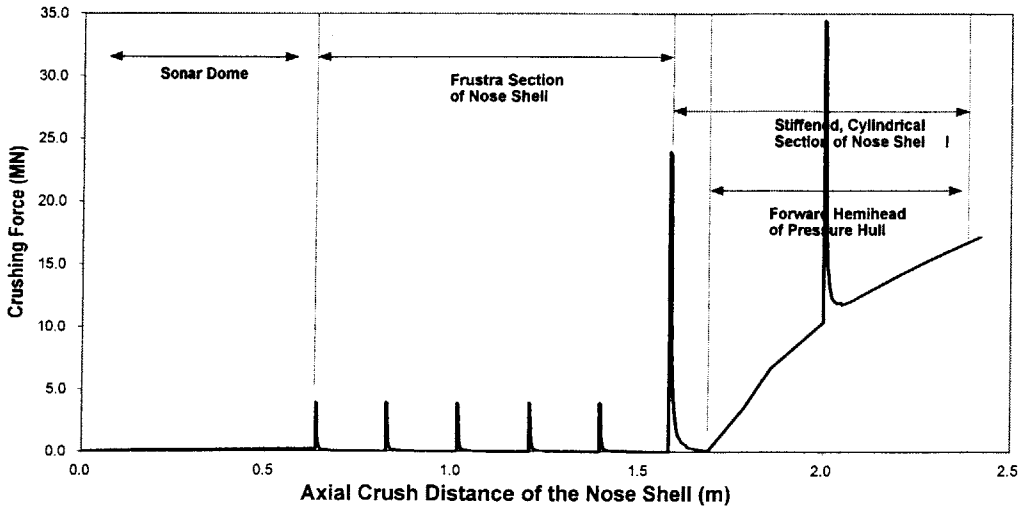

Figure 3-14: Crushing Force Profile for the Entire Deformation Process.

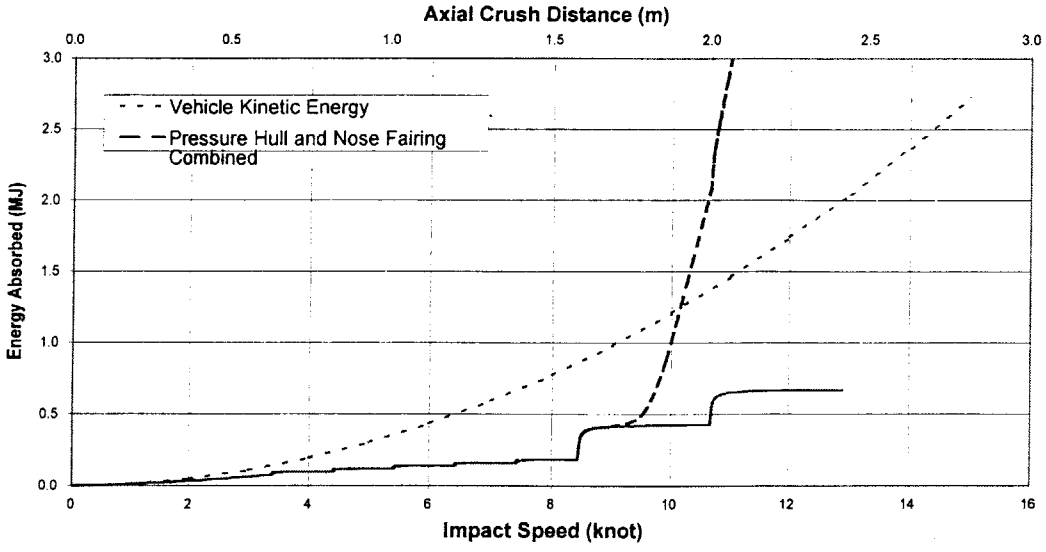

Figure 3-15: Total Cumulative Energy Absorption and Vehicle Kinetic Energy.

Chapter 4

Summary and Conclusions

Throughout the course of this analysis, several new deformation models have been developed. The force required to deform a hemispherical shell loaded axially with a rigid plate by axisymmetric dishing was related to shell thickness, material flow stress (compressive and tensile), and axial deflection using a rigid-plastic analysis technique. Additionally, a deformation model for a cylindrical shell composed of elastic material, crushed axially by a rigid flat plate, was proposed. This model assumed a concertina type deformation mode and used shell thickness, cylinder radius, material stiffness, and axial displacement to determine the force required to crush the shell. Further, methods were set forth to include the effects of cutout sections and internal stiffening members on the crushing force characteristics of the shells. The effect of the cutout section was taken to be a reduction of the intact shell crushing force by a ratio equal to the shell area remaining divided by the total area of the intact shell in the local vicinity of the cutout. The effect of internal stiffeners was incorporated by increasing the thickness of the shell material to a new effective thickness determined by making the load carried by the effective structure equal to the combined load on the stiffeners and shell.

These tools were used to determine the crushing force and energy absorption characteristics of the composite nose fairing structure and forward pressure hull of the U.S. Navy's Advanced Seal Delivery System in a head-on impact with a rigid wall. The complex structure of the ASDS was first simplified and modeled to permit the use of the tools described above. The shell structures were approximated as rotationally symmetric shells (i.e.- cylinders, frustum, hemispherical domes) with the internal shell stiffeners being incorporated into the model in

two ways. The energy absorption of the longitudinal elements was captured by increasing the effective thickness of the shell in the vicinity of the longitudinal beams, while the transverse stiffening elements served only to force nodal points in the shell buckling pattern since their energy absorption during a head-on collision is minimal. Further, major internal components, such as the titanium clevises (used to connect the internal beams) and the forward anchor, were treated as rigid, massless objects.

The structure was divided into a hemispherical sonar dome, a frustum and stiffened cylindrical nose shell, and a hemispherical forward pressure hull based on the shape, material composition, and thickness of the actual structure. Using laminated plate theory and a progressive failure model, stiffness versus crush distance and material thickness versus crush distance relationships were developed for each of the material systems used. These relationships were then used in conjunction with the rigid-plastic hemispherical and elastic cylindrical shell models to predict the force deflection and energy absorption of each component. The component-level energy absorptions were then summed to approximate these characteristics for the overall structure. Finally, the absorbed energy was equated to the vehicle's pre-impact kinetic energy in order to determine an initial speed just prior to the collision. The composite nose fairing structure was deemed capable of absorbing the impact energy associated with a vehicle speed of 7.5 knots. If the effects of the pressure hull were included, the structure could absorb the kinetic energy from a 26.4 knot impact.

4.1 Areas Additional for Study

This analysis has taken the first step in determining the energy absorption capability of the ASDS. However, considerable work remains to be done before a final assessment can be made of the vehicle's overall crashworthiness. The following is a list of topics for further study in this project:

- **Model validation and calibration**: The models developed herein have not been calibrated or confirmed via actual test data. Cylindrical and hemispherical composite sections of the appropriate length to radius and thickness to radius ratios need to be constructed for each composite material and crushed under quasi-static and dynamic conditions. The

results should be used to confirm, improve, and calibrate the methods developed in this thesis.

- **Rupture Point of Forward Pressure Hull**: The overall objective of the project is to determine a safe impact speed for the vehicle such that during an impact the pressure hull will not rupture and the crew will survive the collision. The rupture or collapse point of the forward pressure hull needs to be determined and may vary with depth of the vehicle.

- **Strength Analysis of Nose Fairing Mounting Plates:** The composite nose fairing is mounted to reinforced metal plates that are welded to the forward hemi-head of the pressure hull. An analysis needs to be done to determine whether these structures will be capable of withstanding the force of the impact or if they will bend or shear off completely.

- **Energy Absorption of Internal Components**: The energy absorption potential of the internal components (such as clevises, angle bulkheads, the anchor, the sonar equipment, etc.) have not been included in this analysis. The effects of each of these components can be determined individually and added to the curves developed in this report to get a more accurate approximation of the energy absorption of the vehicle.

- **Effect of Impact Angle on Energy Absorption**: This analysis looked at an "impact sequence" for a head-on impact angle. In reality, this situation is likely never to happen. A relationship should be developed for various impact angles using model testing or other means to relate the reduction in energy absorption that is realized by an off-axis impact to that of an orthogonal impact.

Bibliography

[1] D. Updike, "On the Large Deformation of a Rigid Plastic Spherical Shell Compressed by a Rigid Plate," Journal of Engineering for Industry, 1972, pp. 949-955.

[2] D. Updike and A. Kalnins, "Axisymmetric Behavior of an Elastic Spherical Shell Compressed Between Rigid Plates," Journal of Applied Mechanics, 1970, pp. 635-640.

[3] D. Updike and A. Kalnins, "Axisymmetric Postbuckling and Nonsymmetric Buckling of a Spherical Shell Compressed Between Rigid Plates," Journal of Applied Mechanics, 1972, pp. 172-178.

[4] T. Wierzbicki. and J. Oliveira, "Crushing Analysis of Rotationally Symmetric Plastic Shells," Journal of Strain Analysis, 1982, Vol. 17, No. 4, pp. 229-236.

[5] R. Kitching, R. Houlston, and W. Johnson, "A Theoretical and Experimental Study of Hemispherical Shell Subjected to Axial Loads Between Flat Plates," International Journal of Mechanical Science, 1975, Vol. 17, pp. 693-703.

[6] A. Kinkead, A. Jennings, J. Newel, and J.C. Lienster, "Spherical Shells in Inelastic Collision with a Rigid Wall – Tentative Analysis and Recent Quasi-static Testing," Journal of Strain Analysis, 1994, Vol. 29, pp. 17-41.

[7] N. Gupta, G. Easwara Prasad, and S. Gupta, "Axial Compression of Metallic Spherical Shells Between Rigid Plates," Thin Walled Structures, 1998, (accepted).

[8] N. Gupta, R. Velmurugan, and S. Gupta, "An Analysis of Axial Crushing of Composite Tubes," Journal of Composite Materials, 1997, Vol. 31, No 13, pp. 1262-1286.

[9] P. Thornton and P. Edwards, "Energy Absorption in Composite Tubes," Journal of Composite Materials, 1982, Vol. 16, pp. 521-545.

[10] G. Farley and R. Jones, "The Effects of Crushing Speed on the Energy-Absorption Capability of Composite Tubes," Journal of Composite Materials, 1991, Vol 25, pp. 1314-1329.

[11] G. Farley and R. Jones, "Crushing Characteristic of Continuous Fiber-Reinforced Composite Tubes," Journal of Composite Materials, 1992, Vol. 26, pp. 37-50.

[12] G. Farley and R. Jones, "Analogy for the Effect of Materials and Geometrical Variables on Energy-Absorption Capability of Composite Tubes," Journal of Composite Materials, 1992, Vol. 26, pp. 78-89.

[13] G. Farley and R. Jones, "Prediction of Energy-Absorption Capability of Composite Tubes," Journal of Composite Materials, 1992, Vol. 26, pp. 388-404.

[14] D. Hull, "A Unified Aproach to Progressive Crushing of Fiber-Reinforced Composite Tubes," Composites Science and Technology, 1992, Vol. 40, pp. 377-421.

[15] T. Wierzbicki and E. Hanefi, "Axial Resistance and Energy Absorption of Externally Reinforced Metal Tubes," Composites, 1996, Vol. 27B, pp. 387-394.

[16] ASDS 4^{th} Quarter Weight Report, Northrop Grumman Oceanic Systems, 1998.

[17] J.N. Newman, *Marine Hydrodynamics*, Cambridge: The MIT Press, 1977.

[18] D.Brush and B. Almroth, *Buckling of Bars, Plates, and Shells*, New York: McGraw-Hill, Inc, 1975.

[19] Detailed Design History Notebook for Advanced SEAL Delivery System, Northrop Grumman Oceanic Systems, Vol. 2, 1998.

[20] ASDS Detailed Drawings, Northrop Grumman Oceanic Systems, 1998.

[21] S.W. Tsai, *Theory of Composites Design*, Dayton: Think Composites, 1992.

[22] S.W. Tsai and K. Liu, "A Progressive Quadratic Failure Criterion for a Laminate," Composites Science and Technology, 1998, Vol. 58, pp. 1023-1032.

Appendix A

Sonar Dome Analysis

Ply Stiffness and Layup Inputs:

1. Material System: Kevlar (K285)/ epoxy (7714) woven cloth

2. Layup Configuration: $[90,0]_5,0,0,[90,0]_5$

$N_0 := 12$ $N_{n45} := 0$

$N_{90} := 10$ $N_{p45} := 0$

3. Total Number of Plys $Total\_plys := N_0 + N_{n45} + N_{p45} + N_{90}$

4. Ply Thickness $h := .01 \cdot in$ $h_{rubber} := .15 \cdot in$

5. Laminate Thickness $t_L := Total\_plys \cdot h + h_{rubber}$ $t_L = 9.398 \cdot mm$

6. Strain Applied to the Material (circumferential):

$\beta = atan(\varepsilon_y/\varepsilon_x)$ $\beta := 0 \cdot deg$

Shear Strain: $\varepsilon_s := 0$

7. Number and Orientation of Ply Angles:

$Plys := 4$

$a := 1 .. Plys$

$c := 1 .. 3 \cdot Plys$

$$\theta := \begin{bmatrix} 0 \\ 90 \\ 45 \\ -45 \end{bmatrix} \cdot deg$$

8. Engineering Constants:

Kevlar

$E_x := 4.7 \cdot MSI$ $E_s := .45 \cdot MSI$

$E_y := 4.7 \cdot MSI$ $E_m := 3.4 \cdot GPa$

$v_f := .5$ $G_m := 1.26 \cdot GPa$

$v_m := .5$ $v_x := .15$

Rubber

$E_{rubber} := 1304 \cdot psi$

$v_{rubber} := .499$

Model Parameters

1. Radius of Base of Sonar Dome: $R_{model} := 36.\cdot in$
2. Axial Depth: $D_{model} := 25\cdot in$
3. Radius of Curvature $R_{curvature} := \frac{1}{2}\cdot\frac{D_{model}^2 + R_{model}^2}{D_{model}}$ $R_{curvature} = 0.976\cdot m$
4. Radius to Center of Cutouts $R_{cutout} := 27\cdot in$
5. Axial Distance to Center of Cutout $D_{cutout} := R_{curvature} - \sqrt{R_{curvature}^2 - R_{cutout}^2}$ $D_{cutout} = 0.282\cdot m$
6. Slope of Dome Surface at Cutout Center $\omega := \frac{-D_{cutout} + R_{curvature}}{\sqrt{D_{cutout}}\cdot\sqrt{-D_{cutout} + 2\cdot R_{curvature}}}$ $\omega = 58.003\cdot deg$
7. Diameter of Cutout $d_{cutout} := 11\cdot in$
8. Radius where Cutout Starts $r_0 := 23.693\cdot in$
9. Radius where Cutout Ends $r_f := 29.66\cdot in$
10. Number of Cutouts $n_{cutouts} := 3$

Ply Strength Parameter Inputs:

1. Tensile Strength in Longitudinal Direction $X := 56\cdot KSI$
2. Compressive Strength in Longitudinal Direction $X_{prime} := 14\cdot KSI$
3. Tensile Strength in Transverse Direction $Y := 56\cdot KSI$
4. Compressive Strength in the Transverse Direction $Y_{prime} := 14\cdot KSI$
5. Shear Strength $S := 4.5\cdot KSI$

Matrix and Fiber Damage Inputs

$E_{f\_star} := .01$ $\eta_y := .5161$ $n := .1$

$E_{m\_star} := .15$ $\eta_s := .316$ $F_{xy\_star} := -.5$

Damage Ply Calculations:

$$E_{fx} := \frac{E_x}{v_f} \qquad G_{fx} := \left[\frac{1+\eta_s \frac{v_m}{v_f}}{E_s} - \frac{\eta_s \frac{v_m}{v_f}}{G_m} \right]^{-1} \qquad E_{fy} := \left[\frac{1+\eta_y \frac{v_m}{v_f}}{E_y} - \frac{\eta_y \frac{v_m}{v_f}}{E_m} \right]^{-1}$$

$$E_{y\_damaged}(F) := \left[\frac{1}{1+\eta_y \frac{v_m}{v_f}} \cdot \left[\frac{1}{E_{fy}} + \frac{1}{F} - \frac{\eta_y \frac{v_m}{v_f}}{E_m} \right] \right]^{-1}$$

$$E_{s\_damaged}(F) := \left[\frac{1}{1+\eta_s \frac{v_m}{v_f}} \cdot \left[\frac{1}{G_{fx}} + \frac{1}{F} - \frac{\eta_s \frac{v_m}{v_f}}{G_m} \right] \right]^{-1}$$

Building Ply Data:

Undamaged ply, ply with matrix damage and ply with fiber damage.

$$E_{xx} := \begin{bmatrix} E_x \\ E_x \\ E_x \cdot E_{f\_star} \end{bmatrix} \qquad E_{yy} := \begin{bmatrix} E_y \\ E_{y\_damaged} \\ E_{y\_damaged} \cdot E_{f\_star} \end{bmatrix} \qquad E_{ss} := \begin{bmatrix} E_s \\ E_{s\_damaged} \\ E_{s\_damaged} \cdot E_{f\_star} \end{bmatrix}$$

$$v_{xx} := \begin{bmatrix} v_x \\ v_x \cdot E_{m\_star} \\ v_x \cdot E_{f\_star} \end{bmatrix} \qquad FF_{xy\_star} := \begin{bmatrix} F_{xy\_star} \\ F_{xy\_star} \cdot E_{m\_star} \\ F_{xy\_star} \cdot E_{f\_star} \end{bmatrix}$$

$$XX_q := X \qquad XX_{prime_q} := X_{prime} \cdot \left(\frac{E_{ss_q}}{E_s} \right)^n$$

$$YY_q := Y \qquad YY_{prime_q} := Y_{prime} \qquad SS_q := S \qquad v_{yy_q} := v_{xx_q} \frac{E_{yy_q}}{E_{xx_q}}$$

Rotation Matrices:

$$ml_a := \cos\theta_a \qquad n_a := \sin\theta_a$$

$$J_a := \begin{bmatrix} ml_a^2 & n_a^2 & 2 \cdot ml_a \cdot n_a \\ n_a^2 & ml_a^2 & -2 \cdot ml_a \cdot n_a \\ -ml_a \cdot n_a & ml_a \cdot n_a & ml_a^2 - n_a^2 \end{bmatrix}$$

$$Rotation1_a := \begin{bmatrix} ml_a^4 & n_a^4 & 2 \cdot ml_a^2 \cdot n_a^2 & 4\, ml_a^2 \cdot n_a^2 \\ n_a^4 & ml_a^4 & 2\, ml_a^2 \cdot n_a^2 & 4\, ml_a^2 \cdot n_a^2 \\ ml_a^2 \cdot n_a^2 & ml_a^2 \cdot n_a^2 & ml_a^4 + n_a^4 & -4\, ml_a^2 \cdot n_a^2 \\ ml_a^2 \cdot n_a^2 & ml_a^2 \cdot n_a^2 & -2\, ml_a^2 \cdot n_a^2 & \left[ml_a^2 - n_a^2 \right]^2 \\ ml_a^3 \cdot n_a & -ml_a \cdot n_a^3 & ml_a \cdot n_a^3 - ml_a^3 \cdot n_a & 2 \cdot \left[ml_a \cdot n_a^3 - ml_a^3 \cdot n_a \right] \\ ml_a \cdot n_a^3 & -ml_a^3 \cdot n_a & ml_a^3 \cdot n_a - ml_a \cdot n_a^3 & 2 \cdot \left[ml_a^3 \cdot n_a - ml_a \cdot n_a^3 \right] \end{bmatrix}$$

$$Rotation2_a := \begin{bmatrix} ml_a^2 & n_a^2 \\ n_a^2 & ml_a^2 \\ ml_a \cdot n_a & -ml_a \cdot n_a \end{bmatrix}$$

Ply Stiffness Calculation:

Calculates the zero direction stiffness matrix for the various ply states (undamaged, matrix damaged, and fiber damaged)

$$Q_q := \begin{bmatrix} \frac{E_{xx_q}}{1-\nu_{xx_q}\cdot\nu_{yy_q}} & \frac{\nu_{yy_q}\cdot E_{xx_q}}{1-\nu_{xx_q}\cdot\nu_{yy_q}} & 0 \\ \frac{\nu_{xx_q}\cdot E_{yy_q}}{1-\nu_{xx_q}\cdot\nu_{yy_q}} & \frac{E_{yy_q}}{1-\nu_{xx_q}\cdot\nu_{yy_q}} & 0 \\ 0 & 0 & E_{ss_q} \end{bmatrix} \qquad Q_{rubber} := \begin{bmatrix} \frac{E_{rubber}}{1-\nu_{rubber}^2} & \frac{\nu_{rubber}\cdot E_{rubber}}{1-\nu_{rubber}^2} & 0 \\ \frac{\nu_{rubber}\cdot E_{rubber}}{1-\nu_{rubber}^2} & \frac{E_{rubber}}{1-\nu_{rubber}^2} & 0 \\ 0 & 0 & \frac{2\cdot E_{rubber}}{1+\nu_{rubber}} \end{bmatrix}$$

Creates the stiffness matrices for every combination of ply angle and ply state. Qnew is a 3 x 4 matrix

$$Q_{rot_{q,a}} := \text{Rotation1}_a \begin{bmatrix} Q_{q\,1,1} \\ Q_{q\,2,2} \\ Q_{q\,1,2} \\ Q_{q\,3,3} \end{bmatrix} \qquad Q_{new_{q,a}} := \begin{bmatrix} Q_{rot_{q,a\,1}} & Q_{rot_{q,a\,3}} & Q_{rot_{q,a\,5}} \\ Q_{rot_{q,a\,3}} & Q_{rot_{q,a\,2}} & Q_{rot_{q,a\,6}} \\ Q_{rot_{q,a\,5}} & Q_{rot_{q,a\,6}} & Q_{rot_{q,a\,4}} \end{bmatrix}$$

Stress Space Strength Parameters:

A separate F must be calculated for each ply state

$$F_{a_q} := \begin{bmatrix} \frac{1}{XX_q\cdot XX\,prime_q} & \frac{FF_{xy\_star_q}}{\sqrt{XX_q\cdot XX\,prime_q\cdot YY_q\cdot YY\,prime_q}} & 0 \\ \frac{FF_{xy\_star_q}}{\sqrt{XX_q\cdot XX\,prime_q\cdot YY_q\cdot YY\,prime_q}} & \frac{1}{YY_q\cdot YY\,prime_q} & 0 \\ 0 & 0 & \frac{1}{SS_q^2} \end{bmatrix}$$

$$F_{b_q} := \begin{bmatrix} \frac{1}{XX_q} - \frac{1}{XX\,prime_q} \\ \frac{1}{YY_q} - \frac{1}{YY\,prime_q} \end{bmatrix}$$

Strain Space Strength Parameters:

1. Strain strength parameter for each ply state

$$G_{base1_q} := \begin{bmatrix} F_{aq_{1,1}}\left[Q_{q_{1,1}}\right]^2 \cdots & F_{aq_{1,1}} \cdot Q_{q_{1,1}} \cdot Q_{q_{1,2}} \cdots & 0 \\ +2 \cdot F_{aq_{1,2}} \cdot Q_{q_{1,1}} \cdot Q_{q_{1,2}} \cdots & + F_{aq_{1,2}}\left[Q_{q_{1,1}} \cdot Q_{q_{2,2}} + \left[Q_{q_{1,2}}\right]^2\right] \cdots & \\ + F_{aq_{2,2}}\left[Q_{q_{1,2}}\right]^2 & + F_{aq_{2,2}} \cdot Q_{q_{1,2}} \cdot Q_{q_{2,2}} & \\ F_{aq_{1,1}} \cdot Q_{q_{1,1}} \cdot Q_{q_{1,2}} \cdots & F_{aq_{1,1}}\left[Q_{q_{1,2}}\right]^2 \cdots & 0 \\ + F_{aq_{1,2}}\left[Q_{q_{1,1}} \cdot Q_{q_{2,2}} + \left[Q_{q_{1,2}}\right]^2\right] \cdots & +2 \cdot F_{aq_{1,2}} \cdot Q_{q_{1,2}} \cdot Q_{q_{2,2}} \cdots & \\ + F_{aq_{2,2}} \cdot Q_{q_{1,2}} \cdot Q_{q_{2,2}} & + F_{aq_{2,2}}\left[Q_{q_{2,2}}\right]^2 & \\ 0 & 0 & F_{aq_{3,3}}\left[Q_{q_{3,3}}\right]^2 \end{bmatrix}$$

$$G_{base2_q} := \begin{bmatrix} F_{bq_1} \cdot Q_{q_{1,1}} + F_{bq_2} \cdot Q_{q_{1,2}} \\ F_{bq_1} \cdot Q_{q_{1,2}} + F_{bq_2} \cdot Q_{q_{2,2}} \end{bmatrix}$$

2. Calculating G matrices for all combinations of ply state and angle:

$$\begin{bmatrix} \text{Rotation1}_1 \cdot \begin{bmatrix} G_{base1_1\ 1,1} \\ G_{base1_1\ 2,2} \\ G_{base1_1\ 1,2} \\ G_{base1_1\ 3,3} \end{bmatrix} \\ \text{Rotation1}_1 \cdot \begin{bmatrix} G_{base1_2\ 1,1} \\ G_{base1_2\ 2,2} \\ G_{base1_2\ 1,2} \\ G_{base1_2\ 3,3} \end{bmatrix} \\ \text{Rotation1}_1 \cdot \begin{bmatrix} G_{base1_3\ 1,1} \\ G_{base1_3\ 2,2} \\ G_{base1_3\ 1,2} \\ G_{base1_3\ 3,3} \end{bmatrix} \\ \begin{bmatrix} G_{base1_1\ 1,1} \\ G_{base1_1\ 2,2} \end{bmatrix} \end{bmatrix}$$

$$G_{2trans} := \begin{bmatrix} \text{Rotation2}_1 \cdot \begin{bmatrix} G_{base2_1\ 1} \\ G_{base2_1\ 2} \end{bmatrix} \\ \text{Rotation2}_1 \cdot \begin{bmatrix} G_{base2_2\ 1} \\ G_{base2_2\ 2} \end{bmatrix} \\ \text{Rotation2}_1 \cdot \begin{bmatrix} G_{base2_3\ 1} \\ G_{base2_3\ 2} \end{bmatrix} \\ \text{Rotation2}_2 \cdot \begin{bmatrix} G_{base2_1\ 1} \\ G_{base2_1\ 2} \end{bmatrix} \\ \text{Rotation2}_2 \cdot \begin{bmatrix} G_{base2_2\ 1} \\ G_{base2_2\ 2} \end{bmatrix} \\ \text{Rotation2}_2 \cdot \begin{bmatrix} G_{base2_3\ 1} \\ G_{base2_3\ 2} \end{bmatrix} \\ \text{Rotation2}_3 \cdot \begin{bmatrix} G_{base2_1\ 1} \\ G_{base2_1\ 2} \end{bmatrix} \\ \text{Rotation2}_3 \cdot \begin{bmatrix} G_{base2_2\ 1} \\ G_{base2_2\ 2} \end{bmatrix} \\ \begin{bmatrix} G_{base2_3\ 1} \end{bmatrix} \end{bmatrix}$$

$$G_{1trans} := \begin{bmatrix} \text{Rotation1}_2 \cdot \begin{bmatrix} {}^{1}G_{base1_1}{}_{1,2} \\ G_{base1_1}{}_{2,2} \\ G_{base1_1}{}_{3,3} \end{bmatrix} \\ \text{Rotation1}_2 \cdot \begin{bmatrix} G_{base1_2}{}_{1,1} \\ G_{base1_2}{}_{2,2} \\ G_{base1_2}{}_{1,2} \\ G_{base1_2}{}_{3,3} \end{bmatrix} \\ \text{Rotation1}_2 \cdot \begin{bmatrix} G_{base1_3}{}_{1,1} \\ G_{base1_3}{}_{2,2} \\ G_{base1_3}{}_{1,2} \\ G_{base1_3}{}_{3,3} \end{bmatrix} \\ \text{Rotation1}_3 \cdot \begin{bmatrix} G_{base1_1}{}_{1,1} \\ G_{base1_1}{}_{2,2} \\ G_{base1_1}{}_{1,2} \\ G_{base1_1}{}_{3,3} \end{bmatrix} \\ \text{Rotation1}_3 \cdot \begin{bmatrix} G_{base1_2}{}_{1,1} \\ G_{base1_2}{}_{2,2} \\ G_{base1_2}{}_{1,2} \\ G_{base1_2}{}_{3,3} \end{bmatrix} \\ \text{Rotation1}_3 \cdot \begin{bmatrix} G_{base1_3}{}_{1,1} \\ G_{base1_3}{}_{2,2} \\ G_{base1_3}{}_{1,2} \\ G_{base1_3}{}_{3,3} \end{bmatrix} \\ \text{Rotation1}_4 \cdot \begin{bmatrix} G_{base1_1}{}_{1,1} \\ G_{base1_1}{}_{2,2} \\ G_{base1_1}{}_{1,2} \\ G_{base1_1}{}_{3,3} \end{bmatrix} \\ \text{Rotation1}_4 \cdot \begin{bmatrix} G_{base1_2}{}_{1,1} \\ G_{base1_2}{}_{2,2} \\ G_{base1_2}{}_{1,2} \\ G_{base1_2}{}_{3,3} \end{bmatrix} \\ \text{Rotation1}_4 \cdot \begin{bmatrix} G_{base1_3}{}_{1,1} \\ G_{base1_3}{}_{2,2} \\ G_{base1_3}{}_{1,2} \\ G_{base1_3}{}_{3,3} \end{bmatrix} \end{bmatrix}$$

$$\begin{bmatrix} \text{Rotation2}_3 \cdot \begin{bmatrix} {}^{3}G_{base2_3}{}_{1} \\ G_{base2_3}{}_{2} \end{bmatrix} \\ \text{Rotation2}_4 \cdot \begin{bmatrix} G_{base2_1}{}_{1} \\ G_{base2_1}{}_{2} \end{bmatrix} \\ \text{Rotation2}_4 \cdot \begin{bmatrix} G_{base2_2}{}_{1} \\ G_{base2_2}{}_{2} \end{bmatrix} \\ \text{Rotation2}_4 \cdot \begin{bmatrix} G_{base2_3}{}_{1} \\ G_{base2_3}{}_{2} \end{bmatrix} \end{bmatrix}$$

$$G_c := \begin{bmatrix} G_{1trans_c 1} & G_{1trans_c 3} & G_{1trans_c 5} & G_{2trans_c 1} \\ G_{1trans_c 3} & G_{1trans_c 2} & G_{1trans_c 6} & G_{2trans_c 2} \\ G_{1trans_c 5} & G_{1trans_c 6} & G_{1trans_c 4} & G_{2trans_c 3} \end{bmatrix}$$

Formation of Strain Space Failure Envelopes:

1. The following relationship is used to determine the failure envelope: $G_{i,j}\cdot\varepsilon_i\cdot\varepsilon_j + G_i\cdot\varepsilon_i = 1$

2. After shifting to polar coordinates, the above equation can be solved for r using the quadratic equation:

   $\varepsilon_1 = r\cdot\cos\phi \quad \varepsilon_2 = r\cdot\sin\phi \quad A\cdot r^2 + B\cdot r - 1 = 0$

3. Calculation of coefficients for the quadratic formula

$$A(\phi,b) := G_{b\,2,2}\cdot\sin(\phi)^2 + 2\cdot G_{b\,1,2}\cdot\cos(\phi)\cdot\sin(\phi) + G_{b\,1,1}\cdot\cos(\phi)^2$$

$$B(\phi,b,\varepsilon_s) := 2\cdot G_{b\,2,3}\cdot\sin(\phi)\cdot\varepsilon_s + G_{b\,2,4}\cdot\sin(\phi) + 2\cdot G_{b\,1,3}\cdot\cos(\phi)\cdot\varepsilon_s + G_{b\,1,4}\cdot\cos(\phi)$$

$$C(\phi,b,\varepsilon_s) := G_{b\,3,4}\cdot\varepsilon_s + G_{b\,3,3}\cdot\varepsilon_s^2 - 1$$

$$r(\phi,b,\varepsilon_s) := \frac{-B(\phi,b,\varepsilon_s) + \sqrt{B(\phi,b,\varepsilon_s)^2 - 4\cdot A(\phi,b)\cdot C(\phi,b,\varepsilon_s)}}{2\cdot A(\phi,b)}$$

Strain Space Failure Envelopes:

$\phi := 0\cdot deg, 1\cdot deg .. 360\cdot deg \quad y(x) := \tan(\beta)\cdot x \quad x := 0, \frac{\cos(\beta)}{10} .. \cos(\beta) \quad \varepsilon_x(\phi,b,\varepsilon_s) := r(\phi,b,\varepsilon_s)\cdot\cos(\phi) \quad \varepsilon_y(\phi,b,\varepsilon_s) := r(\phi,b,\varepsilon_s)\cdot\sin(\phi)$

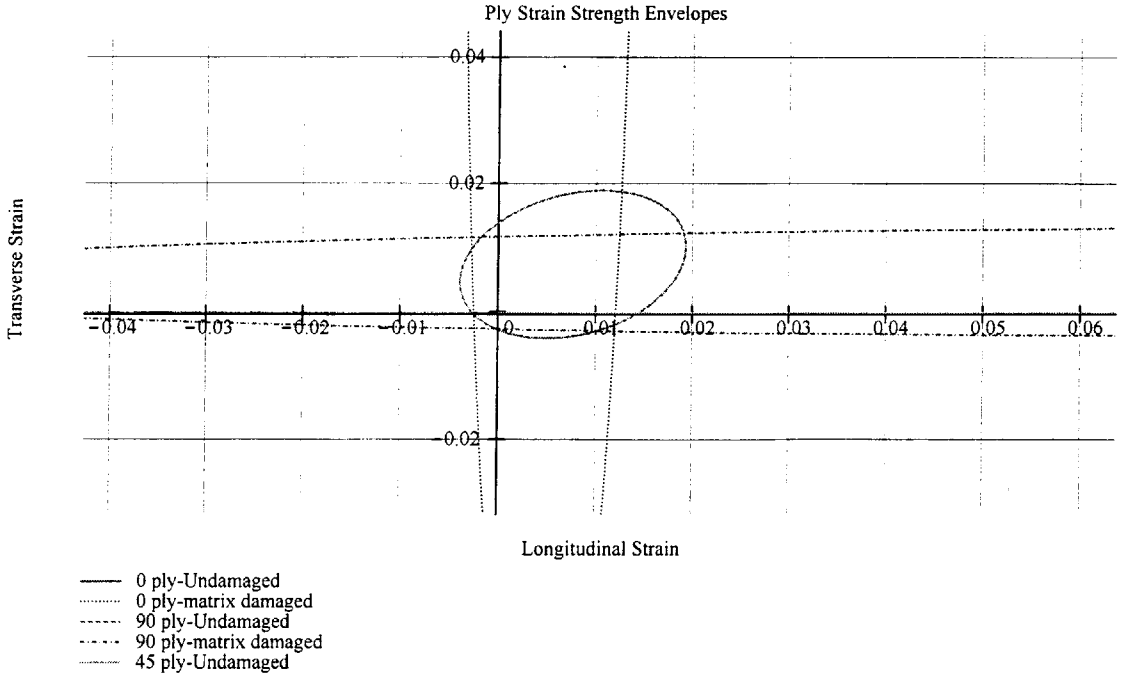

Calculation of Degraded Laminate Stiffness:

The first ply failure strain is first calculated. Subsequently, a progressive failure of plys is allowed and the stiffness calculated based on the ply damage history.

plot1 := al ← 1
bl ← 1
count ← 2
n1 ← 1
s ← 1
while 1
  $\varepsilon 1_1 \leftarrow 0$
  $\sigma 1_1 \leftarrow 0 \cdot MPa$
  $\varepsilon 1_{count} \leftarrow \min \begin{bmatrix} \varepsilon_x(\beta, al, \varepsilon_s) \\ \varepsilon_x(\beta, bl+3, \varepsilon_s) \end{bmatrix}$
  $\varepsilon 2_{count} \leftarrow \varepsilon 1_{count} \cdot \tan(\beta)$
  $A\,star_{count} \leftarrow \frac{1}{N_0 \cdot s + N_{90} \cdot s + \frac{h_{rubber}}{h}} \cdot \left[N_0 \cdot Q_{new_{al,1}} \cdot s + N_{90} \cdot Q_{new_{bl,2}} \cdot s + \frac{h_{rubber}}{h} \cdot Q_{rubber} \right]$
  $E_{y1_{count}} \leftarrow \left[\left[A\,star_{count}^{-1} \right]_{1,1} \right]^{-1}$
  $\sigma 1_{count} \leftarrow \left[A\,star_{count} \cdot \begin{bmatrix} \varepsilon 1_{count} \\ \varepsilon 2_{count} \\ \varepsilon_s \end{bmatrix} \right]_1$
  al ← al + 2 if $\varepsilon 1_{count} = \varepsilon_x(\beta, al, \varepsilon_s)$
  bl ← bl + 1 if $\varepsilon 1_{count} = \varepsilon_x(\beta, bl+3, \varepsilon_s)$
  count ← count + 1
  break if al + bl = 6
  break if al > 3
  break if bl > 3
tempstore ← augment $\left(\varepsilon 1, \frac{\sigma 1}{MPa}\right)$

$\varepsilon_{rubber} := \begin{bmatrix} .236 \\ 1 \end{bmatrix}$ iii := 1 .. rows ε_{rubber} $\sigma_{rubber_{iii}} := \left[Q_{rubber} \cdot \begin{bmatrix} \varepsilon_{rubber_{iii}} \\ 0 \\ 0 \end{bmatrix} \right]_1$ plot := stack (plot1, augment $\left(\varepsilon_{rubber}, \frac{\sigma_{rubber}}{MPa}\right)$

Tensile Flow Stress Determination

curve(x) := linterp $(plot^{\langle 1 \rangle}, plot^{\langle 2 \rangle}, x)$

$$\sigma_t := \frac{1}{plot^{\langle 1 \rangle}_{rows(plot)}} \cdot \int_0^{plot^{\langle 1 \rangle}_{rows(plot)}} curve(x)\,dx \cdot MPa$$

$\sigma_t = 53.354 \cdot MPa$

Calculation of Degraded Laminate Stiffness (Compressive):

The first ply failure strain is first calculated. Subsequently, a progressive failure of plys is allowed and the stiffness calculated based on the ply damage history.

$\beta := 180 \cdot deg$

plot1 :=
- $a1 \leftarrow 1$
- $b1 \leftarrow 1$
- $count \leftarrow 2$
- $n1 \leftarrow 1$
- $s \leftarrow 1$
- while 1
  - $\varepsilon 1_1 \leftarrow 0$
  - $\sigma 1_1 \leftarrow 0 \cdot MPa$
  - $a_{count,1} \leftarrow a1$
  - $a_{count,2} \leftarrow b1$
  - $\varepsilon 1_{count} \leftarrow \min \begin{bmatrix} \varepsilon_x(\beta, a1, \varepsilon_s) \\ \varepsilon_x(\beta, b1+3, \varepsilon_s) \end{bmatrix}$
  - $\varepsilon 2_{count} \leftarrow \varepsilon 1_{count} \cdot \tan(\beta)$
  - $A\,star_{count} \leftarrow \frac{1}{N_0 \cdot s + N_{90} \cdot s + \frac{h_{rubber}}{h}} \cdot \left[N_0 \cdot Q_{new_{a1,1}} \cdot s + N_{90} \cdot Q_{new_{b1,2}} \cdot s + \frac{h_{rubber}}{h} \cdot Q_{rubber} \right]$
  - $E_{y1_{count}} \leftarrow \left[\left[A\,star_{count}^{-1} \right]_{1,1} \right]^{-1}$
  - $\sigma 1_{count} \leftarrow \left[A\,star_{count} \cdot \begin{bmatrix} \varepsilon 1_{count} \\ \varepsilon 2_{count} \\ \varepsilon_s \end{bmatrix} \right]_1$
  - $a1 \leftarrow a1 + 2$ if $\varepsilon 1_{count} = \varepsilon_x(\beta, a1, \varepsilon_s)$
  - $b1 \leftarrow b1 + 1$ if $\varepsilon 1_{count} = \varepsilon_x(\beta, b1+3, \varepsilon_s)$
  - $count \leftarrow count + 1$
  - break if $a1 + b1 = 6$
  - break if $a1 > 3$
  - break if $b1 > 3$
- $tempstore \leftarrow augment(\varepsilon 1, \frac{\sigma 1}{MPa})$

$\varepsilon_{rubber} := \begin{bmatrix} .06 \\ 1 \end{bmatrix}$ $iii := 1 .. rows(\varepsilon_{rubber})$ $\sigma_{rubber_{iii}} := \left[Q_{rubber} \cdot \begin{bmatrix} \varepsilon_{rubber_{iii}} \\ 0 \\ 0 \end{bmatrix} \right]_1$ $plot := stack(plot1, augment(\varepsilon_{rubber}, \frac{\sigma_{rubber}}{MPa}))$

Compressive Flow Stress Determination

$curve(x) := linterp(plot^{\langle 1 \rangle}, plot^{\langle 2 \rangle}, x)$

$\sigma_c := \frac{1}{plot^{\langle 1 \rangle}_{rows(plot)}} \cdot \int_0^{plot^{\langle 1 \rangle}_{rows(plot)}} curve(x)\,dx \cdot MPa$ $\sigma_c = 8.41 \cdot MPa$

Force vs Axial Crush Distance Determination:

$nn := 30$ $bbb := 1 .. nn$

1. Establishing Displacement Array $\delta_{bbb} := \frac{D_{model} \cdot (bbb - 1)}{nn - 1}$

2. Calculate Open Section Correction Factor

$$a(\delta) := \sqrt{\delta \cdot (2 \cdot R_{curvature} - \delta)}$$

$$\phi(\delta) := 2 \cdot \operatorname{asin}\left[\frac{\sqrt{\frac{r_o + d_{cutout} \cdot \cos(\omega) - a(\delta)}{\cos(\omega)}} \cdot d_{cutout} - \frac{r_o + d_{cutout} \cdot \cos(\omega) - a(\delta)}{\cos(\omega)}}{a(\delta)}\right]$$

$$\varepsilon(\delta) := 1 - \frac{n_{cutouts} \cdot \phi(\delta)}{2 \cdot \pi}$$

3. Calculate Unbalance Flow Stress Correction Factor

$$\alpha := \frac{2 \cdot \sigma_t}{\sigma_c + \sigma_t} \qquad \alpha = 1.728$$

4. Calculate Crushing Force for Displacement Array

$$P_{bbb} := \text{if}\left[a \cdot \delta_{bbb} \le r_o, 4 \cdot \pi \cdot \sqrt{2} \cdot \sigma_c \cdot \alpha^{\frac{1}{2}} \cdot t_L^{\frac{3}{2}} \cdot \delta_{bbb}^{\frac{1}{2}}, \text{if}\left[a \cdot \delta_{bbb} \le r_f, \varepsilon \cdot \delta_{bbb} \cdot \left[4 \cdot \pi \cdot \sqrt{2} \cdot \sigma_c \cdot \alpha^{\frac{1}{2}} \cdot t_L^{\frac{3}{2}} \cdot \delta_{bbb}^{\frac{1}{2}}\right], 4 \cdot \pi \cdot \sqrt{2} \cdot \sigma_c \cdot \alpha^{\frac{1}{2}} \cdot t_L^{\frac{3}{2}} \cdot \delta_{bbb}^{\frac{1}{2}}\right]\right]$$

$P1(xx) := (\text{linterp}(\delta, P, xx))$

Energy Absorption of the Structure:

$Energy(\delta 11) := \text{linterp}(\delta, P, \delta 11)$

$$Cumulative\_Energy_{bbb} := \int_{0 \cdot m}^{\delta_{bbb}} Energy(x)\,dx \qquad Cumulative\_Energy_{rows(\delta)} = 0.058 \cdot MJ$$

Appendix B

Frustum Section Analysis

Ply Stiffness and Layup Inputs:

1. Material System: E-Glass (1583)/Epoxy (7780) woven cloth

2. Layup Configuration: $[90,45,0,-45]_2,90,45,0,0,45,90,[90,45,0,-45]_2$

$N_0 := 6$ $N_{n45} := 4$

$N_{90} := 6$ $N_{p45} := 6$

3. Total Number of Plys $Total\_plys := N_0 + N_{n45} + N_{p45} + N_{90}$

4. Ply Thickness $h := .018 \cdot in$

5. Laminate Thickness $t_L := Total\_plys \cdot h$ $t_L = 0.0101\,m$

$$sequence := \begin{bmatrix} 90 \\ 45 \\ 0 \\ -45 \\ 90 \\ 45 \\ 0 \\ -45 \\ 90 \\ 45 \\ 0 \\ 0 \\ 45 \\ 90 \\ -45 \\ 0 \\ 45 \\ 90 \\ -45 \\ 0 \\ 45 \\ 90 \end{bmatrix} \cdot deg$$

6. Strain Applied to the Material (circumferential):

$\beta = \text{atan}(\varepsilon_y/\varepsilon_x)$ $\beta := 89.5 \cdot deg$

Shear Strain: $\varepsilon_s := 0$

7. Number and Orientation of Ply Angles:

$Plys := 4$

$a := 1 .. Plys$

$c := 1 .. 3 \cdot Plys$

$$\theta := \begin{bmatrix} 0 \\ 90 \\ 45 \\ -45 \end{bmatrix} \cdot deg$$

8. Engineering Constants:

$E_x := 3 \cdot MSI$ $E_s := .55 \cdot MSI$ $G_m := 1.26 \cdot GPa$

$E_y := 2.7 \cdot MSI$ $E_m := 3.4 \cdot GPa$

$v_f := .5$

$v_m := .5$

$v_x := .15$

Component Parameters:

1. Radius of Shell: $R_{shell} := 3.25 \cdot ft$
2. Length of Shell: $L_{shell} := 3.1 \cdot ft$
3. Wave Length of Elastic Buckling Wave: $H := \sqrt{R_{shell} \cdot t \, L}$
4. Number of Buckling Waves Along Shell

$$Number_{waves} := \frac{L_{shell}}{2 \cdot H} \qquad Number_{waves} = 4.733$$

$$Number_{waves} := 5 \qquad H_{eff} := \frac{L_{shell}}{2 \cdot Number_{waves}}$$

Ply Strength Parameter Inputs:

1. Tensile Strength in Longitudinal Direction $X := 39.1 \cdot KSI$
2. Compressive Strength in Longitudinal Direction $X_{prime} := 33.8 \cdot KSI$
3. Tensile Strength in Transverse Direction $Y := 39.1 \cdot KSI$
4. Compressive Strength in the Transverse Direction $Y_{prime} := 33.8 \cdot KSI$
5. Shear Strength $S := 9.41 \cdot KSI$

Matrix and Fiber Damage Inputs

$E_{f\_star} := .01$ $\quad \eta_y := .5161$ $\quad n := .1$

$E_{m\_star} := .15$ $\quad \eta_s := .316$ $\quad F_{xy\_star} := -.5$

Damage Ply Calculations:

$$E_{fx} := \frac{E_x}{v_f} \qquad G_{fx} := \left[\frac{1 + \eta_s \frac{v_m}{v_f}}{E_s} - \frac{\eta_s \frac{v_m}{v_f}}{G_m} \right]^{-1} \qquad E_{fy} := \left[\frac{1 + \eta_y \frac{v_m}{v_f}}{E_y} - \frac{\eta_y \frac{v_m}{v_f}}{E_m} \right]^{-1}$$

$$E_{y\_damaged}(F) := \left[\frac{1}{1 + \eta_y \frac{v_m}{v_f}} \cdot \left[\frac{1}{E_{fy}} + \frac{1}{F} \frac{\eta_y \frac{v_m}{v_f}}{E_m} \right] \right]^{-1}$$

$$E_{s\_damaged}(F) := \left[\frac{1}{1 + \eta_s \frac{v_m}{v_f}} \cdot \left[\frac{1}{G_{fx}} + \frac{1}{F} \frac{\eta_s \frac{v_m}{v_f}}{G_m} \right] \right]^{-1}$$

Building Ply Data:

Undamaged ply, ply with matrix damage and ply with fiber damage.

$$E_{xx} := \begin{bmatrix} E_x \\ E_x \\ E_x \cdot E_{f\_star} \end{bmatrix} \qquad E_{yy} := \begin{bmatrix} E_y \\ E_{y\_damaged} \cdot E_{m\_star} \\ E_{y\_damaged} \cdot E_{f\_star} \end{bmatrix} \qquad E_{ss} := \begin{bmatrix} E_s \\ E_{s\_damaged} \cdot E_{m\_star} \\ E_{s\_damaged} \cdot E_{f\_star} \end{bmatrix}$$

$$\nu_{xx} := \begin{bmatrix} \nu_x \\ \nu_x \cdot E_{m\_star} \\ \nu_x \cdot E_{f\_star} \end{bmatrix} \qquad FF_{xy\_star} := \begin{bmatrix} F_{xy\_star} \\ F_{xy\_star} \cdot E_{m\_star} \\ F_{xy\_star} \cdot E_{f\_star} \end{bmatrix}$$

$$XX_q := X \qquad XX_{prime_q} := X_{prime} \cdot \left(\frac{E_{ss_q}}{E_s}\right)^n$$

$$YY_q := Y \qquad YY_{prime_q} := Y_{prime} \qquad SS_q := S \qquad \nu_{yy_q} := \nu_{xx_q} \cdot \frac{E_{yy_q}}{E_{xx_q}}$$

Rotation Matrices:

$$ml_a := \cos(\theta_a) \qquad n_a := \sin(\theta_a)$$

$$J_a := \begin{bmatrix} ml_a^2 & n_a^2 & 2 \cdot ml_a \cdot n_a \\ n_a^2 & ml_a^2 & -2 \cdot ml_a \cdot n_a \\ -ml_a \cdot n_a & ml_a \cdot n_a & ml_a^2 - n_a^2 \end{bmatrix}$$

$$Rotation1_a := \begin{bmatrix} ml_a^4 & n_a^4 & 2 \cdot ml_a^2 \cdot n_a^2 & 4\, ml_a^2 \cdot n_a^2 \\ n_a^4 & ml_a^4 & 2\, ml_a^2 \cdot n_a^2 & 4\, ml_a^2 \cdot n_a^2 \\ ml_a^2 \cdot n_a^2 & ml_a^2 \cdot n_a^2 & ml_a^4 + n_a^4 & -4\, ml_a^2 \cdot n_a^2 \\ ml_a^2 \cdot n_a^2 & ml_a^2 \cdot n_a^2 & -2\, ml_a^2 \cdot n_a^2 & \left[ml_a^2 - n_a^2\right]^2 \\ ml_a^3 \cdot n_a & -ml_a \cdot n_a^3 & ml_a \cdot n_a^3 - ml_a^3 \cdot n_a & 2 \cdot \left[ml_a \cdot n_a^3 - ml_a^3 \cdot n_a\right] \\ ml_a \cdot n_a^3 & -ml_a^3 \cdot n_a & ml_a^3 \cdot n_a - ml_a \cdot n_a^3 & 2 \cdot \left[ml_a^3 \cdot n_a - ml_a \cdot n_a^3\right] \end{bmatrix}$$

$$Rotation2_a := \begin{bmatrix} ml_a^2 & n_a^2 \\ n_a^2 & ml_a^2 \\ ml_a \cdot n_a & -ml_a \cdot n_a \end{bmatrix}$$

Ply Stiffness Calculation:

Calculates the zero direction stiffness matrix for the various ply states (undamaged, matrix damaged, and fiber damaged)

$$Q_q := \begin{bmatrix} \frac{E_{xx_q}}{1 - \nu_{xx_q} \cdot \nu_{yy_q}} & \frac{\nu_{yy_q} \cdot E_{xx_q}}{1 - \nu_{xx_q} \cdot \nu_{yy_q}} & 0 \\ \frac{\nu_{xx_q} \cdot E_{yy_q}}{1 - \nu_{xx_q} \cdot \nu_{yy_q}} & \frac{E_{yy_q}}{1 - \nu_{xx_q} \cdot \nu_{yy_q}} & 0 \\ 0 & 0 & E_{ss_q} \end{bmatrix}$$

Creates the stiffness matrices for every combination of ply angle and ply state. Qnew is a 3 x 4 matrix

$$Q_{rot_{q,a}} := \text{Rotation1}_a \cdot \begin{bmatrix} Q_{q\,1,1} \\ Q_{q\,2,2} \\ Q_{q\,1,2} \\ Q_{q\,3,3} \end{bmatrix}$$

$$Q_{new_{q,a}} := \begin{bmatrix} Q_{rot_{q,a\,1}} & Q_{rot_{q,a\,3}} & Q_{rot_{q,a\,5}} \\ Q_{rot_{q,a\,3}} & Q_{rot_{q,a\,2}} & Q_{rot_{q,a\,6}} \\ Q_{rot_{q,a\,5}} & Q_{rot_{q,a\,6}} & Q_{rot_{q,a\,4}} \end{bmatrix}$$

Flexural Stiffness:

1. Indexing variables $ff := 1 .. Total\_plys + 1$

   $gg := 1 .. Total\_plys$

2. Establishing an array of thickness positions for each ply

$$z_{ff} := \frac{-t_L}{2} + (ff - 1) \cdot h$$

3. Assigns the appropriate stiffness matrix based on the layup sequence

$$Q_{flex_{gg}} := \begin{cases} Q_{new_{1,1}} & \text{if } sequence_{gg} = 0 \cdot deg \\ Q_{new_{1,2}} & \text{if } sequence_{gg} = 90 \cdot deg \\ Q_{new_{1,3}} & \text{if } sequence_{gg} = 45 \cdot deg \\ Q_{new_{1,4}} & \text{otherwise} \end{cases}$$

Stress Space Strength Parameters:

A separate F must be calculated for each ply state

$$F_{a_q} := \begin{bmatrix} \frac{1}{XX_q \cdot XX\,prime_q} & \frac{FF_{xy\_star_q}}{\sqrt{XX_q \cdot XX\,prime_q \cdot YY_q \cdot YY\,prime_q}} & 0 \\ \frac{FF_{xy\_star_q}}{\sqrt{XX_q \cdot XX\,prime_q \cdot YY_q \cdot YY\,prime_q}} & \frac{1}{YY_q \cdot YY\,prime_q} & 0 \\ 0 & 0 & \frac{1}{SS_q^{\,2}} \end{bmatrix}$$

$$F_{b_q} := \begin{bmatrix} \frac{1}{XX_q} - \frac{1}{XX\,prime_q} \\ \frac{1}{YY_q} - \frac{1}{YY\,prime_q} \end{bmatrix}$$

Strain Space Strength Parameters:

1. Strain strength parameter for each ply state

$$G_{base1_q} := \begin{bmatrix} F_{a_{q\,1,1}} \cdot \left[Q_{q\,1,1}\right]^2 \cdots & F_{a_{q\,1,1}} \cdot Q_{q\,1,1} \cdot Q_{q\,1,2} \cdots & 0 \\ +2 \cdot F_{a_{q\,1,2}} \cdot Q_{q\,1,1} \cdot Q_{q\,1,2} \cdots & + F_{a_{q\,1,2}} \cdot \left[Q_{q\,1,1} \cdot Q_{q\,2,2} + \left[Q_{q\,1,2}\right]^2\right] \cdots & \\ + F_{a_{q\,2,2}} \cdot \left[Q_{q\,1,2}\right]^2 & + F_{a_{q\,2,2}} \cdot Q_{q\,1,2} \cdot Q_{q\,2,2} & \\ F_{a_{q\,1,1}} \cdot Q_{q\,1,1} \cdot Q_{q\,1,2} \cdots & F_{a_{q\,1,1}} \cdot \left[Q_{q\,1,2}\right]^2 \cdots & 0 \\ + F_{a_{q\,1,2}} \cdot \left[Q_{q\,1,1} \cdot Q_{q\,2,2} + \left[Q_{q\,1,2}\right]^2\right] \cdots & +2 \cdot F_{a_{q\,1,2}} \cdot Q_{q\,1,2} \cdot Q_{q\,2,2} \cdots & \\ + F_{a_{q\,2,2}} \cdot Q_{q\,1,2} \cdot Q_{q\,2,2} & + F_{a_{q\,2,2}} \cdot \left[Q_{q\,2,2}\right]^2 & \\ 0 & 0 & F_{a_{q\,3,3}} \cdot \left[Q_{q\,3,3}\right]^2 \end{bmatrix}$$

$$G_{base2_q} := \begin{bmatrix} F_{b_{q\,1}} \cdot Q_{q\,1,1} + F_{b_{q\,2}} \cdot Q_{q\,1,2} \\ F_{b_{q\,1}} \cdot Q_{q\,1,2} + F_{b_{q\,2}} \cdot Q_{q\,2,2} \end{bmatrix}$$

2. Calculating G matrices for all combinations of ply state and angle:

$$G_{1trans} := \begin{bmatrix} Rotation1_1 \cdot \begin{bmatrix} G_{base1_1\,1,1} \\ G_{base1_1\,2,2} \\ G_{base1_1\,1,2} \\ G_{base1_1\,3,3} \end{bmatrix} \\ Rotation1_1 \cdot \begin{bmatrix} G_{base1_2\,1,1} \\ G_{base1_2\,2,2} \\ G_{base1_2\,1,2} \\ G_{base1_2\,3,3} \end{bmatrix} \\ Rotation1_1 \cdot \begin{bmatrix} G_{base1_3\,1,1} \\ G_{base1_3\,2,2} \\ G_{base1_3\,1,2} \\ G_{base1_3\,3,3} \end{bmatrix} \\ Rotation1_2 \cdot \begin{bmatrix} G_{base1_1\,1,1} \\ G_{base1_1\,2,2} \\ G_{base1_1\,1,2} \\ G_{base1_1\,3,3} \end{bmatrix} \\ Rotation1_2 \cdot \begin{bmatrix} G_{base1_2\,1,1} \\ G_{base1_2\,2,2} \\ G_{base1_2\,1,2} \\ G_{base1_2\,3,3} \end{bmatrix} \\ Rotation1_2 \cdot \begin{bmatrix} G_{base1_3\,1,1} \\ G_{base1_3\,2,2} \\ G_{base1_3\,1,2} \\ G_{base1_3\,3,3} \end{bmatrix} \\ Rotation1_3 \cdot \begin{bmatrix} G_{base1_1\,1,1} \\ G_{base1_1\,2,2} \\ G_{base1_1\,1,2} \\ G_{base1_1\,3,3} \end{bmatrix} \end{bmatrix}$$

$$G_{2trans} := \begin{bmatrix} Rotation2_1 \cdot \begin{bmatrix} G_{base2_1\,1} \\ G_{base2_1\,2} \end{bmatrix} \\ Rotation2_1 \cdot \begin{bmatrix} G_{base2_2\,1} \\ G_{base2_2\,2} \end{bmatrix} \\ Rotation2_1 \cdot \begin{bmatrix} G_{base2_3\,1} \\ G_{base2_3\,2} \end{bmatrix} \\ Rotation2_2 \cdot \begin{bmatrix} G_{base2_1\,1} \\ G_{base2_1\,2} \end{bmatrix} \\ Rotation2_2 \cdot \begin{bmatrix} G_{base2_2\,1} \\ G_{base2_2\,2} \end{bmatrix} \\ Rotation2_2 \cdot \begin{bmatrix} G_{base2_3\,1} \\ G_{base2_3\,2} \end{bmatrix} \\ Rotation2_3 \cdot \begin{bmatrix} G_{base2_1\,1} \\ G_{base2_1\,2} \end{bmatrix} \\ Rotation2_3 \cdot \begin{bmatrix} G_{base2_2\,1} \\ G_{base2_2\,2} \end{bmatrix} \\ Rotation2_3 \cdot \begin{bmatrix} G_{base2_3\,1} \\ G_{base2_3\,2} \end{bmatrix} \\ Rotation2_4 \cdot \begin{bmatrix} G_{base2_1\,1} \\ G_{base2_1\,2} \end{bmatrix} \\ Rotation2_4 \cdot \begin{bmatrix} G_{base2_2\,1} \\ G_{base2_2\,2} \end{bmatrix} \\ Rotation2_4 \cdot \begin{bmatrix} G_{base2_3\,1} \\ G_{base2_3\,2} \end{bmatrix} \end{bmatrix}$$

$$\left[\begin{array}{l} \left[\begin{array}{c} {}^{1}_{3,3} \end{array}\right] \\ \text{Rotation1}_3 \left[\begin{array}{c} {}^{G}\text{basel}_{2\ 1,1} \\ {}^{G}\text{basel}_{2\ 2,2} \\ {}^{G}\text{basel}_{2\ 1,2} \\ {}^{G}\text{basel}_{2\ 3,3} \end{array}\right] \\ \text{Rotation1}_3 \left[\begin{array}{c} {}^{G}\text{basel}_{3\ 1,1} \\ {}^{G}\text{basel}_{3\ 2,2} \\ {}^{G}\text{basel}_{3\ 1,2} \\ {}^{G}\text{basel}_{3\ 3,3} \end{array}\right] \\ \text{Rotation1}_4 \left[\begin{array}{c} {}^{G}\text{basel}_{1\ 1,1} \\ {}^{G}\text{basel}_{1\ 2,2} \\ {}^{G}\text{basel}_{1\ 1,2} \\ {}^{G}\text{basel}_{1\ 3,3} \end{array}\right] \\ \text{Rotation1}_4 \left[\begin{array}{c} {}^{G}\text{basel}_{2\ 1,1} \\ {}^{G}\text{basel}_{2\ 2,2} \\ {}^{G}\text{basel}_{2\ 1,2} \\ {}^{G}\text{basel}_{2\ 3,3} \end{array}\right] \\ \text{Rotation1}_4 \left[\begin{array}{c} {}^{G}\text{basel}_{3\ 1,1} \\ {}^{G}\text{basel}_{3\ 2,2} \\ {}^{G}\text{basel}_{3\ 1,2} \\ {}^{G}\text{basel}_{3\ 3,3} \end{array}\right] \end{array}\right]$$

$$G_c := \begin{bmatrix} {}^{G}\text{1trans}_{c\ 1} & {}^{G}\text{1trans}_{c\ 3} & {}^{G}\text{1trans}_{c\ 5} & {}^{G}\text{2trans}_{c\ 1} \\ {}^{G}\text{1trans}_{c\ 3} & {}^{G}\text{1trans}_{c\ 2} & {}^{G}\text{1trans}_{c\ 6} & {}^{G}\text{2trans}_{c\ 2} \\ {}^{G}\text{1trans}_{c\ 5} & {}^{G}\text{1trans}_{c\ 6} & {}^{G}\text{1trans}_{c\ 4} & {}^{G}\text{2trans}_{c\ 3} \end{bmatrix}$$

Formation of Strain Space Failure Envelopes:

1. The following relationship is used to determine the failure envelope: $G_{i,j} \cdot \varepsilon_i \cdot \varepsilon_j + G_i \cdot \varepsilon_i = 1$

2. After shifting to polar coordinates, the above equation can be solved for r using the quadratic equation:

$\varepsilon_1 = r \cdot \cos\phi \quad \varepsilon_2 = r \cdot \sin\phi \quad A \cdot r^2 + B \cdot r - 1 = 0$

3. Calculation of coefficients for the quadratic formula

$$A(\phi, b) := G_{b\,2,2} \cdot \sin(\phi)^2 + 2 \cdot G_{b\,1,2} \cdot \cos(\phi) \cdot \sin(\phi) + G_{b\,1,1} \cdot \cos(\phi)^2$$

$$B(\phi, b, \varepsilon_s) := 2 \cdot G_{b\,2,3} \cdot \sin(\phi) \cdot \varepsilon_s + G_{b\,2,4} \cdot \sin(\phi) + 2 \cdot G_{b\,1,3} \cdot \cos(\phi) \cdot \varepsilon_s + G_{b\,1,4} \cdot \cos(\phi)$$

$$C(\phi, b, \varepsilon_s) := G_{b\,3,4} \cdot \varepsilon_s + G_{b\,3,3} \cdot \varepsilon_s^2 - 1$$

$$r(\phi, b, \varepsilon_s) := \frac{-B(\phi, b, \varepsilon_s) + \sqrt{B(\phi, b, \varepsilon_s)^2 - 4 \cdot A(\phi, b) \cdot C(\phi, b, \varepsilon_s)}}{2 \cdot A(\phi, b)}$$

Strain Space Failure Envelopes:

$\phi := 0 \cdot deg, 1 \cdot deg .. 360 \cdot deg \quad y(x) := \tan(\beta) \cdot x \quad x := 0, \frac{\cos(\beta)}{10} .. \cos(\beta) \quad \varepsilon_x(\phi, b, \varepsilon_s) := r(\phi, b, \varepsilon_s) \cdot \cos(\phi) \quad \varepsilon_y(\phi, b, \varepsilon_s) := r(\phi, b, \varepsilon_s) \cdot \sin(\phi)$

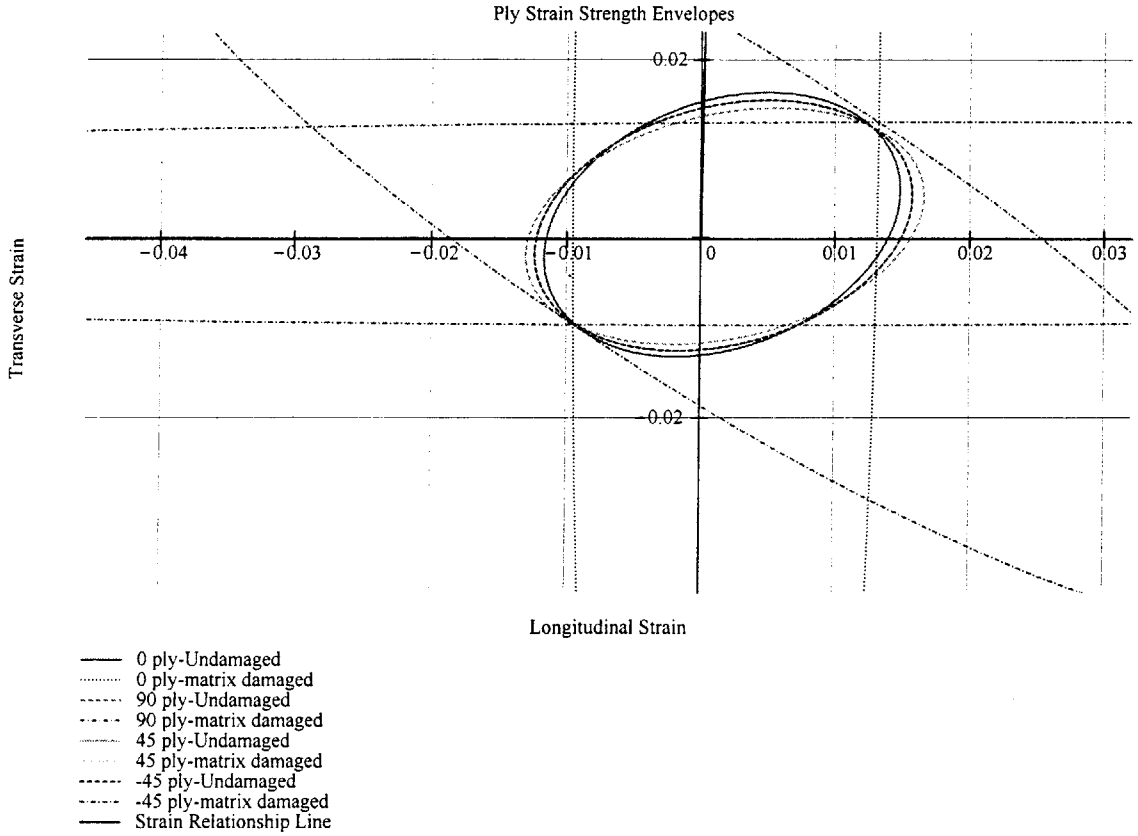

Calculation of Degraded Laminate Stiffness:

The first ply failure strain is first calculated. Subsequently, a progressive failure of plys is allowed and the stiffness calculated based on the ply damage history.

$$
\begin{aligned}
&\text{plot} := \\
&\quad a1 \leftarrow 1 \\
&\quad b1 \leftarrow 1 \\
&\quad c1 \leftarrow 1 \\
&\quad d1 \leftarrow 1 \\
&\quad \text{count} \leftarrow 2 \\
&\quad n1 \leftarrow 1 \\
&\quad \text{while } 1 \\
&\qquad \varepsilon 1_1 \leftarrow 0 \\
&\qquad \sigma 1_1 \leftarrow 0 \cdot \text{MPa} \\
&\qquad \varepsilon 1_{\text{count}} \leftarrow \min\left(\begin{bmatrix} \varepsilon_x(\beta, a1, \varepsilon_s) \\ \varepsilon_x(\beta, b1+3, \varepsilon_s) \\ \varepsilon_x(\beta, c1+6, \varepsilon_s) \\ \varepsilon_x(\beta, d1+9, \varepsilon_s) \end{bmatrix}\right) \\
&\qquad \varepsilon 2_{\text{count}} \leftarrow \varepsilon 1_{\text{count}} \cdot \tan(\beta) \\
&\qquad A\_star_{\text{count}} \leftarrow \frac{1}{N_0 + N_{90} + N_{n45} + N_{p45}} \cdot \left[N_0 \cdot Q\_new_{a1,1} + N_{90} \cdot Q\_new_{b1,2} + N_{n45} \cdot Q\_new_{c1,3} + N_{p45} \cdot Q\_new_{d1,4} \right] \\
&\qquad E_{y1_{\text{count}}} \leftarrow \left[\left[A\_star_{\text{count}}^{-1} \right]_{2,2} \right]^{-1} \\
&\qquad \sigma 1_{\text{count}} \leftarrow \left[A\_star_{\text{count}} \cdot \begin{bmatrix} \varepsilon 1_{\text{count}} \\ \varepsilon 2_{\text{count}} \\ \varepsilon_s \end{bmatrix} \right]_2 \\
&\qquad a1 \leftarrow a1 + 1 \text{ if } \varepsilon 1_{\text{count}} = \varepsilon_x(\beta, a1, \varepsilon_s) \\
&\qquad b1 \leftarrow b1 + 2 \text{ if } \varepsilon 1_{\text{count}} = \varepsilon_x(\beta, b1+3, \varepsilon_s) \\
&\qquad c1 \leftarrow c1 + 1 \text{ if } \varepsilon 1_{\text{count}} = \varepsilon_x(\beta, c1+6, \varepsilon_s) \\
&\qquad d1 \leftarrow d1 + 1 \text{ if } \varepsilon 1_{\text{count}} = \varepsilon_x(\beta, d1+9, \varepsilon_s) \\
&\qquad \text{count} \leftarrow \text{count} + 1 \\
&\qquad \text{break if } a1 + b1 + c1 + d1 = 12 \\
&\qquad \text{break if } a1 > 3 \\
&\qquad \text{break if } b1 > 3 \\
&\qquad \text{break if } c1 > 3 \\
&\qquad \text{break if } d1 > 3 \\
&\quad \text{tempstore} \leftarrow \text{augment}\left(\varepsilon 2, \frac{\sigma 1}{\text{MPa}}\right) \\
&\quad \text{augment}\left(\text{tempstore}, \frac{E_{y1}}{\text{GPa}}\right)
\end{aligned}
$$

Ply Transverse Young's Moduli as a function of Strain

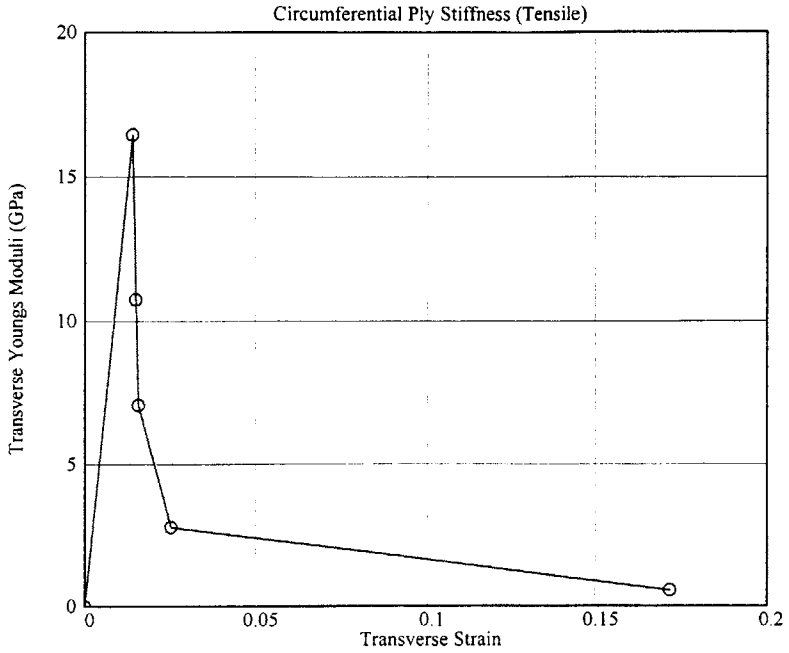

$$plot = \begin{bmatrix} 0 & 0 & 0 \\ 0.014 & 247.801 & 16.449 \\ 0.015 & 180.252 & 10.741 \\ 0.016 & 126.253 & 7.07 \\ 0.025 & 85.233 & 2.765 \\ 0.171 & 94.954 & 0.554 \end{bmatrix}$$

Transverse Stiffness Variations with Axial Location and Axial Crush Distance:

1. Setting up stations along the x' axis and axial crush distances at which E_y is to be calculated

$n := 2000 \qquad yyy := 1..17 \qquad zzz := 1..n$

$$x\,prime_{zzz} := \frac{zzz}{n} - \frac{1}{2 \cdot n} \cdot H_{eff} \qquad \delta_{temp} := \begin{bmatrix} 0 \\ 2 \cdot 10^{-3} \\ 3 \cdot 10^{-3} \\ 5 \cdot 10^{-3} \\ 6 \cdot 10^{-3} \\ 7 \cdot 10^{-3} \\ 8 \cdot 10^{-3} \\ 9 \cdot 10^{-3} \\ 0.011 \\ 0.014 \\ 0.02 \\ 0.029 \\ 0.041 \\ 0.068 \\ 0.093 \\ 0.1 \\ .2 \end{bmatrix} \cdot \frac{H_{eff}}{H} \cdot m$$

2. Calculation of circumferential strain based on axial position and crush distance

$$\varepsilon_{\theta zzz,yyy} := \frac{x\,prime_{zzz} \cdot \delta\,temp_{yyy}}{R_{shell} \cdot H_{eff}} \cdot \sqrt{\frac{H_{eff}}{\delta\,temp_{yyy}} - \frac{1}{4}}$$

3. Assignment of the appropriate Young's moduli to the correct axial position and crush distance based on the transverse Young's Moduli vs strain plot and circumferential strain.

$$E_{\theta zzz,yyy} := \begin{cases} 0 \cdot GPa & \text{if } \varepsilon_{\theta zzz,yyy} \geq .171 \\ .554 \cdot GPa & \text{if } .171 > \varepsilon_{\theta zzz,yyy} \geq .025 \\ 2.765 \cdot GPa & \text{if } .025 > \varepsilon_{\theta zzz,yyy} \geq .016 \\ 7.07 \cdot GPa & \text{if } .016 > \varepsilon_{\theta zzz,yyy} \geq .015 \\ 10.741 \cdot GPa & \text{if } .015 > \varepsilon_{\theta zzz,yyy} \geq .014 \\ 16.449 \cdot GPa & \text{otherwise} \end{cases}$$

$$plot = \begin{bmatrix} 0 & 0 & 0 \\ 0.014 & 247.801 & 16.449 \\ 0.015 & 180.252 & 10.741 \\ 0.016 & 126.253 & 7.07 \\ 0.025 & 85.233 & 2.765 \\ 0.171 & 94.954 & 0.554 \end{bmatrix}$$

Flexural Strain and Stiffness Calculations, and Thickness Variations:

1. Flexural Strain as a function of crush distance $.018 \cdot in = 4.572 \cdot 10^{-4}\ m$

$$\varepsilon_{xf}(\delta, gg) := 2 \cdot \frac{z_{gg+1} + z_{gg}}{2 \cdot R_{shell} \cdot t_L} \cdot \sqrt{\delta \cdot \sqrt{R_{shell} \cdot t_L} - \frac{\delta^2}{4}} \qquad \delta := 0, .001 .. 2 \cdot \sqrt{R_{shell} \cdot t_L}$$

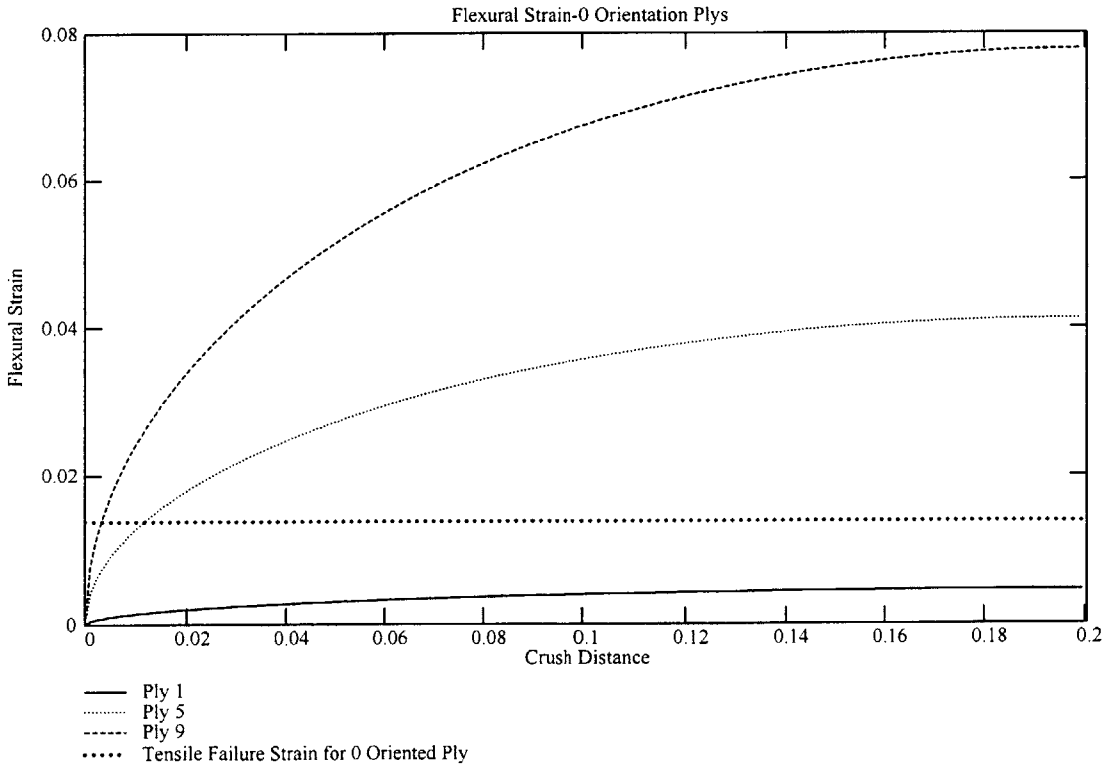

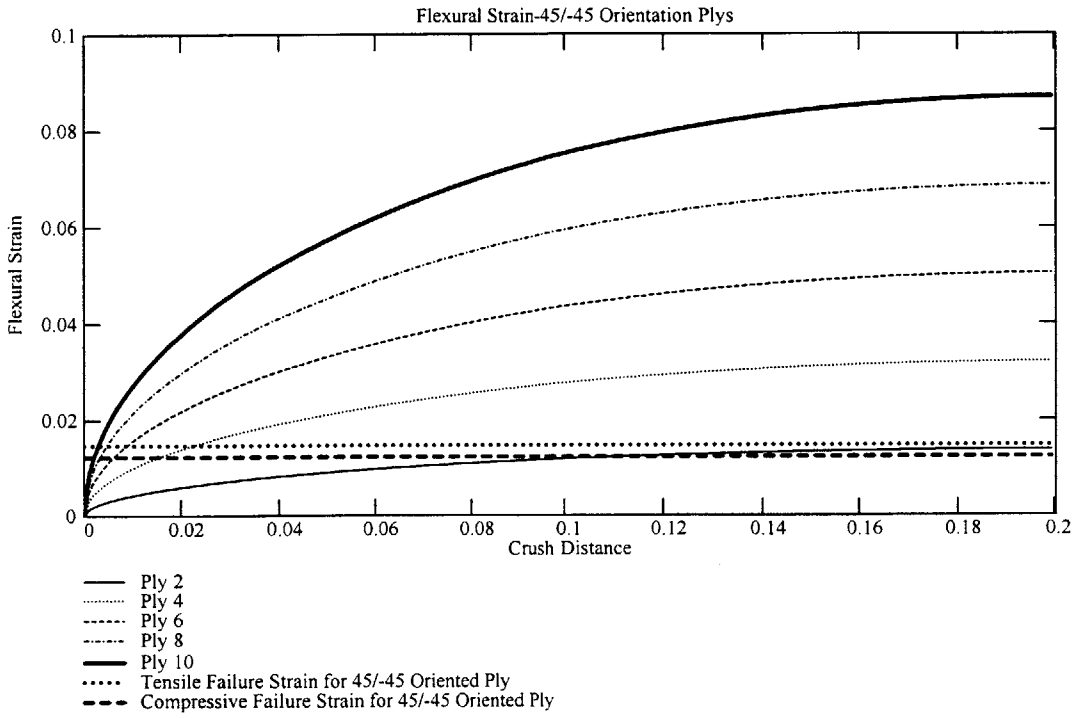
Flexural Strain-45/-45 Orientation Plys
Flexural Strain
0.1
0.08
0.06
0.04
0.02
0
0
0.02
0.04
0.06
0.08
0.1
0.12
0.14
0.16
0.18
0.2
Crush Distance
Ply 2
Ply 4
Ply 6
Ply 8
Ply 10
Tensile Failure Strain for 45/-45 Oriented Ply
Compressive Failure Strain for 45/-45 Oriented Ply

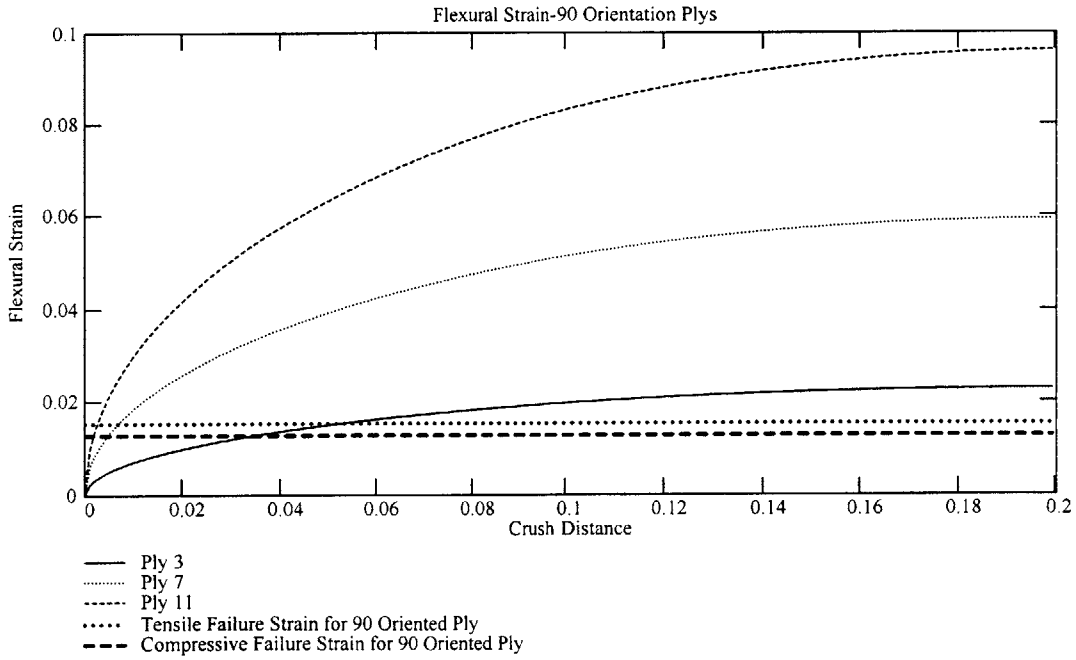
Flexural Strain-90 Orientation Plys
Flexural Strain
0.1
0.08
0.06
0.04
0.02
0
0
0.02
0.04
0.06
0.08
0.1
0.12
0.14
0.16
0.18
0.2
Crush Distance
Ply 3
Ply 7
Ply 11
Tensile Failure Strain for 90 Oriented Ply
Compressive Failure Strain for 90 Oriented Ply

2. Determination of flexural stiffness and thickness variations with crush distance. This a manual operation where the plys are failed progressively as crush distance is increased to 2H using the graphs above and the included ply strain limits. The thickness is determined by removing ply thicknesses as they fail.

$$ss := \begin{bmatrix} 0 \\ 0 \\ 0 \\ 0 \\ 0 \\ 0 \\ 0 \\ 0 \\ 0 \\ 0 \\ 1 \\ 1 \\ 0 \\ 0 \\ 0 \\ 0 \\ 0 \\ 0 \\ 0 \\ 0 \\ 0 \\ 0 \end{bmatrix}$$

$$D_{star} := \frac{12}{(2 \cdot h)^3} \cdot \frac{1}{3} \cdot \sum_{xx=1}^{Total\_plys} Q_{flex_{xx}} \cdot \left[\left[z_{(xx+1)} \right]^3 - z_{xx}^{\ 3} \right] \cdot ss_{xx}$$

$$d_{star} := D_{star}^{-1} \qquad E_{xf} := d_{star_{1,1}}^{-1} \qquad E_{xf} = 20.6843 \cdot GPa$$

$$\delta := \begin{bmatrix} 0 \\ .002 \\ .003 \\ .005 \\ .006 \\ .007 \\ .008 \\ .009 \\ .011 \\ .014 \\ .02 \\ .029 \\ .041 \\ .068 \\ .093 \\ \frac{H}{m} \\ \frac{2 \cdot H}{m} \end{bmatrix} \cdot \frac{H_{eff}}{H} \cdot m \qquad E_{flexure} := \begin{bmatrix} 16.4811 \\ 16.4811 \\ 17.3293 \\ 15.9983 \\ 16.4377 \\ 18.3322 \\ 16.5229 \\ 16.7947 \\ 17.0984 \\ 14.2239 \\ 16.142 \\ 17.2425 \\ 18.3592 \\ 12.799 \\ 18.4517 \\ 20.6843 \\ 20.6843 \end{bmatrix} \cdot GPa \qquad t_f := \begin{bmatrix} 22 \cdot h \\ 22 \cdot h \\ 19 \cdot h \\ 15 \cdot h \\ 13 \cdot h \\ 12 \cdot h \\ 11 \cdot h \\ 10 \cdot h \\ 9 \cdot h \\ 8 \cdot h \\ 7 \cdot h \\ 6 \cdot h \\ 5 \cdot h \\ 4 \cdot h \\ 3 \cdot h \\ 2 \cdot h \\ 2 \cdot h \end{bmatrix}$$

Force vs Axial Crush Distance Determination:

$$P_{yyy} := 2 \cdot \pi \left[\frac{t_L}{R_{shell} \cdot H_{eff}^{2}} \cdot \sum_{ppp=1}^{10} E_{\theta_{ppp,yyy}} \cdot x\,prime_{ppp} \cdot 2 \cdot \frac{H_{eff}}{n} + \frac{E_{flexure_{yyy}} \cdot R_{shell} \cdot t_{f_{yyy}}^{3}}{3 \cdot H_{eff}^{3}} \right] \cdot H_{eff} - \frac{\delta_{yyy}}{2}$$

Energy Absorption of the Structure:

$$Energy(\delta 11) := linterp(\delta, P, \delta 11)$$

$$Cumulative\_Energy_{yyy} := \int_{0 \cdot m}^{\delta_{yyy}} Energy(x)\,dx \qquad Cumulative\_Energy_{rows(\delta)} = 0.021\ MJ$$

Appendix C

Cylindrical Section Analysis

Ply Stiffness and Lay-up Inputs:

1. Material System: E-Glass (1583)/Epoxy (7780) woven cloth

2. Lay-up Configuration: $[90,45,0,-45]_3,90,45,45,90,[90,45,0,-45]_3$

$N_0 := 6$ $N_{n45} := 6$

$N_{90} := 8$ $N_{p45} := 8$

3. Total Number of Plys $Total\_plys := N_0 + N_{n45} + N_{p45} + N_{90}$

4. Ply Thickness $h := .018 \cdot in$

5. Laminate Thickness $t_L := Total\_plys \cdot h$

6. Strain Applied to the Material (circumferential):

$\beta = \text{atan}(\varepsilon_y/\varepsilon_x)$ $\beta := 89.5 \cdot deg$

Shear Strain: $\varepsilon_s := 0$

7. Number and Orientation of Ply Angles:

$Plys := 4$

$a := 1 .. Plys$

$c := 1 .. 3 \cdot Plys$

$\theta := \begin{bmatrix} 0 \\ 90 \\ 45 \\ -45 \end{bmatrix} \cdot deg$

$sequence := \begin{bmatrix} 90 \\ 45 \\ 0 \\ -45 \\ 90 \\ 45 \\ 0 \\ -45 \\ 90 \\ 45 \\ 0 \\ -45 \\ 90 \\ 45 \\ 45 \\ 90 \\ -45 \\ 0 \\ 45 \\ 90 \\ -45 \\ 0 \\ 45 \\ 90 \\ -45 \\ 0 \\ 45 \\ 90 \end{bmatrix} \cdot deg$

8. Engineering Constants:

$E_x := 3 \cdot MSI$ $E_s := .55 \cdot MSI$ $G_m := 1.26 \cdot GPa$

$E_y := 2.7 \cdot MSI$ $E_m := 3.4 \cdot GPa$

$v_f := .5$

$v_m := .5$

$v_x := .15$

Component Parameters:

1. Radius of Shell: $R_{shell} := 3.5 \cdot ft$
2. Length of Shell: $L_{shell} := 33 \cdot in$
3. Wave Length of Elastic Buckling Wave: (shell only, no stiffener effect) $H := \sqrt{R_{shell} \cdot t \, L}$
4. Stiffener Parameters
   - Undamaged Stiffness
   - Number $E_{carbon} := 53.793 \cdot GPa$
   - Area of Single Stiffener $N_{stiffener} := 8$
5. Open Section Parameters
   - Reduction Parameter $A_{stiffener} := (5.526 \cdot in + (8 \cdot in - 2 \cdot .45 \cdot in)) \cdot .45 \cdot in$

$\zeta := 62.5 \cdot deg$

$\gamma := \frac{\pi - \zeta}{\pi}$ $\gamma = 0.653$

Ply Strength Parameter Inputs:

1. Tensile Strength in Longitudinal Direction $X := 39.1 \cdot KSI$
2. Compressive Strength in Longitudinal Direction $X_{prime} := 33.8 \cdot KSI$
3. Tensile Strength in Transverse Direction $Y := 39.1 \cdot KSI$
4. Compressive Strength in the Transverse Direction $Y_{prime} := 33.8 \cdot KSI$
5. Shear Strength $S := 9.41 \cdot KSI$

Matrix and Fiber Damage Inputs

$E_{f\_star} := .01$ $\eta_y := .5161$ $n := .1$

$E_{m\_star} := .15$ $\eta_s := .316$ $F_{xy\_star} := -.5$

Damage Ply Calculations:

$$E_{fx} := \frac{E_x}{v_f} \qquad G_{fx} := \left[\frac{1 + \eta_s \cdot \frac{v_m}{v_f}}{E_s} - \frac{\eta_s \cdot \frac{v_m}{v_f}}{G_m} \right]^{-1} \qquad E_{fy} := \left[\frac{1 + \eta_y \cdot \frac{v_m}{v_f}}{E_y} - \frac{\eta_y \cdot \frac{v_m}{v_f}}{E_m} \right]^{-1}$$

$$E_{y\_damaged}(F) := \left[\frac{1}{1 + \eta_y \cdot \frac{v_m}{v_f}} \cdot \left[\frac{1}{E_{fy}} + \frac{1}{F} \cdot \frac{\eta_y \cdot \frac{v_m}{v_f}}{E_m} \right] \right]^{-1}$$

$$E_{s\_damaged}(F) := \left[\frac{1}{1 + \eta_s \cdot \frac{v_m}{v_f}} \cdot \left[\frac{1}{G_{fx}} + \frac{1}{F} \cdot \frac{\eta_s \cdot \frac{v_m}{v_f}}{G_m} \right] \right]^{-1}$$

Building Ply Data:

Undamaged ply, ply with matrix damage and ply with fiber damage.

$$E_{xx} := \begin{bmatrix} E_x \\ E_x \\ E_x \cdot E_{f\_star} \end{bmatrix} \qquad E_{yy} := \begin{bmatrix} E_y \\ E_{y\_damaged} \cdot E_{m\_star} \\ E_{y\_damaged} \cdot E_{f\_star} \end{bmatrix} \qquad E_{ss} := \begin{bmatrix} E_s \\ E_{s\_damaged} \cdot E_{m\_star} \\ E_{s\_damaged} \cdot E_{f\_star} \end{bmatrix}$$

$$v_{xx} := \begin{bmatrix} v_x \\ v_x \cdot E_{m\_star} \\ v_x \cdot E_{f\_star} \end{bmatrix} \qquad FF_{xy\_star} := \begin{bmatrix} F_{xy\_star} \\ F_{xy\_star} \cdot E_{m\_star} \\ F_{xy\_star} \cdot E_{f\_star} \end{bmatrix}$$

$$XX_q := X$$

$$XX_{prime_q} := X_{prime} \cdot \left(\frac{E_{ss_q}}{E_s} \right)^n$$

$$YY_q := Y \qquad YY_{prime_q} := Y_{prime} \qquad SS_q := S \qquad v_{yy_q} := v_{xx_q} \cdot \frac{E_{yy_q}}{E_{xx_q}}$$

Rotation Matrices:

$$ml_a := \cos\theta_a \qquad n_a := \sin\theta_a$$

$$J_a := \begin{bmatrix} ml_a^2 & n_a^2 & 2 \cdot ml_a \cdot n_a \\ n_a^2 & ml_a^2 & -2 \cdot ml_a \cdot n_a \\ -ml_a \cdot n_a & ml_a \cdot n_a & ml_a^2 - n_a^2 \end{bmatrix}$$

$$\text{Rotation1}_a := \begin{bmatrix} ml_a^4 & n_a^4 & 2 \cdot ml_a^2 \cdot n_a^2 & 4 \cdot ml_a^2 \cdot n_a^2 \\ n_a^4 & ml_a^4 & 2 \cdot ml_a^2 \cdot n_a^2 & 4 \cdot ml_a^2 \cdot n_a^2 \\ ml_a^2 \cdot n_a^2 & ml_a^2 \cdot n_a^2 & ml_a^4 + n_a^4 & -4 \cdot ml_a^2 \cdot n_a^2 \\ ml_a^2 \cdot n_a^2 & ml_a^2 \cdot n_a^2 & -2 \cdot ml_a^2 \cdot n_a^2 & \left[ml_a^2 - n_a^2\right]^2 \\ ml_a^3 \cdot n_a & -ml_a \cdot n_a^3 & ml_a \cdot n_a^3 - ml_a^3 \cdot n_a & 2 \cdot \left[ml_a \cdot n_a^3 - ml_a^3 \cdot n_a\right] \\ ml_a \cdot n_a^3 & -ml_a^3 \cdot n_a & ml_a^3 \cdot n_a - ml_a \cdot n_a^3 & 2 \cdot \left[ml_a^3 \cdot n_a - ml_a \cdot n_a^3\right] \end{bmatrix}$$

$$\text{Rotation2}_a := \begin{bmatrix} ml_a^2 & n_a^2 \\ n_a^2 & ml_a^2 \\ ml_a \cdot n_a & -ml_a \cdot n_a \end{bmatrix}$$

Ply Stiffness Calculation:

Calculates the zero direction stiffness matrix for the various ply states (undamaged, matrix damaged, and fiber damaged)

$$Q_q := \begin{bmatrix} \frac{E_{xx_q}}{1 - \nu_{xx_q} \cdot \nu_{yy_q}} & \frac{\nu_{yy_q} \cdot E_{xx_q}}{1 - \nu_{xx_q} \cdot \nu_{yy_q}} & 0 \\ \frac{\nu_{xx_q} \cdot E_{yy_q}}{1 - \nu_{xx_q} \cdot \nu_{yy_q}} & \frac{E_{yy_q}}{1 - \nu_{xx_q} \cdot \nu_{yy_q}} & 0 \\ 0 & 0 & E_{ss_q} \end{bmatrix}$$

Creates the stiffness matrices for every combination of ply angle and ply state. Qnew is a 3 x 4 matrix

$$Q_{rot_{q,a}} := \text{Rotation1}_a \cdot \begin{bmatrix} Q_{q\,1,1} \\ Q_{q\,2,2} \\ Q_{q\,1,2} \\ Q_{q\,3,3} \end{bmatrix} \qquad Q_{new_{q,a}} := \begin{bmatrix} Q_{rot_{q,a}\,1} & Q_{rot_{q,a}\,3} & Q_{rot_{q,a}\,5} \\ Q_{rot_{q,a}\,3} & Q_{rot_{q,a}\,2} & Q_{rot_{q,a}\,6} \\ Q_{rot_{q,a}\,5} & Q_{rot_{q,a}\,6} & Q_{rot_{q,a}\,4} \end{bmatrix}$$

Undamaged Elastic Stiffness of Laminate:

$$Q_{laminate} := \frac{1}{N_0 + N_{90} + N_{n45} + N_{p45}} \cdot \left[N_0 \cdot Q_{new_{1,1}} + N_{90} \cdot Q_{new_{1,2}} + N_{n45} \cdot Q_{new_{1,3}} + N_{p45} \cdot Q_{new_{1,4}}\right]$$

$$Q_{laminate} = \begin{bmatrix} 17.575 & 5.256 & -0.038 \\ 5.256 & 17.726 & -0.038 \\ -0.038 & -0.038 & 6.198 \end{bmatrix} \cdot GPa \qquad S := Q_{laminate}^{-1} \qquad E_{Eglass} := \frac{1}{S_{1,1}}$$

Effective Thickness Calculations:

$$t_{eff} := t_L + \frac{A_{stiffener} \cdot N_{stiffener}}{(2 \cdot \pi - 2\zeta) \cdot R_{shell}} \cdot \frac{E_{carbon}}{E_{Eglass}}$$

$t_{eff} = 0.035\,m$ $t_L = 0.0128\,m$

$$H_{eff} := \sqrt{R_{shell} \cdot t_{eff}}$$

$H_{eff} = 0.194\,m$ $H = 0.117\,m$

$$Number_{waves} := \frac{L_{shell}}{2 \cdot H_{eff}}$$

$Number_{waves} = 2.159$

$Number_{waves} := 2$ $\quad H_{eff} := \frac{L_{shell}}{Number_{waves} \cdot 2}$ $\quad H_{eff} = 0.21\,m$

Flexural Stiffness:

1. Indexing variables $\quad ff := 1 .. Total\_plys + 1$

   $gg := 1 .. Total\_plys$

2. Establishing an array of thickness positions for each ply

$$z_{ff} := \frac{-t_L}{2} + (ff - 1) \cdot h$$

3. Assigns the appropriate stiffness matrix based on the lay-up sequence

$$Q_{flex_{gg}} := \begin{cases} Q_{new_{1,1}} & \text{if } sequence_{gg} = 0 \cdot deg \\ Q_{new_{1,2}} & \text{if } sequence_{gg} = 90 \cdot deg \\ Q_{new_{1,3}} & \text{if } sequence_{gg} = 45 \cdot deg \\ Q_{new_{1,4}} & \text{otherwise} \end{cases}$$

Stress Space Strength Parameters:

A separate F must be calculated for each ply state

$$F_{a_q} := \begin{bmatrix} \frac{1}{XX_q \cdot XX\,prime_q} & \frac{FF_{xy\_star_q}}{\sqrt{XX_q \cdot XX\,prime_q \cdot YY_q \cdot YY\,prime_q}} & 0 \\ \frac{FF_{xy\_star_q}}{\sqrt{XX_q \cdot XX\,prime_q \cdot YY_q \cdot YY\,prime_q}} & \frac{1}{YY_q \cdot YY\,prime_q} & 0 \\ 0 & 0 & \frac{1}{SS_q^{\,2}} \end{bmatrix}$$

$$F_{b_q} := \begin{bmatrix} \frac{1}{XX_q} - \frac{1}{XX\,prime_q} \\ \frac{1}{YY_q} - \frac{1}{YY\,prime_q} \end{bmatrix}$$

Strain Space Strength Parameters:

1. Strain strength parameter for each ply state

$$G_{base1_q} := \begin{bmatrix} F_{aq_{1,1}}\cdot\left[Q_{q_{1,1}}\right]^2 \cdots & F_{aq_{1,1}}\cdot Q_{q_{1,1}}\cdot Q_{q_{1,2}} \cdots & 0 \\ +2\cdot F_{aq_{1,2}}\cdot Q_{q_{1,1}}\cdot Q_{q_{1,2}} \cdots & +F_{aq_{1,2}}\left[Q_{q_{1,1}}\cdot Q_{q_{2,2}}+\left[Q_{q_{1,2}}\right]^2\right] \cdots & \\ +F_{aq_{2,2}}\left[Q_{q_{1,2}}\right]^2 & +F_{aq_{2,2}}\cdot Q_{q_{1,2}}\cdot Q_{q_{2,2}} & \\ F_{aq_{1,1}}\cdot Q_{q_{1,1}}\cdot Q_{q_{1,2}} \cdots & F_{aq_{1,1}}\left[Q_{q_{1,2}}\right]^2 \cdots & 0 \\ +F_{aq_{1,2}}\left[Q_{q_{1,1}}\cdot Q_{q_{2,2}}+\left[Q_{q_{1,2}}\right]^2\right] \cdots & +2\cdot F_{aq_{1,2}}\cdot Q_{q_{1,2}}\cdot Q_{q_{2,2}} \cdots & \\ +F_{aq_{2,2}}\cdot Q_{q_{1,2}}\cdot Q_{q_{2,2}} & +F_{aq_{2,2}}\left[Q_{q_{2,2}}\right]^2 & \\ 0 & 0 & F_{aq_{3,3}}\left[Q_{q_{3,3}}\right]^2 \end{bmatrix}$$

$$G_{base2_q} := \begin{bmatrix} F_{bq_1}\cdot Q_{q_{1,1}} + F_{bq_2}\cdot Q_{q_{1,2}} \\ F_{bq_1}\cdot Q_{q_{1,2}} + F_{bq_2}\cdot Q_{q_{2,2}} \end{bmatrix}$$

2. Calculating G matrices for all combinations of ply state and angle:

$$\begin{bmatrix} \text{Rotation1}_1\cdot\begin{bmatrix} G_{base1_1\ 1,1} \\ G_{base1_1\ 2,2} \\ G_{base1_1\ 1,2} \\ G_{base1_1\ 3,3} \end{bmatrix} \\ \text{Rotation1}_1\cdot\begin{bmatrix} G_{base1_2\ 1,1} \\ G_{base1_2\ 2,2} \\ G_{base1_2\ 1,2} \\ G_{base1_2\ 3,3} \end{bmatrix} \\ \text{Rotation1}_1\cdot\begin{bmatrix} G_{base1_3\ 1,1} \\ G_{base1_3\ 2,2} \end{bmatrix} \end{bmatrix}$$

$$G_{2trans} := \begin{bmatrix} \text{Rotation2}_1\cdot\begin{bmatrix} G_{base2_1\ 1} \\ G_{base2_1\ 2} \end{bmatrix} \\ \text{Rotation2}_1\cdot\begin{bmatrix} G_{base2_2\ 1} \\ G_{base2_2\ 2} \end{bmatrix} \\ \text{Rotation2}_1\cdot\begin{bmatrix} G_{base2_3\ 1} \\ G_{base2_3\ 2} \end{bmatrix} \\ \text{Rotation2}_2\cdot\begin{bmatrix} G_{base2_1\ 1} \\ G_{base2_1\ 2} \end{bmatrix} \\ \text{Rotation2}_2\cdot\begin{bmatrix} G_{base2_2\ 1} \\ G_{base2_2\ 2} \end{bmatrix} \\ \text{Rotation2}_2\cdot\begin{bmatrix} G_{base2_3\ 1} \\ G_{base2_3\ 2} \end{bmatrix} \\ \text{Rotation2}_3\cdot\begin{bmatrix} G_{base2_1\ 1} \end{bmatrix} \end{bmatrix}$$

$$G_{1trans} := \begin{vmatrix} \text{Rotation1}_1 \cdot \begin{bmatrix} G_{base1_3\,1,2} \\ G_{base1_3\,3,3} \end{bmatrix} \\ \text{Rotation1}_2 \cdot \begin{bmatrix} G_{base1_1\,1,1} \\ G_{base1_1\,2,2} \\ G_{base1_1\,1,2} \\ G_{base1_1\,3,3} \end{bmatrix} \\ \text{Rotation1}_2 \cdot \begin{bmatrix} G_{base1_2\,1,1} \\ G_{base1_2\,2,2} \\ G_{base1_2\,1,2} \\ G_{base1_2\,3,3} \end{bmatrix} \\ \text{Rotation1}_2 \cdot \begin{bmatrix} G_{base1_3\,1,1} \\ G_{base1_3\,2,2} \\ G_{base1_3\,1,2} \\ G_{base1_3\,3,3} \end{bmatrix} \\ \text{Rotation1}_3 \cdot \begin{bmatrix} G_{base1_1\,1,1} \\ G_{base1_1\,2,2} \\ G_{base1_1\,1,2} \\ G_{base1_1\,3,3} \end{bmatrix} \\ \text{Rotation1}_3 \cdot \begin{bmatrix} G_{base1_2\,1,1} \\ G_{base1_2\,2,2} \\ G_{base1_2\,1,2} \\ G_{base1_2\,3,3} \end{bmatrix} \\ \text{Rotation1}_3 \cdot \begin{bmatrix} G_{base1_3\,1,1} \\ G_{base1_3\,2,2} \\ G_{base1_3\,1,2} \\ G_{base1_3\,3,3} \end{bmatrix} \\ \text{Rotation1}_4 \cdot \begin{bmatrix} G_{base1_1\,1,1} \\ G_{base1_1\,2,2} \\ G_{base1_1\,1,2} \\ G_{base1_1\,3,3} \end{bmatrix} \\ \text{Rotation1}_4 \cdot \begin{bmatrix} G_{base1_2\,1,1} \\ G_{base1_2\,2,2} \\ G_{base1_2\,1,2} \\ G_{base1_2\,3,3} \end{bmatrix} \\ \text{Rotation1}_4 \cdot \begin{bmatrix} G_{base1_3\,1,1} \\ G_{base1_3\,2,2} \end{bmatrix} \end{vmatrix} * \begin{vmatrix} \text{Rotation2}_3 \cdot \begin{bmatrix} G_{base2_1\,2} \end{bmatrix} \\ \text{Rotation2}_3 \cdot \begin{bmatrix} G_{base2_2\,1} \\ G_{base2_2\,2} \end{bmatrix} \\ \text{Rotation2}_3 \cdot \begin{bmatrix} G_{base2_3\,1} \\ G_{base2_3\,2} \end{bmatrix} \\ \text{Rotation2}_4 \cdot \begin{bmatrix} G_{base2_1\,1} \\ G_{base2_1\,2} \end{bmatrix} \\ \text{Rotation2}_4 \cdot \begin{bmatrix} G_{base2_2\,1} \\ G_{base2_2\,2} \end{bmatrix} \\ \text{Rotation2}_4 \cdot \begin{bmatrix} G_{base2_3\,1} \\ G_{base2_3\,2} \end{bmatrix} \end{vmatrix}$$

$$\left[\left[\text{Rotation1}_4 \right] \left[G_{\text{basel3}_{1,2}} \right] \left[G_{\text{basel3}_{3,3}} \right] \right]$$

$$G_c := \begin{bmatrix} G_{\text{1trans}_{c_1}} & G_{\text{1trans}_{c_3}} & G_{\text{1trans}_{c_5}} & G_{\text{2trans}_{c_1}} \\ G_{\text{1trans}_{c_3}} & G_{\text{1trans}_{c_2}} & G_{\text{1trans}_{c_6}} & G_{\text{2trans}_{c_2}} \\ G_{\text{1trans}_{c_5}} & G_{\text{1trans}_{c_6}} & G_{\text{1trans}_{c_4}} & G_{\text{2trans}_{c_3}} \end{bmatrix}$$

Formation of Strain Space Failure Envelopes:

1. The following relationship is used to determine the failure envelope: $G_{i,j} \cdot \varepsilon_i \cdot \varepsilon_j + G_i \cdot \varepsilon_i = 1$

2. After shifting to polar coordinates, the above equation can be solved for r using the quadratic equation:

   $\varepsilon_1 = r \cdot \cos\phi \quad \varepsilon_2 = r \cdot \sin\phi \quad A \cdot r^2 + B \cdot r - 1 = 0$

3. Calculation of coefficients for the quadratic formula

$$A(\phi, b) := G_{b_{2,2}} \cdot \sin(\phi)^2 + 2 \cdot G_{b_{1,2}} \cdot \cos(\phi) \cdot \sin(\phi) + G_{b_{1,1}} \cdot \cos(\phi)^2$$

$$B(\phi, b, \varepsilon_s) := 2 \cdot G_{b_{2,3}} \cdot \sin(\phi) \cdot \varepsilon_s + G_{b_{2,4}} \cdot \sin(\phi) + 2 \cdot G_{b_{1,3}} \cdot \cos(\phi) \cdot \varepsilon_s + G_{b_{1,4}} \cdot \cos(\phi)$$

$$C(\phi, b, \varepsilon_s) := G_{b_{3,4}} \cdot \varepsilon_s + G_{b_{3,3}} \cdot \varepsilon_s^2 - 1$$

$$r(\phi, b, \varepsilon_s) := \frac{-B(\phi, b, \varepsilon_s) + \sqrt{B(\phi, b, \varepsilon_s)^2 - 4 \cdot A(\phi, b) \cdot C(\phi, b, \varepsilon_s)}}{2 \cdot A(\phi, b)}$$

Strain Space Failure Envelopes:

$\phi := 0 \cdot deg, 1 \cdot deg .. 360 \cdot deg \quad y(x) := \tan(\beta) \cdot x \quad x := 0, \frac{\cos(\beta)}{10} .. \cos(\beta) \quad \varepsilon_x(\phi, b, \varepsilon_s) := r(\phi, b, \varepsilon_s) \cdot \cos(\phi) \quad \varepsilon_y(\phi, b, \varepsilon_s) := r(\phi, b, \varepsilon_s) \cdot \sin(\phi)$

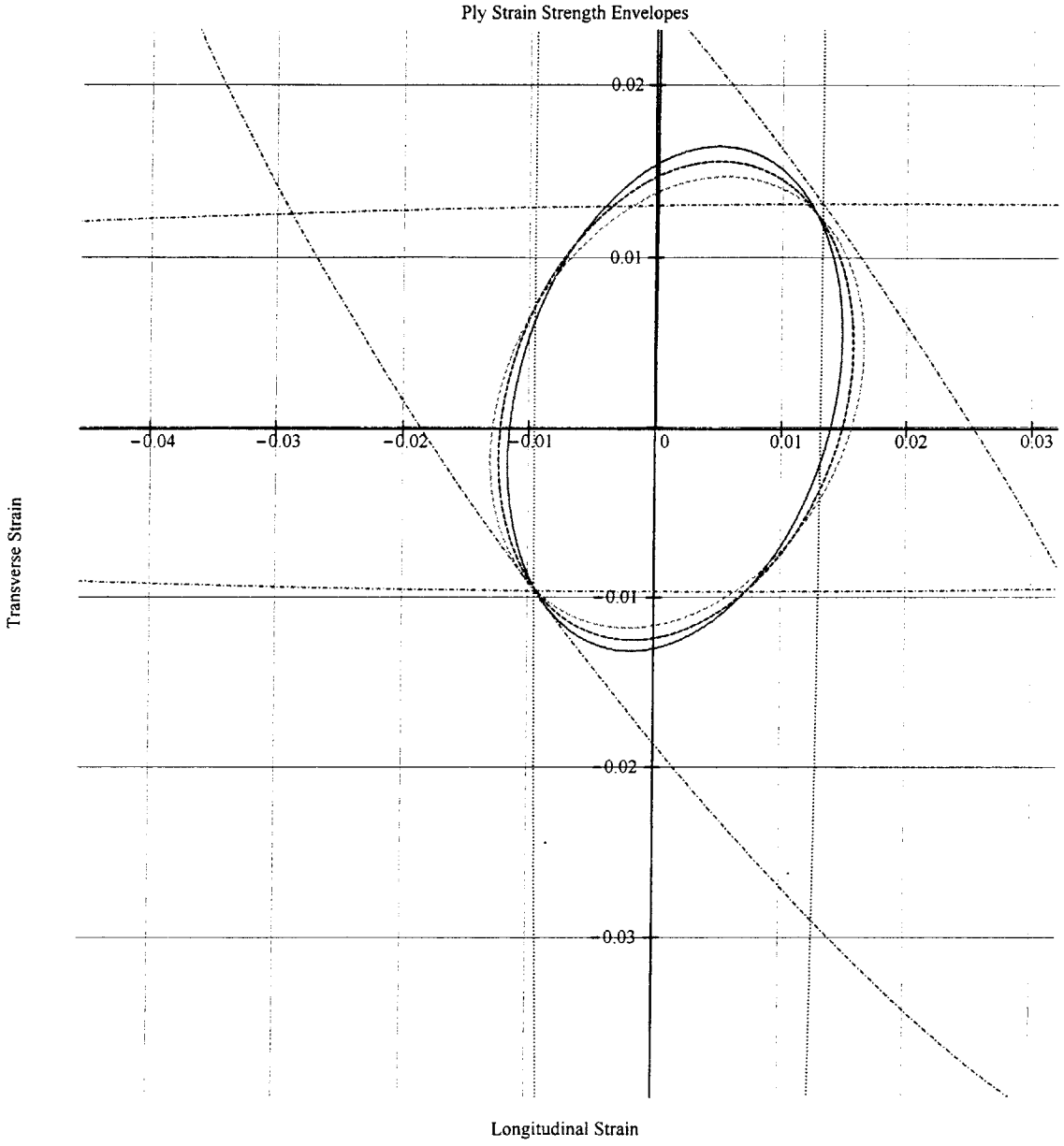

Calculation of Degraded Laminate Stiffness:

The first ply failure strain is first calculated. Subsequently, a progressive failure of plys is allowed and the stiffness calculated based on the ply damage history.

$$
\begin{aligned}
&\text{plot} := \left|\begin{array}{l}
a1 \leftarrow 1 \\
b1 \leftarrow 1 \\
c1 \leftarrow 1 \\
d1 \leftarrow 1 \\
\text{count} \leftarrow 2 \\
n1 \leftarrow 1 \\
\text{while } 1 \\
\quad \left|\begin{array}{l}
\varepsilon 1_1 \leftarrow 0 \\
\sigma 1_1 \leftarrow 0 \cdot \text{MPa} \\
\varepsilon 1_{\text{count}} \leftarrow \min\left(\begin{bmatrix} \varepsilon_x(\beta, a1, \varepsilon_s) \\ \varepsilon_x(\beta, b1+3, \varepsilon_s) \\ \varepsilon_x(\beta, c1+6, \varepsilon_s) \\ \varepsilon_x(\beta, d1+9, \varepsilon_s) \end{bmatrix}\right) \\
\varepsilon 2_{\text{count}} \leftarrow \varepsilon 1_{\text{count}} \cdot \tan(\beta) \\
A\,\text{star}_{\text{count}} \leftarrow \dfrac{1}{N_0 + N_{90} + N_{n45} + N_{p45}} \cdot \left[N_0 \cdot Q\,\text{new}_{a1,1} + N_{90} \cdot Q\,\text{new}_{b1,2} + N_{n45} \cdot Q\,\text{new}_{c1,3} + N_{p45} \cdot Q\,\text{new}_{d1,4}\right] \\
E_{y1_{\text{count}}} \leftarrow \left[\left[A\,\text{star}_{\text{count}}^{-1}\right]_{2,2}\right]^{-1} \\
\sigma 1_{\text{count}} \leftarrow \left[A\,\text{star}_{\text{count}} \cdot \begin{bmatrix} \varepsilon 1_{\text{count}} \\ \varepsilon 2_{\text{count}} \\ \varepsilon_s \end{bmatrix}\right]_2 \\
a1 \leftarrow a1 + 1 \text{ if } \varepsilon 1_{\text{count}} = \varepsilon_x(\beta, a1, \varepsilon_s) \\
b1 \leftarrow b1 + 2 \text{ if } \varepsilon 1_{\text{count}} = \varepsilon_x(\beta, b1+3, \varepsilon_s) \\
c1 \leftarrow c1 + 1 \text{ if } \varepsilon 1_{\text{count}} = \varepsilon_x(\beta, c1+6, \varepsilon_s) \\
d1 \leftarrow d1 + 1 \text{ if } \varepsilon 1_{\text{count}} = \varepsilon_x(\beta, d1+9, \varepsilon_s) \\
\text{count} \leftarrow \text{count} + 1 \\
\text{break if } a1 + b1 + c1 + d1 = 12 \\
\text{break if } a1 > 3 \\
\text{break if } b1 > 3 \\
\text{break if } c1 > 3 \\
\text{break if } d1 > 3
\end{array}\right. \\
\text{tempstore} \leftarrow \text{augment}\left(\varepsilon 2, \dfrac{\sigma 1}{\text{MPa}}\right) \\
\text{augment}\left(\text{tempstore}, \dfrac{E_{y1}}{\text{GPa}}\right)
\end{array}\right.
\end{aligned}
$$

Transverse Stiffness Variations with Axial Location and Axial Crush Distance:

1. Setting up stations along the x' axis and axial crush distances at which E_y is to be calculated

$yyy := 1..18 \qquad n := 2000 \qquad zzz := 1..n$

$$x\,prime_{zzz} := \frac{zzz}{n} - \frac{1}{2 \cdot n} \cdot H_{eff}$$

$$\delta_{temp} := \begin{bmatrix} 0 \\ .002 \\ .003 \\ .004 \\ .005 \\ .006 \\ .007 \\ .01 \\ .013 \\ .015 \\ .02 \\ .027 \\ .028 \\ .043 \\ .06 \\ .115 \\ .155 \\ .234 \end{bmatrix} \cdot \frac{H_{eff}}{H} \cdot m$$

2. Calculation of circumferential strain based on axial position and crush distance

$$\varepsilon_{\theta_{zzz,yyy}} := \frac{x\,prime_{zzz} \cdot \delta_{temp_{yyy}}}{R_{shell} \cdot H_{eff}} \cdot \sqrt{\frac{H_{eff}}{\delta_{temp_{yyy}}} - \frac{1}{4}}$$

3. Assignment of the appropriate Young's moduli to the correct axial position and crush distance based on the transverse Young's Moduli vs strain plot and circumferential strain.

$$E_{\theta_{zzz,yyy}} := \begin{cases} 0 \cdot GPa & \text{if } \varepsilon_{\theta_{zzz,yyy}} \geq .171 \\ .469 \cdot GPa & \text{if } .171 > \varepsilon_{\theta_{zzz,yyy}} \geq .025 \\ 2.779 \cdot GPa & \text{if } .025 > \varepsilon_{\theta_{zzz,yyy}} \geq .016 \\ 6.094 \cdot GPa & \text{if } .016 > \varepsilon_{\theta_{zzz,yyy}} \geq .015 \\ 10.133 \cdot GPa & \text{if } .015 > \varepsilon_{\theta_{zzz,yyy}} \geq .014 \\ 16.154 \cdot GPa & \text{otherwise} \end{cases}$$

$$plot = \begin{bmatrix} 0 & 0 & 0 \\ 0.014 & 245.846 & 16.154 \\ 0.015 & 174.15 & 10.133 \\ 0.016 & 113.553 & 6.094 \\ 0.025 & 90.216 & 2.779 \\ 0.171 & 80.302 & 0.469 \end{bmatrix}$$

Flexural Strain and Stiffness Calculations, and Thickness Variations:

1. Flexural Strain as a function of crush distance

$$\varepsilon_{xf}(\delta, gg) := 2 \cdot \frac{z_{gg+1} + z_{gg}}{2 \cdot R_{shell} \cdot t_L} \cdot \sqrt{\delta \cdot \sqrt{R_{shell} \cdot t_L} + \frac{\delta^2}{4}} \qquad \delta := 0, .001 .. 2 \cdot \sqrt{R_{shell} \cdot t_L}$$

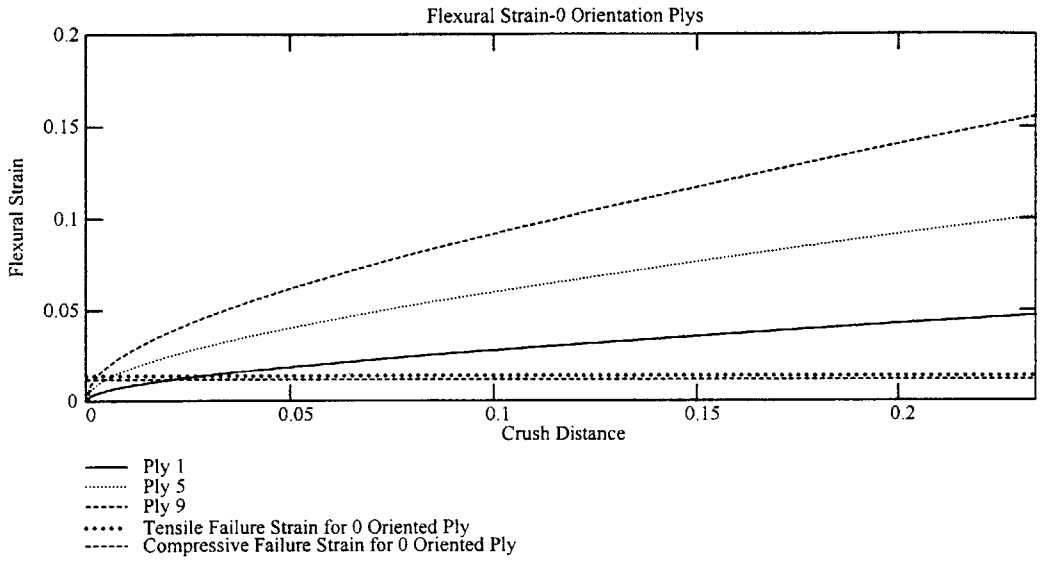

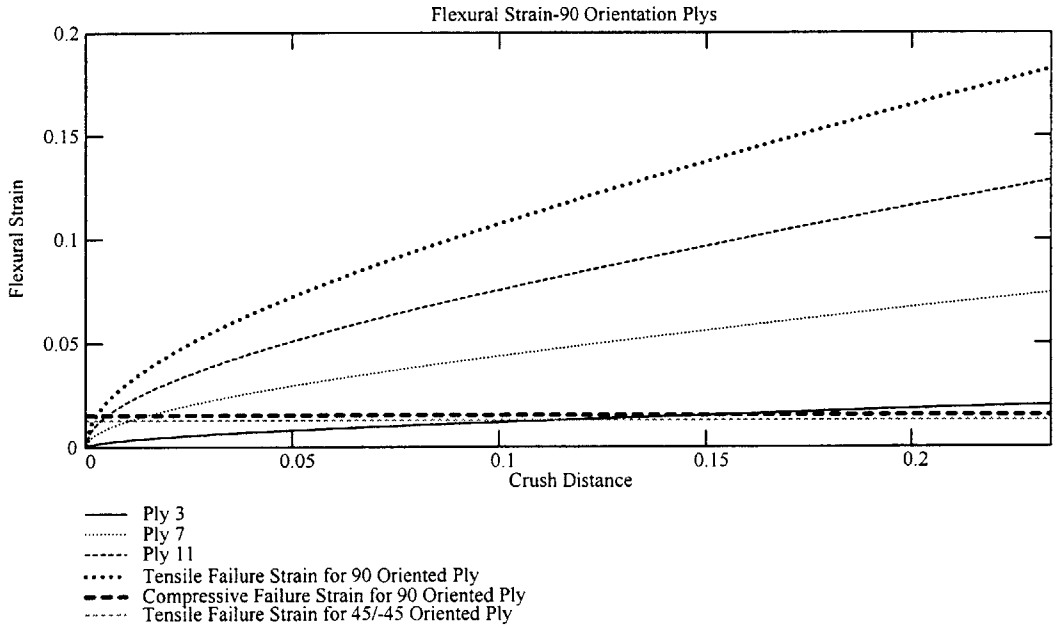

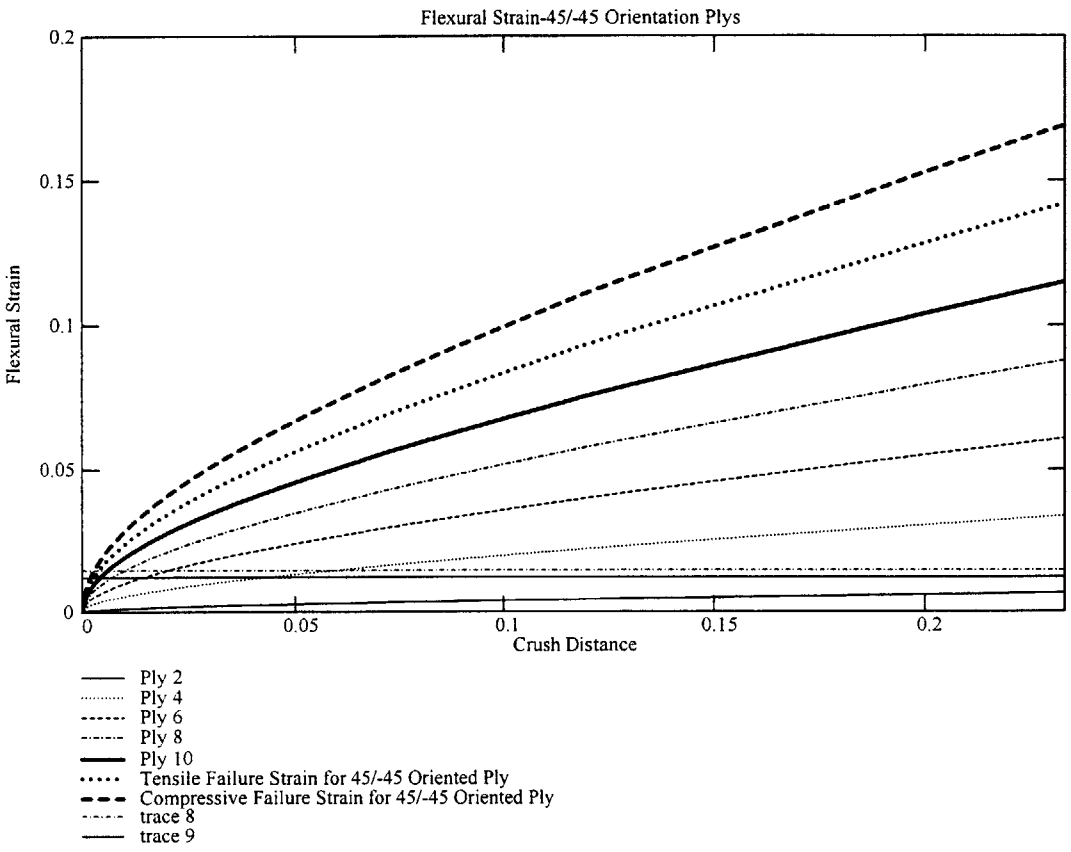

$$ss := \begin{bmatrix} 0 \\ 0 \\ 0 \\ 0 \\ 0 \\ 0 \\ 0 \\ 0 \\ 0 \\ 0 \\ 0 \\ 0 \\ 0 \\ 0 \\ 0 \\ 1 \\ 1 \\ 0 \\ 0 \\ 0 \\ 0 \\ 0 \\ 0 \\ 0 \\ 0 \\ 0 \\ 0 \\ 0 \\ 0 \end{bmatrix}$$

2. Determination of flexural stiffness and thickness variations with crush distance. This a manual operation where the plys are failed progressively as crush distance is increased to 2H using the graphs above and the included ply strain limits. The thickness is determined by removing ply thicknesses as they fail.

$$D_{star} := \frac{12}{(2 \cdot h)^3} \cdot \frac{1}{3} \cdot \sum_{xx=1}^{Total\_plys} Q_{flex_{xx}} \cdot \left[\left[z_{(xx+1)} \right]^3 - z_{xx}^{\ 3} \right] \cdot ss_{xx}$$

$$d_{star} := D_{star}^{-1}$$

$$E_{xf} := d_{star_{1,1}}^{-1}$$

$$E_{xf} = 11.3874 \cdot GPa$$

$$\delta := \begin{bmatrix} 0 \\ .002 \\ .003 \\ .004 \\ .005 \\ .006 \\ .007 \\ .01 \\ .013 \\ .015 \\ .02 \\ .027 \\ .028 \\ .043 \\ .06 \\ .115 \\ .155 \\ \frac{2 \cdot H}{m} \end{bmatrix} \quad \frac{H_{eff}}{H} \cdot m \quad E_{flexure} := \begin{bmatrix} 16.4023 \\ 16.4023 \\ 16.7798 \\ 15.9182 \\ 17.3134 \\ 16.0961 \\ 16.4632 \\ 16.0174 \\ 16.5986 \\ 19.1109 \\ 16.703 \\ 17.9956 \\ 17.8391 \\ 13.7589 \\ 16.6569 \\ 17.9459 \\ 23.1851 \\ 11.3874 \end{bmatrix} \cdot GPa \quad t_f := \begin{bmatrix} 28 \cdot h \\ 28 \cdot h \\ 25 \cdot h \\ 20 \cdot h \\ 18 \cdot h \\ 16 \cdot h \\ 15 \cdot h \\ 13 \cdot h \\ 11 \cdot h \\ 10 \cdot h \\ 9 \cdot h \\ 8 \cdot h \\ 7 \cdot h \\ 6 \cdot h \\ 5 \cdot h \\ 4 \cdot h \\ 3 \cdot h \\ 2 \cdot h \end{bmatrix} \cdot \frac{t_{eff}}{t_L}$$

Force vs Axial Crush Distance Determination:

$$P_{yyy} := 2 \cdot \pi \left[\frac{t_{eff}}{R_{shell} \cdot H_{eff}^{2}} \cdot \sum_{ppp=1}^{10} E\theta_{ppp,yyy} \cdot x\,prime_{ppp} \cdot 2 \frac{H_{eff}}{n} + \frac{E_{flexure_{yyy}} \cdot R_{shell} \cdot t_{f_{yyy}}^{3}}{3 \cdot H_{eff}^{3}} \right] \cdot H_{eff} - \frac{\delta_{yyy}}{2} \cdot \gamma$$

Energy Absorption of the Structure:

$$Energy(\delta 11) := linterp(\delta, P, \delta 11)$$

$$Cumulative\_Energy_{yyy} := \int_{0 \cdot m}^{\delta_{yyy}} Energy(x)\,dx \qquad Cumulative\_Energy_{rows(\delta)} = 0.244 \cdot MJ$$

$$Instant\_Energy_{yyy} := if\ yyy = 1, Cumulative\_Energy_{yyy}, Cumulative\_Energy_{yyy} - Cumulative\_Energy_{yyy-1}$$

Appendix D

Stiffener Analysis

Ply Stiffness and Lay-up Inputs:

1. Material System: Carbon, woven cloth (6K 5HS satin weave IM7)

2. Lay-up Configuration: $[90,45,0,-45]_4[90,45,0,-45]_4$

$N_0 := 8$ $N_{n45} := 8$

$N_{90} := 8$ $N_{p45} := 8$

3. Total Number of Plys $Total\_plys := N_0 + N_{n45} + N_{p45} + N_{90}$

4. Ply Thickness $h := .0135 \cdot in$

5. Laminate Thickness $t_L := Total\_plys \cdot h$

6. Strain Applied to the Material (circumferential):

$\beta = \text{atan}(\varepsilon_y/\varepsilon_x)$ $\beta := 89.5 \cdot deg$

Shear Strain: $\varepsilon_s := 0$

7. Number and Orientation of Ply Angles:

$Plys := 4$

$a := 1 .. Plys$

$c := 1 .. 3 \cdot Plys$

$$\theta := \begin{bmatrix} 0 \\ 90 \\ 45 \\ -45 \end{bmatrix} \cdot deg$$

8. Engineering Constants:

$E_x := 11.6 \cdot MSI$ $E_s := .37 \cdot MSI$ $G_m := 1.26 \cdot GPa$

$E_y := 11.6 \cdot MSI$ $E_m := 3.4 \cdot GPa$

$v_f := .5$

$v_m := .5$

$v_x := .124$

Component Parameters:

1. Radius of Shell: $R_{shell} := 3.5 \cdot ft$
2. Length of Shell: $L_{shell} := 4.471 \cdot ft$
3. Wave Length of Elastic Buckling Wave: $H := \sqrt{R_{shell} \cdot t \cdot L}$
4. Number of Buckling Waves Along Shell $Number_{waves} := \frac{L_{shell}}{2 \cdot H}$

Ply Strength Parameter Inputs:

1. Tensile Strength in Longitudinal Direction $X := 39.1 \cdot KSI$
2. Compressive Strength in Longitudinal Direction $X_{prime} := 33.8 \cdot KSI$
3. Tensile Strength in Transverse Direction $Y := 39.1 \cdot KSI$
4. Compressive Strength in the Transverse Direction $Y_{prime} := 33.8 \cdot KSI$
5. Shear Strength $S := 9.41 \cdot KSI$

Matrix and Fiber Damage Inputs

$E_{f\_star} := .01$ $\eta_y := .5161$ $n := .1$

$E_{m\_star} := .15$ $\eta_s := .316$ $F_{xy\_star} := -.5$

Damage Ply Calculations:

$$E_{fx} := \frac{E_x}{v_f} \qquad G_{fx} := \left[\frac{1+\eta_s \frac{v_m}{v_f}}{E_s} - \frac{\eta_s \frac{v_m}{v_f}}{G_m}\right]^{-1} \qquad E_{fy} := \left[\frac{1+\eta_y \frac{v_m}{v_f}}{E_y} - \frac{\eta_y \frac{v_m}{v_f}}{E_m}\right]^{-1}$$

$$E_{y\_damaged}(F) := \left[\frac{1}{1+\eta_y \frac{v_m}{v_f}} \cdot \left[\frac{1}{E_{fy}} + \frac{1}{F} \cdot \frac{\eta_y \frac{v_m}{v_f}}{E_m}\right]\right]^{-1}$$

$$E_{s\_damaged}(F) := \left[\frac{1}{1+\eta_s \frac{v_m}{v_f}} \cdot \left[\frac{1}{G_{fx}} + \frac{1}{F} \cdot \frac{\eta_s \frac{v_m}{v_f}}{G_m}\right]\right]^{-1}$$

Building Ply Data:

Undamaged ply, ply with matrix damage and ply with fiber damage.

$$E_{xx} := \begin{bmatrix} E_x \\ E_x \\ E_x \cdot E_{f\_star} \end{bmatrix} \qquad E_{yy} := \begin{bmatrix} E_y \\ E_{y\_damaged} \cdot E_{m\_star} \\ E_{y\_damaged} \cdot E_{f\_star} \end{bmatrix} \qquad E_{ss} := \begin{bmatrix} E_s \\ E_{s\_damaged} \cdot E_{m\_star} \\ E_{s\_damaged} \cdot E_{f\_star} \end{bmatrix}$$

$$\nu_{xx} := \begin{bmatrix} \nu_x \\ \nu_x \cdot E_{m\_star} \\ \nu_x \cdot E_{f\_star} \end{bmatrix} \qquad FF_{xy\_star} := \begin{bmatrix} F_{xy\_star} \\ F_{xy\_star} \cdot E_{m\_star} \\ F_{xy\_star} \cdot E_{f\_star} \end{bmatrix}$$

$$XX_q := X \qquad XX_{prime_q} := X_{prime} \cdot \left(\frac{E_{ss_q}}{E_s}\right)^n$$

$$YY_q := Y \qquad YY_{prime_q} := Y_{prime} \qquad SS_q := S \qquad \nu_{yy_q} := \nu_{xx_q} \frac{E_{yy_q}}{E_{xx_q}}$$

Rotation Matrices:

$$ml_a := \cos\theta_a \qquad n_a := \sin\theta_a$$

$$J_a := \begin{bmatrix} ml_a^2 & n_a^2 & 2 \cdot ml_a \cdot n_a \\ n_a^2 & ml_a^2 & -2 \cdot ml_a \cdot n_a \\ -ml_a \cdot n_a & ml_a \cdot n_a & ml_a^2 - n_a^2 \end{bmatrix}$$

$$Rotation1_a := \begin{bmatrix} ml_a^4 & n_a^4 & 2 \cdot ml_a^2 \cdot n_a^2 & 4 \cdot ml_a^2 \cdot n_a^2 \\ n_a^4 & ml_a^4 & 2 \cdot ml_a^2 \cdot n_a^2 & 4 \cdot ml_a^2 \cdot n_a^2 \\ ml_a^2 \cdot n_a^2 & ml_a^2 \cdot n_a^2 & ml_a^4 + n_a^4 & -4 \cdot ml_a^2 \cdot n_a^2 \\ ml_a^2 \cdot n_a^2 & ml_a^2 \cdot n_a^2 & -2 \cdot ml_a^2 \cdot n_a^2 & \left[ml_a^2 - n_a^2\right]^2 \\ ml_a^3 \cdot n_a & -ml_a \cdot n_a^3 & ml_a \cdot n_a^3 - ml_a^3 \cdot n_a & 2 \cdot \left[ml_a \cdot n_a^3 - ml_a^3 \cdot n_a\right] \\ ml_a \cdot n_a^3 & -ml_a^3 \cdot n_a & ml_a^3 \cdot n_a - ml_a \cdot n_a^3 & 2 \cdot \left[ml_a^3 \cdot n_a - ml_a \cdot n_a^3\right] \end{bmatrix}$$

$$Rotation2_a := \begin{bmatrix} ml_a^2 & n_a^2 \\ n_a^2 & ml_a^2 \\ ml_a \cdot n_a & -ml_a \cdot n_a \end{bmatrix}$$

Ply Stiffness Calculation:

Calculates the zero direction stiffness matrix for the various ply states (undamaged, matrix damaged, and fiber damaged)

$$Q_q := \begin{bmatrix} \frac{E_{xx_q}}{1-\nu_{xx_q}\cdot\nu_{yy_q}} & \frac{\nu_{yy_q}\cdot E_{xx_q}}{1-\nu_{xx_q}\cdot\nu_{yy_q}} & 0 \\ \frac{\nu_{xx_q}\cdot E_{yy_q}}{1-\nu_{xx_q}\cdot\nu_{yy_q}} & \frac{E_{yy_q}}{1-\nu_{xx_q}\cdot\nu_{yy_q}} & 0 \\ 0 & 0 & E_{ss_q} \end{bmatrix}$$

Creates the stiffness matrices for every combination of ply angle and ply state. Qnew is a 3 x 4 matrix

$$Q_{rot_{q,a}} := \text{Rotation1}_a \cdot \begin{bmatrix} Q_{q\,1,1} \\ Q_{q\,2,2} \\ Q_{q\,1,2} \\ Q_{q\,3,3} \end{bmatrix} \qquad Q_{new_{q,a}} := \begin{bmatrix} Q_{rot_{q,a}\,1} & Q_{rot_{q,a}\,3} & Q_{rot_{q,a}\,5} \\ Q_{rot_{q,a}\,3} & Q_{rot_{q,a}\,2} & Q_{rot_{q,a}\,6} \\ Q_{rot_{q,a}\,5} & Q_{rot_{q,a}\,6} & Q_{rot_{q,a}\,4} \end{bmatrix}$$

Undamaged Elastic Stiffness of Laminate:

$$Q_{laminate} := \frac{1}{N_0+N_{90}+N_{n45}+N_{p45}} \cdot \left[N_0 \cdot Q_{new_{1,1}} + N_{90} \cdot Q_{new_{1,2}} + N_{n45} \cdot Q_{new_{1,3}} + N_{p45} \cdot Q_{new_{1,4}} \right]$$

$$Q_{laminate} = \begin{bmatrix} 64.715 & 26.586 & 6.322 \cdot 10^{-15} \\ 26.586 & 64.715 & -6.322 \cdot 10^{-15} \\ 6.322 \cdot 10^{-15} & -6.322 \cdot 10^{-15} & 19.064 \end{bmatrix} \cdot \text{GPa} \qquad S := Q_{laminate}^{-1}$$

$$\frac{1}{S_{1,1}} = 53.793 \cdot \text{GPa}$$

$$\frac{1}{S_{2,2}} = 53.793 \cdot \text{GPa}$$

Appendix E

Forward Hemi-head Pressure Hull Analysis

Analysis of HY-80 Forward Pressure Hull Hemihead

Stress Strain Relationship for HY-80

$$\varepsilon := \begin{bmatrix} 0 \\ .002567 \\ .0027 \\ .0029 \\ .0031 \\ .0046 \\ .01 \\ .02 \end{bmatrix} \qquad \sigma := \begin{bmatrix} 0 \\ 77 \\ 78 \\ 79 \\ 79.5 \\ 80 \\ 80.5 \\ 81 \end{bmatrix} \cdot KSI$$

$$x := 0, \frac{\varepsilon_{rows(\varepsilon)}}{100} .. \varepsilon_{rows(\varepsilon)} \qquad curve(x) := linterp(\varepsilon, \sigma, x)$$

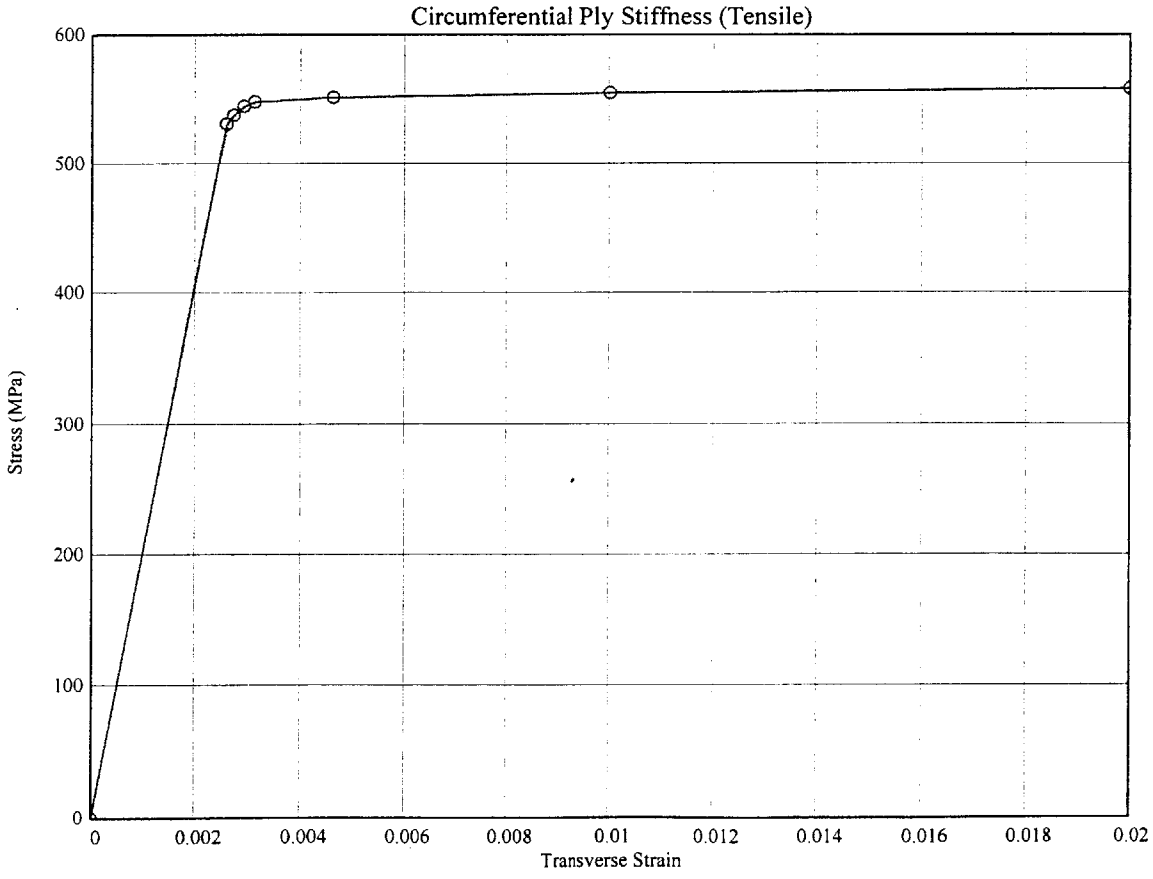

Material Flow Stress Determination:

$$\sigma_c := \frac{1}{\varepsilon_{rows(\varepsilon)}} \cdot \int_0^{\varepsilon_{rows(\varepsilon)}} curve(x)\,dx \qquad \sigma_c = 517.499 \cdot MPa$$

Structural Properties:

$$t_L := \frac{11}{16} \cdot in$$

$$\alpha := 1$$

$$bbb := 1 .. rows(\delta)$$

$$\delta := \begin{bmatrix} 0.028 \\ 0.1 \\ 0.241 \\ 0.242 \\ 0.245 \\ 0.247 \\ 0.248 \\ 0.25 \\ 0.252 \\ 0.254 \\ 0.259 \\ 0.264 \\ 0.268 \\ 0.277 \\ 0.289 \\ 0.291 \\ 0.318 \\ 0.349 \\ 0.447 \\ 0.519 \\ 0.66 \end{bmatrix} \cdot m$$

Crushing Force Prediction:

$$P_{bbb} := 4 \cdot \pi \cdot \sqrt{2} \cdot \sigma_c \cdot \alpha \cdot t_L^{\frac{3}{2}} \cdot \delta_{bbb}^{\frac{1}{2}}$$

Energy Absorption:

$$Energy(\delta 11) := linterp(\delta, P, \delta 11)$$

$$Cumulative\_Energy_{bbb} := \int_{0 \cdot m}^{\delta_{bbb}} Energy(x)\,dx$$

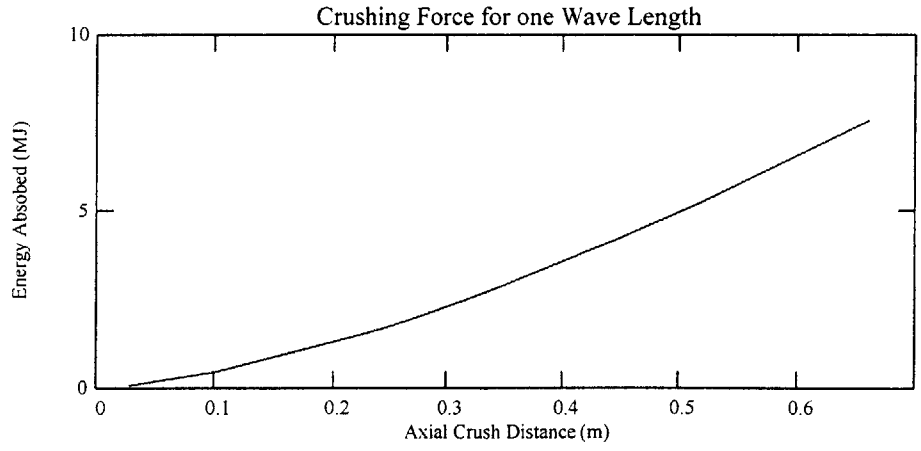

$\delta =$

	1
1	0.028
2	0.1
3	0.241
4	0.242
5	0.245
6	0.247
7	0.248
8	0.25
9	0.252
10	0.254
11	0.259
12	0.264
13	0.268
14	0.277
15	0.289
16	0.291
17	0.318
18	0.349
19	0.447
20	0.519
21	0.66

$\cdot m$

$P =$

	1
1	3.551
2	6.711
3	10.418
4	10.44
5	10.505
6	10.547
7	10.569
8	10.611
9	10.654
10	10.696
11	10.801
12	10.904
13	10.987
14	11.17
15	11.409
16	11.448
17	11.968
18	12.537
19	14.189
20	15.289
21	17.241

$\cdot MN$

$Cumulative\_Energy =$

	1
1	0.082
2	0.452
3	1.659
4	1.67
5	1.701
6	1.722
7	1.733
8	1.754
9	1.775
10	1.797
11	1.85
12	1.905
13	1.948
14	2.048
15	2.184
16	2.207
17	2.522
18	2.902
19	4.212
20	5.273
21	7.566

$\cdot MJ$